Volume 7, Issue 2, 2025

Print ISSN: 2663-1954

Online ISSN: 2663-1962

JOURNAL OF PHARMACEUTICAL

AND MEDICAL RESEARCH



Copyright© Upubscience Publisher

Volume 7, Issue 2, 2025



Published by Upubscience Publisher

Copyright© The Authors

Upubscience Publisher adheres to the principles of Creative Commons, meaning that we do not claim

copyright of the work we publish. We only ask people using one of our publications to respect the integrity

of the work and to refer to the original location, title and author(s).

Copyright on any article is retained by the author(s) under the Creative Commons

Attribution license, which permits unrestricted use, distribution, and reproduction in any medium, provided

the original work is properly cited.

Authors grant us a license to publish the article and identify us as the original publisher.

Authors also grant any third party the right to use, distribute and reproduce the article in any medium,

provided the original work is properly cited.

Journal of Pharmaceutical and Medical Research

Print ISSN: 2663-1954 Online ISSN: 2663-1962

Email: info@upubscience.com

Website: http://www.upubscience.com/

Table of Content

CHINESE MEDICINE FORMULAS FOR STROKE TREATMENT XiaoMiao Gui, XinQi Hu, KeFan Yuan, RuiNa Wang*	1-4
EFFECT OF NPC1 AS AN INDEPENDENT RISK FACTOR ON THE PROGNOSIS OF CERVICAL CANCER ZheYu Luan	5-13
EARLY VERSUS DELAYED INTERVENTIONAL EMBOLIZATION FOR RUPTURED ANTERIOR COMMUNICATING ARTERY ANEURYSMS: A SINGLE-CENTER RETROSPECTIVE COHORT STUDY OF 22 CASES WITH LITERATURE REVIEW ZhanLiang Wei, JianRong Huang*, Jie Bin, Feng Lai	14-18
THE CORRELATION BETWEEN LIFESTYLE AND PREVALENCE OF KNEE JOINT DISEASE IN PLATEAU AREAS $\operatorname{JianCheng} \operatorname{Li}^*, \operatorname{NaNa} \operatorname{Ma}$	19-25
RESEARCH PROGRESS ON LONG NON-CODING RNA-MEDIATED SEPSIS PROGRESSION HongYan Ren, JianQuan Li*	26-30
ESTABLISHMENT OF A METHOD FOR MONITORING MEROPENEM CONCENTRATIONS IN PATIENTS WITH SEVERE ACUTE PANCREATITIS Min Luo#, Wei Bu#, Lu Yao, Liu Shi, HongBo Xu, WenMei Liang, Yan Chen, Tao Chen, Bao Fu*, Lei Gong*	31-36
POST-MARKET CLINICAL FOLLOW-UP STUDY OF THE COLOR DOPPLER ULTRASOUND SYSTEM: A PROSPECTIVE, COMPARATIVE EVALUATION OF SAFETY AND PERFORMANCE Sheng Zhao, FuCheng Wang, Tao Hu*, Dan Wu, JieBing Ma, BaoLi Zhang	37-43
MICRO-ADJUSTMENT MANIPULATION COMBINED WITH TRADITIONAL MANIPULATION FOR KNEE OSTEOARTHRITIS WITH VARUS DEFORMITY KaiLong Sun, ShangJun Xia, Jian Zhang*	44-51
OPTIMIZATION OF NIPT TIMING FOR MALE FETUSES AND ABNORMALITY DETECTION IN FEMALE FETUSES BASED ON QUALITY-CORRECTED MODELS ZhiJian Dai*, LinYv Yang, Kun Li, ZongSheng Wang, YiFeng Liu, JunRan Zhao, Liang Xia	52-58
RECENT ADVANCES IN THE NEUROPROTECTIVE EFFECTS OF TRADITIONAL CHINESE MEDICINE: FOCUS ON ACTIVE INGREDIENTS AND MECHANISMS OF ACTION IN ALZHEIMER'S DISEASE YiWen Zhang	59-65

Print ISSN: 2663-1954 Online ISSN: 2663-1962

DOI: https://doi.org/10.61784/jpmr3037

ANALYSIS OF PRESCRIPTION PATTERNS OF TRADITIONAL CHINESE MEDICINE FORMULAS FOR STROKE TREATMENT

XiaoMiao Gui^{1,2}, XinQi Hu², KeFan Yuan³, RuiNa Wang^{2*}

¹Institute of Scientific and Technical Information of China, Beijing 100038, China.

Corresponding Author: RuiNa Wang, Email: 2317517175@gg.com

Abstract: Stroke is a leading cause of death and disability worldwide. Despite the extensive use of traditional Chinese medicine (TCM) formulas in stroke treatment, systematic analyses of their multi-drug synergy and compatibility patterns remain scarce. This study leverages knowledge graph technology to integrate multi-source TCM formula data and constructs a knowledge graph for stroke-related TCM prescriptions. By combining frequency analysis, cluster analysis, and association rule mining, the study systematically uncovers medication patterns. A total of 1,403 validated formulas were included, identifying nine high-frequency herbs (frequency \geq 200), such as Saposhnikoviae Radix and Glycyrrhizae Radix. These were categorized into four synergistic clusters. Five strong association rules were identified (e.g., "Ligustici Rhizoma and Almond \rightarrow Ephedrae Herba" and "Scutellaria Baicalensis and Saposhnikoviae Radix \rightarrow Glycyrrhizae Radix"). The utility of the knowledge graph in multidimensional retrieval and intelligent reasoning was validated. This study provides data support and a methodological paradigm for the standardized application and modernization of TCM in stroke treatment.

Keywords: Knowledge graph; Traditional Chinese medicine formulas; Prescription pattern; Stroke

1 INTRODUCTION

Stroke poses a major challenge to global public health due to its high disability rate and long-term rehabilitation needs[1], demanding more precise clinical interventions. Owing to their multi-target and multi-pathway synergistic effects, TCM formulas have unique advantages in stroke therapy[2]. However, the formulation principles often rely on empirical knowledge and lack systematic, data-driven validation[3]. Traditional studies based on single statistical methods have been inadequate in revealing hidden associations and synergistic modes among herbs[4], limiting the precision medicine potential of TCM[5].

Knowledge graphs, as an emerging tool for knowledge representation, integrate heterogeneous data through graph structures to visualize complex relationships among entities such as herbs, formulas, diseases, and symptoms[6]. They support intelligent reasoning and pattern discovery, offering new possibilities for the modernization of TCM[7]. In this study, we constructed a knowledge graph using Neo4j for stroke-related TCM prescriptions and applied frequency analysis, clustering, and association rule mining to systematically analyze medication patterns. The goal is to provide scientific evidence for clinical decision-making and new drug development.

2 MATERIALS AND METHODS

2.1 Data Sources and Preprocessing

Data were sourced from the *Encyclopedia of Chinese Medicine Prescriptions* and the TCM Formula Database (https://www.piccc.com/), covering classical texts and modern clinical prescriptions. A total of 1,692 raw records were collected through manual extraction and web scraping. The following preprocessing steps were applied:

Data cleaning: Duplicate entries and records lacking key information (e.g., formula name, composition) were removed, retaining 1,403 valid entries.

Standardization: Herb names were standardized based on the *Pharmacopoeia of the People's Republic of China (2020 edition)* (e.g., "Nanxing" standardized to "Tian Nanxing"), and traditional units (e.g., "liang," "qian") were converted to grams.

Structuring: The formula compositions were split into individual herbs using Python regular expressions to generate a structured CSV dataset.

2.2 Knowledge Graph Construction

Tools: Neo4j (v4.4.6) was used for graph data storage and management, and data import and querying were performed using the py2neo library.

²School of Public Health, Hubei University of Medicine, Shiyan 442000, Hubei, China.

³Xiantao Hospital of Traditional Chinese Medicine, Xiantao 433000, Hubei, China.

2 XiaoMiao Gui, et al.

Entity and relationship definitions: Four types of entities were defined: formulas, herbs, diseases, and symptoms. Formula attributes included name, usage, and source; herb attributes included dosage. Relationships included "COMPOSES" (herb \rightarrow formula) and "TREATS" (formula \rightarrow symptom/disease).

Construction process: Symptom entities were extracted via rule-based matching, assisted by a symptom dictionary based on *Chinese Symptomatology*. The final dataset was imported into Neo4j to complete the graph construction.

2.3 Analytical Methods for Medication Patterns

Frequency analysis: Herbs with occurrence frequency ≥ 200 were identified as high-frequency herbs.

Cluster analysis: Using SPSS 26.0, Euclidean distances between high-frequency herbs were calculated and hierarchical clustering was performed using the between-groups linkage method.

Association rule mining: The Apriori algorithm was applied with a minimum support of 50 and minimum confidence of 85% to discover frequent co-occurrence patterns among herbs.

3 RESULTS

3.1 Knowledge Graph Construction

The resulting stroke TCM knowledge graph comprised 7,451 nodes (diseases in blue, symptoms in red, formulas in orange, herbs in purple) and 9,976 relationships (COMPOSES and TREATS). For example, the "Ligustici Rhizoma Decoction" node clearly shows its herbal components (e.g., Ligustici Rhizoma, Saposhnikoviae Radix, Glycyrrhizae Radix) and target symptoms (e.g., hemiplegia, headache) (Figure 1).

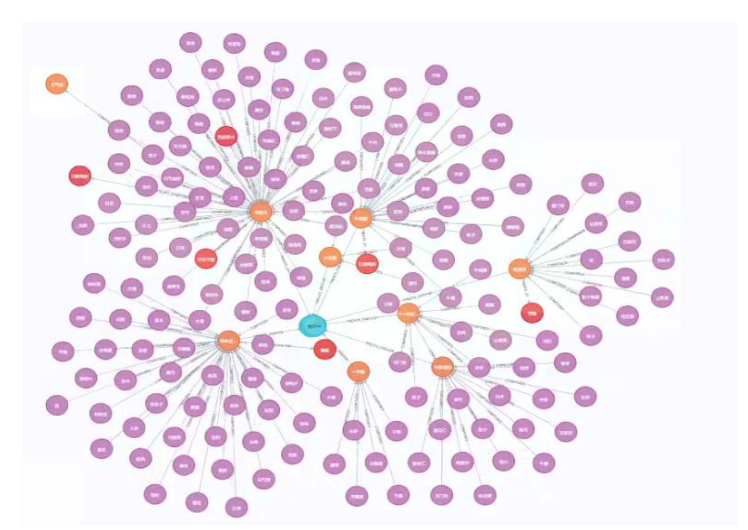


Figure 1 Knowledge Graph of Traditional Chinese Medicine Prescriptions for Stroke

3.2 Medication Pattern Analysis

3.2.1 High-frequency herbs

Nine herbs appeared ≥200 times in the dataset (Table 1): Saposhnikoviae Radix, Glycyrrhizae Radix, Ligustici Rhizoma, Ephedrae Herba, Angelicae Sinensis Radix, Ginseng Radix, Aconiti Lateralis Radix Praeparata, Angelicae Pubescentis Radix, and Notopterygii Rhizoma. These herbs primarily exhibit wind-dispelling, meridian-unblocking, and qi-invigorating effects, aligning with the stroke pathogenesis of "wind-phlegm and blood stasis with qi deficiency." Saposhnikoviae Radix, ranked first, is traditionally used for wind-related conditions and has shown neuroprotective effects via anti-inflammatory and microcirculation improvement mechanisms. Glycyrrhizae Radix is frequently used for its harmonizing and detoxifying properties.

Table 1 Frequency of High-Frequency Drug Use (frequency ≥ 200 times)

Drug Name	Frequency (times)
Saposhnikoviae Radix	443
Glycyrrhizae Radix	357
Ligustici Rhizoma	316
Ephedrae Herba	290
Angelicae Sinensis Radix	288
Ginseng Radix	257
Aconiti Lateralis Radix Praeparata	240
Angelicae Pubescentis Radix	236
Notopterygii Rhizoma	207

3.2.2 Cluster analysis

Using SPSS, the nine high-frequency herbs were grouped into four clusters based on functional similarity:

Cluster A1: Saposhnikoviae Radix

Cluster A2: Glycyrrhizae Radix, Ligustici Rhizoma, Ephedrae Herba, Angelicae Sinensis Radix

Cluster A3: Dioscoreae Hypoglaucae Rhizoma

Cluster A4: Ginseng Radix, Aconiti Lateralis Radix Praeparata, Angelicae Pubescentis Radix, Notopterygii Rhizoma, Arisaema, Cinnamomi Core, Moschus, Gastrodiae Rhizoma, Atractylodes Macrocephala, Pinelliae Rhizoma, Asari Radix, Rhizoma Typhonii, Cinnamomi Cortex, Scutellaria Baicalensis, Ligustici Rhizoma

3.2.3 Association rule mining

Five strong association rules were identified (Table 2), such as:

These rules reflect therapeutic synergies such as "invigorating blood-promoting lung qi-dispelling pathogens," offering evidence for prescription decisions in complex stroke cases with external syndromes.

Table 2 Core Drug Groups and Association Rules

Antecedent Herbs	Consequent Herb	Support	Confidence (%)
Ligustici Rhizoma + Almond	Ephedrae Herba	67	90.54
Almond + Glycyrrhizae Radix	Ephedrae Herba	59	85.51
Scutellaria baicalensis + Saposhnikoviae Radix	Glycyrrhizae Radix	56	86.15
Ligustici Rhizoma + Almond + Glycyrrhizae Radix	Ephedrae Herba	50	92.73
Almond + Glycyrrhizae Radix + Ephedrae Herba	Ligustici Rhizoma	50	86.44

The combination of Ligustici Rhizoma (activating blood circulation and promoting qi movement) and Almond (relieving cough and asthma) results in a 90.54% occurrence probability of Ephedrae Herba (inducing sweating and relieving exterior syndrome). This rule reflects the synergistic effect of "activating blood circulation - ventilating lung - relieving exterior syndrome", which is applicable to the complicating syndrome of lung qi stagnation or external contraction of wind-cold after stroke. When Almond is combined with Glycyrrhizae Radix (harmonizing various medicines), the occurrence probability of Ephedrae Herba reaches 85.51%, indicating that Glycyrrhizae Radix may enhance the synergistic effect between Almond and Ephedrae Herba through alleviating spasm and detoxification. The combination of Scutellaria baicalensis (clearing heat and drying dampness) and Saposhnikoviae Radix (dispelling wind and relieving exterior syndrome) leads to an 86.15% occurrence probability of Glycyrrhizae Radix, reflecting the compatibility pattern of "clearing heat - dispelling wind - harmonizing". After the combination of Ligustici Rhizoma, Almond and Glycyrrhizae Radix, the occurrence probability of Ephedrae Herba is as high as 92.73%, which further verifies the multi-dimensional synergistic effect of "activating blood circulation - ventilating lung - harmonizing - relieving exterior syndrome". When Almond, Glycyrrhizae Radix and Ephedrae Herba are combined, the occurrence probability of Ligustici Rhizoma is 86.44%, embodying the therapeutic idea of strengthening blood circulation and qi promotion on the basis of "ventilating lung - harmonizing - relieving exterior syndrome".

As shown in Figure 2, it displays the correlation network among multiple medicines in stroke TCM prescriptions, visually presenting the compatibility relationships and their strengths between medicines. The nodes in the figure represent TCM medicines, and the edges represent the compositional relationships between medicines. The color, transparency, and label of nodes are displayed according to the degree value: the larger the degree value, the darker the node color, the smaller the transparency, and the larger the label font size, indicating that the corresponding TCM medicine is more important.

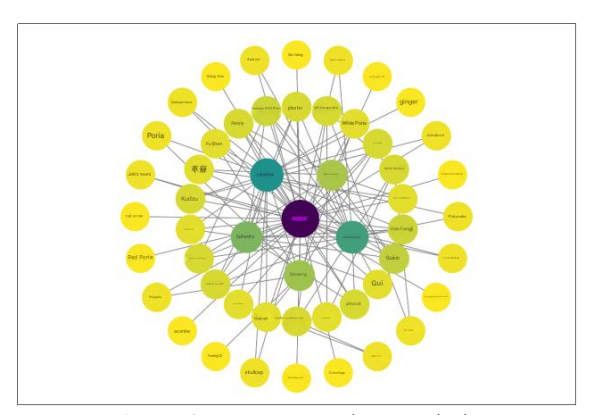


Figure 2 Drug Network Association

3.3 Validation of Knowledge Graph Application

Cypher, the query language used in Neo4j, enables efficient retrieval of formula components. For instance, a Cypher query can extract all herbs in the "Yizisan" formula, visually illustrating its structure and potential mechanism. Cypher also supports multi-tier relational queries, enhancing traceability and interpretability in TCM research.

4 XiaoMiao Gui, et al.

4 DISCUSSION

4.1 Advantages and Challenges of Knowledge Graphs

The constructed knowledge graph breaks the isolation of traditional analyses by integrating multi-source data and visualizing complex herbal-formula-disease-symptom relationships. Its advantages include:

Explicit Relationships: The graph structure visualizes hierarchical links, such as "Saposhnikoviae Radix \rightarrow Qi Deficiency Syndrome \rightarrow Qi-Tonifying and Blood-Activating Therapy," offering new insights into multi-target mechanisms.

Intellignt Inference: Graph algorithms (e.g., link prediction, community detection) can suggest novel herbal combinations for formula development.

Challenges remain:

Data Standardization: TCM terms often have multiple variants (e.g., different processing methods for the same herb), requiring a comprehensive standard dictionary.

Natural Language Processing: Rule-based entity extraction struggles with complex symptom expressions, limiting extraction accuracy.

4.2 Scientific and Clinical Significance of Findings

High-frequency herbs such as Saposhnikoviae Radix and Glycyrrhizae Radix align with classical TCM theories like "treat wind by treating blood" and "harmonize prescriptions." Cluster A2 (Glycyrrhizae Radix, Ligustici Rhizoma, Ephedrae Herba, Angelicae Sinensis Radix) reflects the importance of qi and blood tonification in stroke treatment. The rule "Ligustici Rhizoma + Almond → Ephedrae Herba" illustrates how blood-invigorating and lung-relieving herbs enhance the efficacy of exterior-releasing herbs, guiding treatment for wind-cold syndromes in stroke.

5 CONCLUSION

This study applied knowledge graph technology to systematically explore TCM prescription patterns in stroke treatment. Nine high-frequency herbs were identified as core components with effects on wind expulsion, qi reinforcement, and blood circulation. Cluster and association rule analyses revealed synergistic groupings and compatibility principles. The knowledge graph offers a novel paradigm for the standardized and precise application of TCM in stroke and provides a foundation for future research integrating clinical data and advanced NLP techniques to modernize TCM practices[8-9].

COMPETING INTERESTS

The authors have no relevant financial or non-financial interests to disclose.

REFERENCES

- [1] Parisa Fallahtafti, Amirhossein Habibzadeh, Negar Ghasemloo, et al. Stroke burden in North Africa and the Middle East, 1990-2021: an analysis based on the global burden of disease study. BMC neurology, 2025, 25 (1), 277-277.
- [2] Yin Xinyi, Li Shutang, Wang Junwei, et al. Research progress of active compounds from traditional Chinese medicine in the treatment of stroke. European journal of medicinal chemistry, 2025, 291(5), 117599.
- [3] Xu Min, Wu RuiXia, Li XiaoLi, et al. Traditional medicine in China for ischemic stroke: bioactive components, pharmacology, and mechanisms. Journal of integrative neuroscience, 2022, 21 (1), 26-26.
- [4] Zhao Jianfeng, Zhang Wei, Yu Hai. Prospects and Analysis of Traditional Chinese Medicine Standards Through the Transition of Chinese Pharmacopeia. Journal of Pharmaceutical Innovation, 2022, 18 (2), 349-355.
- [5] Zhang Peng, Zhang Dingfan, Zhou Wuai, et al. Network pharmacology: towards the artificial intelligence-based precision traditional Chinese medicine. Briefings in bioinformatics, 2023, 25 (1), 1-12.
- [6] Zhang Zheng, Wu Hengyang, Wang Na. A Knowledge-Enhanced Disease Diagnosis Method Based on Prompt Learning and BERT Integration. Journal on Artificial Intelligence, 2025, 7 (1), 17-37.
- [7] Gao Yanjun, Li Ruizhe, Emma Croxford, et al. Leveraging Medical Knowledge Graphs Into Large Language Models for Diagnosis Prediction: Design and Application Study. JMIR AI, 2025, 4(1), e58670: p1-p17.
- [8] Alain García Olea, Ane G Domingo Aldama, Marcos Merino, et al. The Application of Deep Learning Tools on Medical Reports to Optimize the Input of an Atrial-Fibrillation-Recurrence Predictive Model. Journal of Clinical Medicine, 2025, 14 (7), 2297-2297.
- [9] Priyanka Khalate, Shilpa Gite, Biswajeet Pradhan, et al. Advancements and gaps in natural language processing and machine learning applications in healthcare: a comprehensive review of electronic medical records and medical imaging. Frontiers in Physics, 2024, 12(12), 1445204-1445204.

Print ISSN: 2663-1954 Online ISSN: 2663-1962

DOI: https://doi.org/10.61784/jpmr3038

EFFECT OF NPC1 AS AN INDEPENDENT RISK FACTOR ON THE PROGNOSIS OF CERVICAL CANCER

ZheYu Luan

Prenatal Diagnosis Center, The Sixth Affiliated Hospital of Harbin Medical University, Harbin Medical University, Harbin 150028, Heilongjiang, China.

Corresponding Email: zyluan2020@163.com

Abstract: Objective: Intracellular cholesterol transporter 1 (NPC1) plays an indispensable role in the pathological process of malignant tumor. But the value of NPC1 as a biomarker in cervical cancer has not yet been revealed. Methods: 191 cervical cancer samples with NPC1 expression data and relevant clinical characteristic information were obtained from the Cancer Genome Atlas (TCGA). A series of bioinformatics analysis methods were performed to explore the biological role of NPC1 in cervical cancer. Results: Firstly, Cox regression and the Kaplan–Meier method showed that the increased expression of NPC1 was related to the decrease of overall survival time in cervical cancer. Secondly, GO enrichment analysis disclosed that some essential physiological processes were significantly correlated with NPC1 over-expression. Thirdly, KEGG enrichment analysis indicated that cancer-related signaling pathways were correlated with NPC1 expression. Fourthly, I found the close relationship between NPC1 expression and tumor immune micro-environment of cervical cancer. Finally, four small molecule drugs with potential inhibitory effect on NPC1 expression were screened by C-Map analysis. Conclusion: The high expression of NPC1 was an independent risk factor for the poor prognosis of cervical cancer. Moreover, NPC1 might be promising biomarker for the diagnosis and treatment of cervical cancer.

Keywords: Cervical cancer; NPC1; Poor prognosis; Biomarker; Bioinformatics analysis

1 INTRODUCTION

Cervical cancer was the first most common cancer in the female reproductive system. In 2018, there were approximately 570,000 women newly diagnosed cervical cancer, and the total number of deaths has reached an incredible 311000 in worldwide [1]. The clinical outcomes of early-staged cervical cancer have greatly improved by HPV screening and vaccination strategies [2-4]. However, the prognosis of advanced cervical cancer is still unsatisfactory, whose 5-year relative survival rate is only 16.5% [5]. The poor prognosis is probably due to the shortage of effectual prediction targets in cervical cancer [6]. Consequently, it is urgent to explore new therapeutic and prognostic biomarkers to improve the prognosis of patients.

Currently, several biomarkers have been identified for the diagnosis and treatment of cervical cancer [7-8]. For example, E6 and E7 promote the malignant evolution of cervical cancer, which has been applied as a detection target in tumor screening [9]. In addition, high circGSE1 expression can predict worse overall survival (OS) and disease-free survival (DFS) [10]. Moreover, the p16/Ki67 is closely related to tumor occurrence, development and prognosis, which is of vital instructive significance for cervical cancer diagnosis [11]. Because the pathogenesis of cervical cancer was extremely complex involving a variety of gene disorders and even epigenetic regulation abnormalities. Therefore, to improve the prognosis of patients, only relying on one or several biomarkers was not enough to achieve the individualized diagnosis and treatment of cervical cancer [12]. It must be emphasized that the exploration of new biomarkers is imperative regarding a better understanding of the progression and prognosis of cervical cancer.

Intracellular cholesterol transporter 1(NPC1), also known as HGNC, encodes a transmembrane protein mediating intracellular cholesterol trafficking. NPC1 plays an essential role in maintaining lipid homeostasis [13]. It is reported that the mutation in NPC1 can be found in about 95% of Niemann-Pick type C (NPC) diseases, which caused the abnormal accumulation of cholesterol in various tissues and cells. In recent years, increasing number of studies has mentioned the role of NPC1 in promoting the malignancies progression and predicting prognosis. It has been revealed that the overexpression of NPC1 could enhance the proliferation of liver carcinoma cell, and the proliferation and migration ability was significantly decreased when NPC1 was silenced [14]. In esophageal cancer, NPC1 with promoter hypomethylation and upregulation, was associated with tumor processions such as extracellular matrix organization, cell adhesion and integrin signaling [15]. Those results suggested that NPC1 might function as an oncogene promote the cancer progression. However, the role of NPC1 in cervical cancer remains unclear to my best knowledge.

This study was the first time to comprehensively and systematically validate the high expression of NPC1 and its prognostic value in cervical cancer through big data analysis. Besides that, I revealed the underlying mechanism of NPC1 may involve in the malignant process of cervical cancer. In summary, the study will provide a new viewpoint on the mechanisms of cervical cancer pathology and a promising biomarker for prognosis and treatment.

2 PATIENTS AND METHODS

6 ZheYu Luan

2.1 TCGA Database

The Tumor Genome Atlas (TCGA) (http://cancergenome.nih.gov/) freely provides various oncology data for researchers all over the world [16]. It contains many kinds of cancer data such as clinical characteristics, genome mutations, mRNA expression, miRNA expression, methylation data. This database has largely helped medical researchers to ameliorate the prevention, diagnosis and management of cancer. After deletion the incomplete data like lack of clinical stage or survival time, I all extract 191 cervical cancer samples for further analysis and processing. Patients' detailed clinical features, such as age, clinical stage, tummy node metastasis classification, were shown in Table 1.

Table 1 Characteristics of Patients with Cervical Cancer Based on TCGA RNA-Seq Data

Covariates	Туре	Total	High	Low	P-value
Age	<=46	96(50.26%)	51(53.68%)	45(46.88%)	0.4258
_	>46	95(49.74%)	44(46.32%)	51(53.12%)	
Clinical Stage	I	105(54.97%)	54(56.84%)	51(53.12%)	0.1533
	II	47(24.61%)	18(18.95%)	29(30.21%)	
	III	25(13.09%)	13(13.68%)	12(12.5%)	
	IV	14(7.33%)	10(10.53%)	4(4.17%)	
Histologic Grade	G1	11(5.76%)	6(6.32%)	5(5.21%)	0.1615
	G2	83(43.46%)	38(40%)	45(46.88%)	
	G3	78(40.84%)	37(38.95%)	41(42.71%)	
	GX	19(9.95%)	14(14.74%)	5(5.21%)	
Pathologic M	M0	93(48.69%)	44(46.32%)	49(51.04%)	0.7113
	M1	7(3.66%)	3(3.16%)	4(4.17%)	
	MX	91(47.64%)	48(50.53%)	43(44.79%)	
Pathologic N	N0	95(49.74%)	44(46.32%)	51(53.12%)	0.0212
	N1	44(23.04%)	17(17.89%)	27(28.12%)	
	NX	52(27.23%)	34(35.79%)	18(18.75%)	
Pathologic T	T1	103(53.93%)	51(53.68%)	52(54.17%)	0.0154
	T2	54(28.27%)	20(21.05%)	34(35.42%)	
	Т3	14(7.33%)	8(8.42%)	6(6.25%)	
	T4	9(4.71%)	6(6.32%)	3(3.12%)	
	TX	11(5.76%)	10(10.53%)	1(1.04%)	
NPC1 Expression	High	95(49.74%)	95(100%)	0(0%)	0
•	Low	96(50.26%)	0(0%)	96(100%)	
Methylation	High	95(49.74%)	46(48.42%)	49(51.04%)	0.8279
-	Low	96(50.26%)	49(51.58%)	47(48.96%)	

2.2 ONCOMINE Analysis

ONCOMINE database (https://www.oncomine.org/) is a prevalent data-mining platform, which is currently the world's largest cancer gene chip database. It contains the genome-wide-sequencing data of 86,733 cancerous tissues and healthy control tissue samples [17]. I collected four datasets *Pyeon Multi-cancer*, *Scotto Cervix*, *Zhai Cervix* and *Biewenga Cervix* to compare the mRNA level of NPC1 between cervical cancer and normal tissue. Threshold value: p < 1E-4, fold change > 1.4, gene rank: 10%, and data type: mRNA.

2.3 HPA database

The Human Protein Atlas (HPA) (http://www.proteinatlas.org/) a massive project based on protein examination, which contains more than 26,000 antibodies that target more than 17,000 human genes [18]. It clearly shows the expression of target genes at RNA and protein levels in different tissue and organs. I obtained six immunohistochemical results from the database on the expression of NPC1 protein in cervical

2.4 Gene Ontology (GO) Analysis

Gene Ontology (GO) analysis aims to provide a consistent description of gene functions in various databases [19]. GO analysis includes three major categories: biological process (BP), cellular component (CC) and molecular function (MF), which describe the possible molecular functions, subcellular structure and location of gene products, as well as the likely involved signaling pathways. GO analysis of differentially expressed genes can obtain more comprehensive gene function information. In this study, the R software Cluster Profiler package was used to annotate the function of the differential gene NPC1.

2.5 KEGG Enrichment Analysis

Kyoto Encyclopedia of Genes and Genomes (KEGG) (https://www.kegg.jp/) is the most commonly used bioinformatics

analysis tool to explore signal pathways. It integrates a large number of high-throughput experimental data such as genome sequencing data into a network for analysis and research. KEGG mainly consists of three databases: the pathway database of interacting molecular networks (Pathway), the gene database of complete and partial sequencing (GENES) and the database of ligand chemical reactions (LIGAND). In this study, KEGG analysis was used to explore the NPC1 gene data set and biological function [20].

2.6 Connectivity Map (C-Map) Analysis

Connectivity map (C-Map) (https://portals.broadinstitute.org/C-Map/) is a biological application database, which can effectively identify candidate drugs for disease [21]. This database quickly matches drug molecules with high relevance to the disease through the use of gene expression data and deduce its related mechanism of action. NPC1 co-expressed genes were screened, positive and negative related genes were considered as up-regulated and down-regulated expression. Then, candidate drugs were screened by setting p < 0.005 and enrichment index < -0.8. Finally, the chemical structure formula and 2D and 3D structures of drugs were found in PubChem.

2.7 Statistical Analysis

R software (version 3.6.1) was used to conduct data analysis and processing in this study. The t-test was sued to compare the expression of NPC1 between cervical cancer and normal cervical tissue. The prognostic value of NPC1 was elevated through plotting Kaplan-Meier survival curves and ROC curves. In addition, Cox regression was utilized to prove whether up-regulation of NPC1 was independently associated with poor prognosis of cervical cancer. The P-values of all statistical analysis results was less than 0.05, which was considered as a significant result in this study.

3 RESULTS

3.1 NPC1 is Abnormally Highly Expressed in Cervical Cancer

I firstly compared the mRNA and protein level of NPC1 in cervical cancer tissue with normal tissue in ONCOMINE database and HPA database. Several datasets in ONCOMINE database reveal that the NPC1 mRNA level in cervical cancerous tissue was significantly increased than that in healthy tissue (Figure 1a-d). The *Pyeon Multi-cancer* dataset showed that the NPC1 mRNA expression in cervical cancer was 3.44 times higher than that in normal tissue (Figure 1a). Then, since proteins are the main executors of gene function, six clinical specimens were selected from the HPA database to analyze the level of NPC1 protein between normal and cervical cancer tissue. I selected three normal tissues and three cancer tissues using the same antibody CAB070132, and they were of similar basic characteristic. As clearly exhibited in Figure 1e-g, NPC1 protein was higher in cervical cancer group versus their expression levels in healthy control group. In summary, both mRNA and protein expression level of NPC1 was highly expressed in cervical cancer.

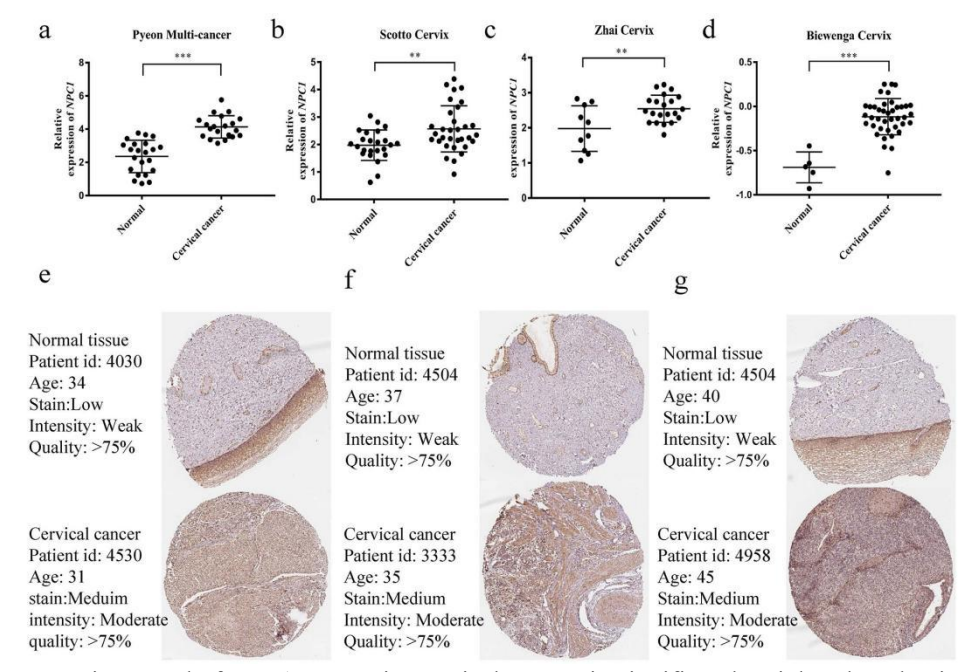


Figure 1 The Expression Level of NPC1 mRNA in Cervical Cancer is Significantly Higher than that in Normal Tissue: a-d: The mRNA Expression of NPC1 in Datasets of ONCOMINE; e-g: The Protein Expression Level of NPC1 Based on HPA Database

8 ZheYu Luan

3.2 NPC1 High Expression Predicts Poor Prognosis in Cervical Cancer

Firstly, the patients were subdivided into high-NPC1 and low-NPC1 expression group according to the median of gene expression. Then, I performed the Kaplan-Meier survival analysis to underlying the association of survival probability and NPC1 expression level in cervical cancer patients. As shown in Figure 2a, the patients with high-NPC1 expression have a worse prognosis than those with low-NPC1 expression. Moreover, drawing ROC curve to evaluate the diagnostic value of NPC1 in cervical cancer. The area under the curve of 3-year and 5-year was respectively 0.683 and 0.762, indicating the overexpression of NPC1 had a relatively diagnostic value (Figure 2b).

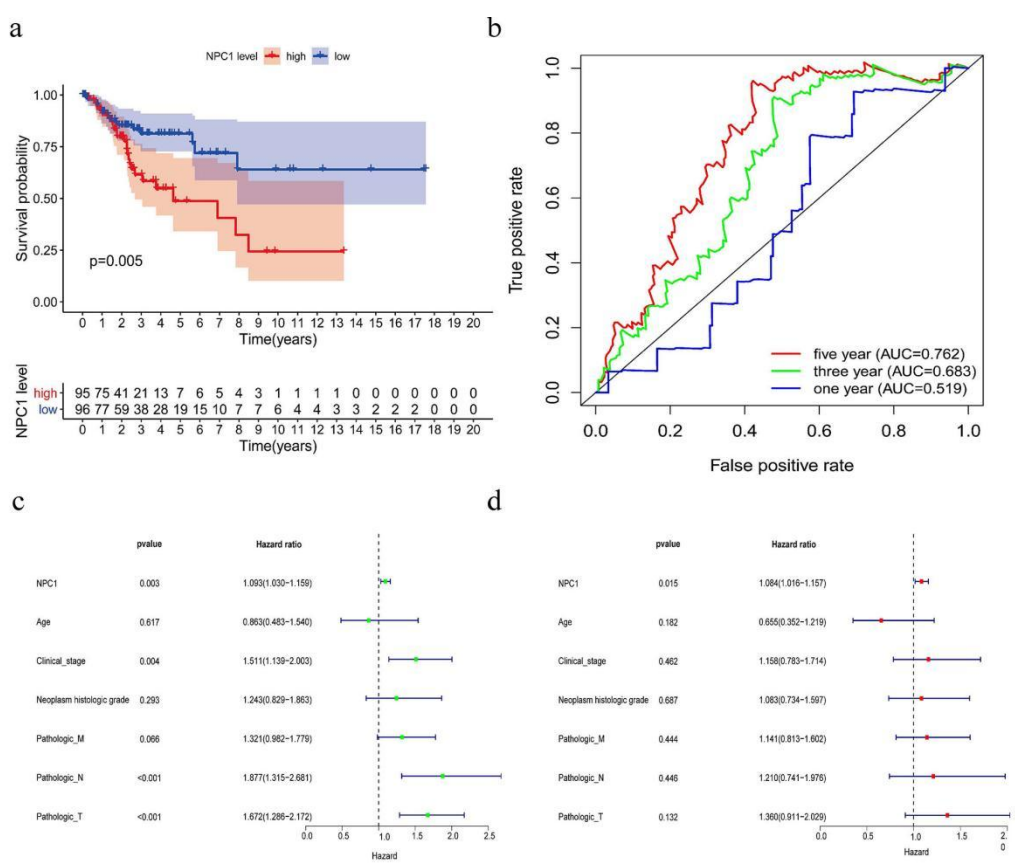


Figure 2 High Expression of NPC1 is Independently Related to the Poor Prognosis of Cervical Cancer: a. High expression of NPC1 indicates poor survival in cervical cancer; b. The ROC curve shows good diagnosis value of NPC1 expression in cervical cancer; c. Univariate regression of prognostic in patients with cervical cancer; d. Multivariate survival model of prognostic in patients with cervical cancer

3.3 NPC1 High Expression is an Independent Risk Factor in Cervical Cancer

Univariate and multivariate Cox regression analysis were conducted to find out factors that might arouse the poor prognosis of patients with cervical cancer. From the univariate Cox regression analysis results shown in Figure 2c, I found that high-NPC1 expression correlated significantly with poor survival (P=0.003, hazard ratio [HR]=1.093(95%CI [1.030-1.159])). Additionally, the clinical stage, pathologic N and pathologic T were risk factors for the poor prognosis as well. The subsequent multivariate Cox regression analysis was performed to eliminate the influence of confounding factors (Figure 2d). NPC1 expression remained independently associated with prognosis, with an HR of 1.084(95%CI [1.016-1.157], p=0.015). The above results emphasized that NPC1 was an independent risk factor for the prognosis of suffers with cervical cancer.

3.4 Functional Annotation and Pathway Enrichment Analysis of NPC1

GO and KEGG analyses were carried out to comprehensively understand the biofunction of NPC1. NPC1 might be of vital importance to gene expression and translation, because the BP results showed that NPC1 was involved in many biological processes such as nuclear transcribed mRNA catalytic process, translation initiation and viral gene expression and transcription (Figure 3a). CC analysis indicated that NPC1 contribute to the formation of cell-subject connection, focal adhesion and mitochondrial protein complex (Figure 3b). Also, MF revealed NPC1 was related to cell adhesion molecule binding, cadherin binding, ribonucleoprotein complex binding and other molecular functions (Figure 3c). Subsequent KEGG analysis showed that NPC1 significantly enriched in the following metabolic pathway: cell cycle, FoxO, wnt and TGF-β signaling pathway (Figure 3d). These signaling pathway are closely related to the malignant

process of tumor and have drawn the attentions of cancer researchers worldwide.

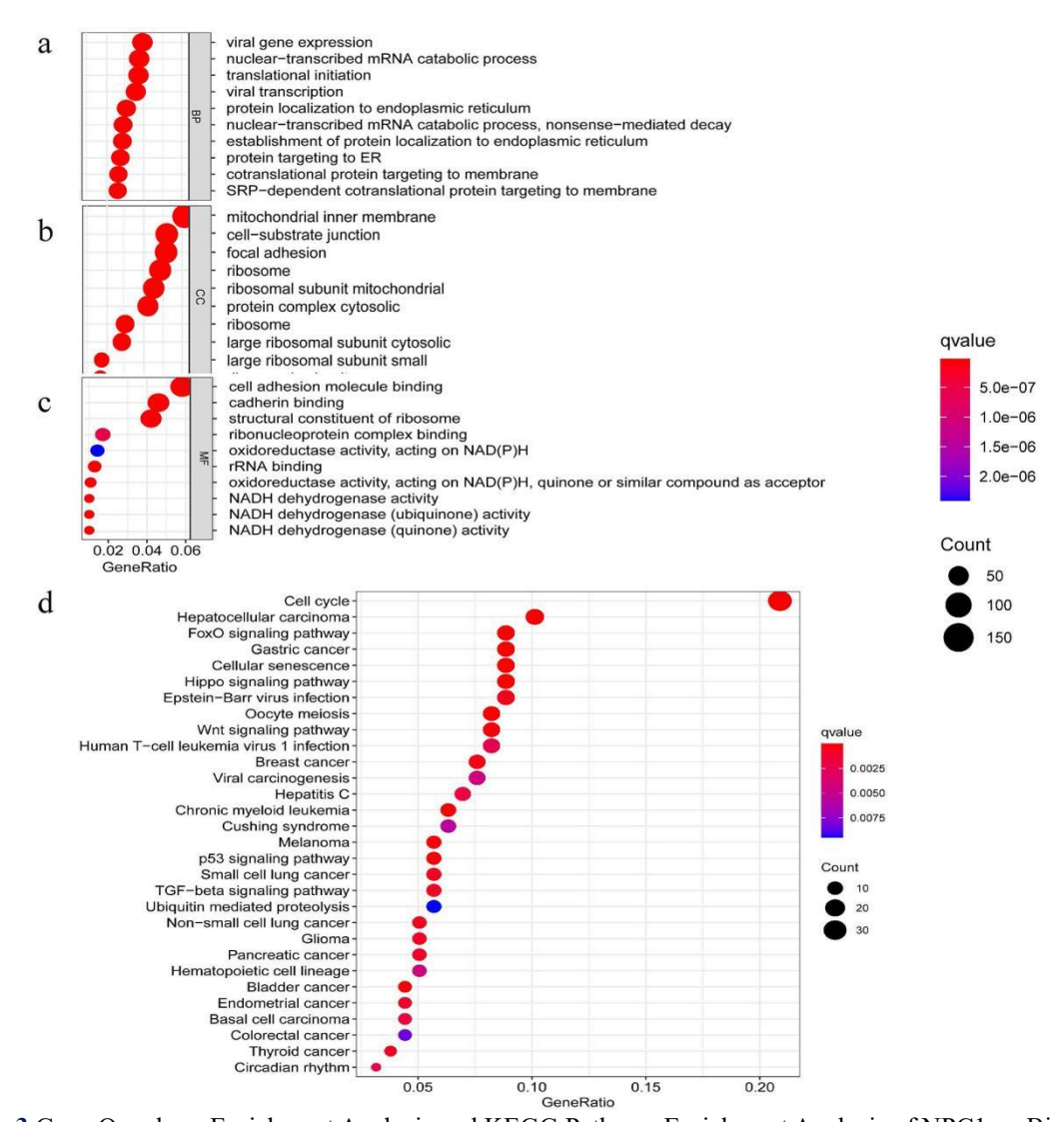


Figure 3 Gene Oncology Enrichment Analysis and KEGG Pathway Enrichment Analysis of NPC1: a. Biological Process (BP); b. Cellular Component (CC); c. Molecular Function (MF); d. The Most Related Signaling Pathway

3.5 Relationships of NPC1 with Immune in Cervical Cancer

The TISDB database was used to identify the relationship between NPC1 expression and the various types of lymphocytes, immunomodulator and chemokine in the tumor microenvironment. In cervical cancer, there was a significant positive correlation between the expression of NPC1 and the infiltration of immune cells, such as Tcm CD8 cell (r = 0.317, p = 1.71e-8), CD56bright (r = 0.201, p = 0.000416), neutrophils (r=0.22, p = 0.000106) and Tcm CD4 (r = 0.281, p = 6.58e-7) (Figure 4a). Notably, this positive correlation in cervical cancer was present between all kind of immune-inhibitors (TGFB1, CD274, PDCD1LG2 and TGFBR1) and NPC1 expression (Figure 4b), and negative correlation was present between all kinds of immune-stimulators (TNFRSF14, TNFRSF3C, CXCR4 and HHLA2) (Figure 4c). Finally, in cervical cancer, NPC1 expression was closely associated with chemokine of the tumor microenvironment (i.e., CXCL8, CDL22, CCL26 and CXCL6) (Figure 4d).

10 ZheYu Luan

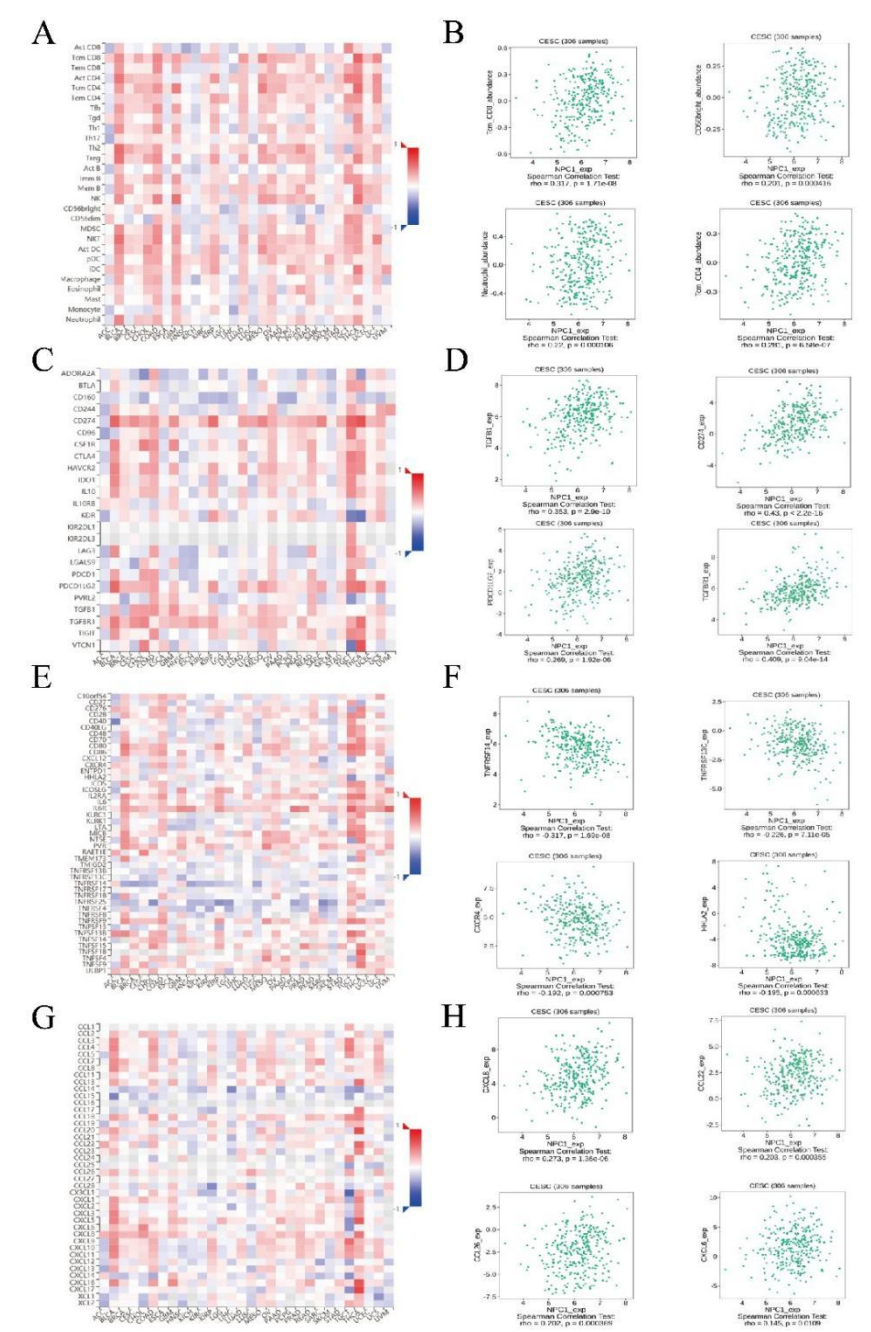


Figure 4 The Correlation of the Expression of NPC1 with Various Types of Lymphocytes, Immunomodulator and Chemokine In Cervical Cancer: a-b. Lymphocytes; c-d. Immune-Inhibitors; e-f. Immune-Stimulators; g-h. Chemokine

3.6 Co-Expression Analysis of NPC1 and Screening of Potential Drugs

Firstly, I used Pearson correlation analysis to explore the co-expression relationship of the NPC1 and other parameters. Based on the correlation coefficient, I obtained the ten genes that most positively or negatively associated with NPC1 expression in patients with cervical cancer. As Figure 5a and 5b showed that there were top five genes with the negative correlation with NPCI (SNRPA, THYN1, ATP5PO, PTOV1, CFAP410) and top-five genes with the positive correlation (CLIP1, ADAM17, MDB1, EDEM1, GNG12). Then, according to the gene principle of the C-Map database, I screened four small molecule compounds with potential therapeutic effects for cervical cancer, including mitoxantrone, harmol, fenoprofen and azacitidine. At last, I searched their chemical structure information in the platform of PubChem (Figure 5c-f).

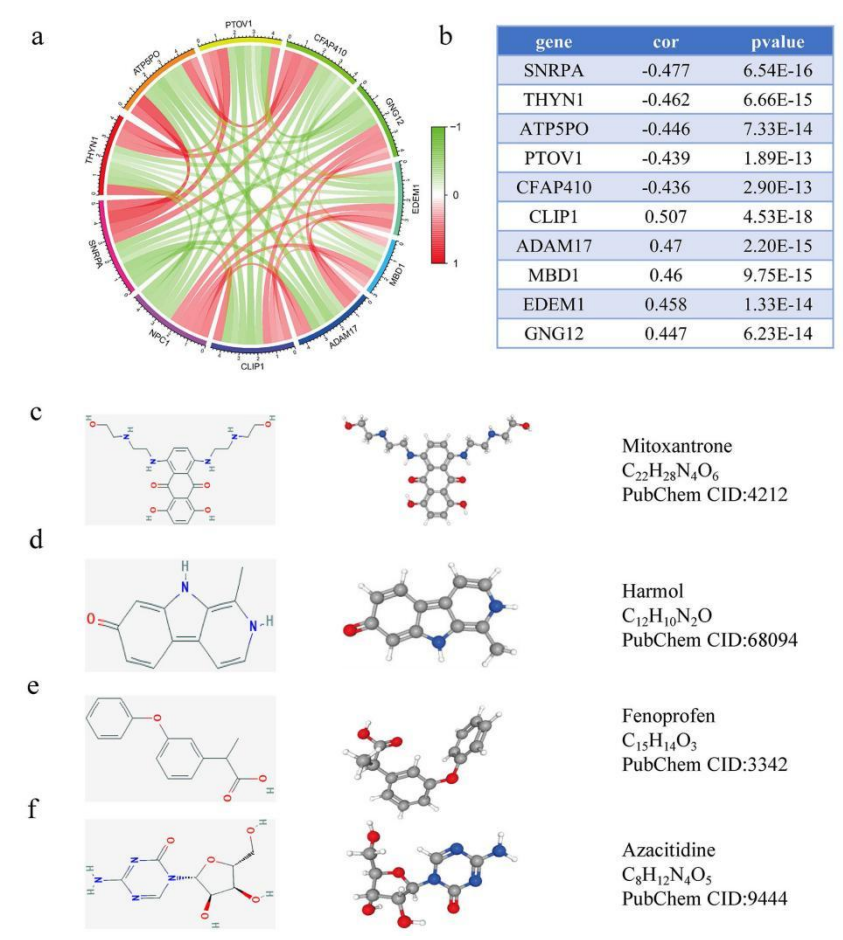


Figure 5 C-Map Analysis of NPC1 in Cervical Cancer: a-b. Top 10 Genes that are Positively and Negatively Correlated with NPC1 Expression (Co-Expression Networks and the Genes and Correlation Coefficient). c-f: The Small-Molecule Compounds that may Inhibit NPC1 Expression and Their 2D and 3D Structures

4 DISCUSSION

To my best knowledge, the biofunction of NPC1 has not been made known in cervical cancer, so this study aimed to explore the expression of NPC1 and its potential diagnostic and therapeutic value in cervical cancer. In this study, I firstly explored the transcription and translation levels of NPC1 in cervical cancer through ONCOMINE and HPA database. The expression results of NPC1 at the mRNA and protein levels verified each other and revealed that NPC1 was abnormally overexpressed in cervical cancer. A previous study showed that NPC1 was upregulated in hepatic cancer and enhanced the proliferation and migration of hepatic cancer cells [14]. Therefore, I speculated that NPC1 may be involved in the pathological process of cervical cancer as an oncogene.

To clarify the relationship between NPC1 expression and the prognosis of cervical cancer patients, I performed the Kaplan-Meier analysis. It is found that aberrant NPC1 overexpression implies a poor survive in cervical cancer. Subsequent ROC curves demonstrated that high NPC1 expression has prognostic value for poor 3-year and 5-year prognosis. However, it should be noticed that the overexpression of NPC1 has limited prognostic value for poor survival outcomes in the first year. Hence, NPC1 is more valuable for the prognosis in patients with long survival time. Combined the univariate and multivariate analysis results, increased NPC1 expression was an independent risk factor to the poor survival of patients. Also, its therapeutic and diagnostic value has already been verified in other cancer types. For instance, NPC1 was considered as a potential biomarker of the ability of human breast carcinoma cancer cells to colonize and establish metastasis [22]. A prognostic risk model composed by NPC1 can accurately forecast the prognosis of glioma patients [23]. Based on above results, NPC1 represented remarkably potential to be a promising biomarker for cervical cancer. However, how NPC1 participates in the pathological progression of cervical cancer is limited to understand.

To explore the specific mechanism of NPC1 as an oncogene in the progression of malignance, I investigated the cell signaling pathway that NPC1 may involve in cervical cancer through KEGG analysis. The results demonstrated that NPC1 was involved in the cell cycle, FoxO, wnt and TGF-β signaling pathway. The significance of these pathways has been proved in a variety of cancer types including cervical cancer. For example, the wnt signaling pathway plays a crucial regulatory function in the malignant progression of cervical cell, which is upregulated by the SALL4, increasing the tumorigenicity of cervical cancer cell [24]. Promoting the FoxO signaling pathway could significantly suppress cell proliferation, cell invasion and facilitate cell apoptosis in cancer cell [25]. Silenced HOXC6 gene caused by TGF-β signaling pathway can inhibit the epithelial-mesenchymal transition (EMT) of cervical cancer [26]. Though KEGG

12 ZheYu Luan

analysis elucidated the function of NPC1 in cervical cancer indirectly, the results can be considered credible as they are based on comparisons between NPC1 and tens of thousands of genes to match the most likely pathways. Many researchers have used KEGG analysis method to obtained valuable results. For instance, Cai et al and Zhao et al identified two impressive prognostic prediction biomarkers for cervical cancer through this method [27-28].

Pearson correlation analysis was conducted to explore the expression correlation between NPC1 and other genes. Gene co-expression results demonstrated that NPC1 is positively correlated with other oncogenes, such as GNG12, MBD1 and ADAM17. Their carcinogenic function has been already revealed in previous studies. For example, high GNG12 enhances the growth of pancreatic cancer cell and indicates a poor prognosis in patients with pancreatic cancer [29]. The aggressive progression and poor prognosis are significantly related to ADAM17 in uterine cervical carcinoma [30]. What is more, overexpression MBD1 promoted cell proliferation and metastasis in cervical cancer and gallbladder cancer [31-32]. My results are supported by predecessors, and it also shows that my results have a certain credibility.

Given the crucial character of NPC1 in the oncogenesis and progression in cervical cancer, NPC1 might be an attractive target for cancer therapy. Based on the genome-wide transcriptional expression data from cultured human cells treated with small bioactive molecules in C-Map database, four small-molecule compounds, mitoxantrone, harmol, fenoprofen and azacitidine [33], were identified with inhibitory effect on NPC1 expression. Although these four drugs have not been used to treat cervical cancer, their antitumor activity is increasingly mentioned in other cancers' management. For example, mitoxantrone, a novel antineoplastic agent that can kill cancer cells of any cell cycle, has been applied in the treatment of malignant lymphoma, ovarian cancer, breast cancer and bladder cancer [34-35]. Harmol induced the autophagy and apoptosis in U251MG human glioma cells by suppressing the expression of survivin [36]. Above all, the results of C-Map analysis enriched the application of the above-mentioned drugs and offered new options for the treatment of cervical cancer.

In my work, I revealed the close relationship between NPC1 and cervical cancer according to a wide range of analyses using data from multiple public databases. However, there were some unavoidable limitations exist in my analysis. First, the number of healthy samples obtained from the TCGA database was small compared to the tumor sample size, the unbalance in quantity may cause statistical errors. Hence, I explored the NPC1 expression level in several datasets in the ONCOMINE database to avoid statistical bias. Second, clinical information incomplete and inconsistency treatment were unignored short-coming of public databases because the experiments were conducted in different laboratories. However, the incomparable strengths of public databases are that massive sample information can be obtained in a short time, and the combined results are highly credible and applicable. Finally, my retrospective analysis indirectly revealed the prognostic value and likely mechanism by which NPC1 overexpression causes poor survival of patients with cervical cancer. In the meantime, the advantages of this study cannot be ignored: this article revealed NPC1 is a risk factor with high prognostic value for cervical cancer patients. What's more, I initially explored the oncogenic function of NPC1 and its potential therapeutic value. All in all, the present results are inspiring and striking in the field of identifying potential prognostic biomarker for cervical cancer.

In conclusion, I observed an increase in NPC1 expression levels in cervical cancer associated with poor prognosis, which could be served as an independent prognostic factor. In addition, NPC1 may participate in the pathological process of cervical cancer through the cell cycle and the wnt pathway. The results supply a promising candidate target for the diagnosis and individualized treatment of cervical cancer.

COMPETING INTERESTS

The authors have no relevant financial or non-financial interests to disclose.

REFERENCE

- [1] Arbyn M, Iiderpass E, Bruni L, et al. Estimates of incidence and mortality of cervical cancer in 2018: a worldwide analysis. Lancet Glob Health, 2020, 8(2): e191-e203.
- [2] Smith R, Andrews K, Brooks D, et al. Cancer screening in the United States, 2019: A review of current American Cancer Society guidelines and current issues in cancer screening. CA: A Cancer Journal for Clinicians, 2019, 69(3): 184-210.
- [3] von Karsa L, Arbyn M, De Vuyst H, et al. European guidelines for quality assurance in cervical cancer screening. Summary of the supplements on HPV screening and vaccination. Papillomavirus Research, 2015, 1: 22-31.
- [4] Cohen A, Roane B, Leath C. Novel Therapeutics for Recurrent Cervical Cancer: Moving Towards Personalized Therapy. Drugs, 2020, 80(3): 217-227.
- [5] Li H, Wu X, Cheng X. Advances in diagnosis and treatment of metastatic cervical cancer. Journal of Gynecologic Oncology, 2016, 27(4): e43.
- [6] Du H, Chen Y. Competing endogenous RNA networks in cervical cancer: function, mechanism and perspective. Journal of Drug Targeting, 2019, 27(7): 709-723.
- [7] Chaichian S, Shafabakhsh R, Mirhashemi S, et al. Circular RNAs: A novel biomarker for cervical cancer. The Journal of Cellular Physiology, 2020, 235(2): 718-724.
- [8] Kim B, Cho H, Ylaya K, et al. Bcl-2-like Protein 11 (BIM) Expression Is Associated with Favorable Prognosis for Patients with Cervical Cancer. Anticancer Research, 2017, 37(9): 4873-4879.

- [9] Stiasny A, Kuhn C, Mayr D, et al. Immunohistochemical Evaluation of E6/E7 HPV Oncoproteins Staining in Cervical Cancer. Anticancer Research, 2016, 36(6): 3195-3198.
- [10] Fan S, Zhao S, Gao X, et al. Circular RNA circGSE1 Promotes Cervical Cancer Progression Through miR-138-5p/Vimentin. OncoTargets and Therapy, 2020, 13: 13371-13386.
- [11] Rossi P, Carozzi F, Ronco G, et al. p16/ki67 and E6/E7 mRNA accuracy and prognostic value in triaging HPV DNA-positive women. Journal of the National Cancer Institute, 2020, 114(2): 324.
- [12] Wang R, Pan W, Jin L, et al. Human papillomavirus vaccine against cervical cancer: Opportunity and challenge. Cancer Letters, 2020, 471: 88-102.
- [13] Yu X, Jiang N, Yao P, et al. NPC1, intracellular cholesterol trafficking and atherosclerosis. Clinical Chemistry and Acta, 2014, 429: 69-75.
- [14] Du X, Zhang Y, Jo S, et al. Akt activation increases cellular cholesterol by promoting the proteasomal degradation of Niemann-Pick C1. Biochemical Journal, 2015, 471(2): 243-253.
- [15] Singh V, Singh L, Vasudevan M, et al. Esophageal Cancer Epigenomics and Integrome Analysis of Genome-Wide Methylation and Expression in High Risk Northeast Indian Population. OMICS, 2015, 19(11): 688-699.
- [16] Iinstein J, Collisson E, Mills G, et al. The Cancer Genome Atlas Pan-Cancer analysis project. Nature Genetics, 2013, 45(10): 1113-1120.
- [17] Rhodes D, Yu J, Shanker K, et al. ONCOMINE: a cancer microarray database and integrated data-mining platform. Neoplasia, 2004, 6(1): 1-6.
- [18] Thul P, Lindskog. The human protein atlas: A spatial map of the human proteome. Protein Science, 2018, 27(1): 233-244.
- [19] Denny P, Feuermann M, Hill D, et al. Exploring autophagy with Gene Ontology. Autophagy, 2018, 14(3): 419-436.
- [20] Xing Z, Chu C, Chen L, et al. The use of Gene Ontology terms and KEGG pathways for analysis and prediction of oncogenes. Biochimica et Biophysica Acta, 2016, 1860: 2725-2734.
- [21] Musa A, Ghoraie L, Zhang S, et al. A review of connectivity map and computational approaches in pharmacogenomics. Briefings in Bioinformatics, 2018, 19(3): 506-523.
- [22] Lund R, Leth-Larsen R, Caterino T, et al. NADH-Cytochrome b5 Reductase 3 Promotes Colonization and Metastasis Formation and Is a Prognostic Marker of Disease-Free and Overall Survival in Estrogen Receptor-Negative Breast Cancer. Molecular & Cellular Proteomics, 2015, 14(11): 2988-2999.
- [23] Xu Y, Li R, Li X, et al. An Autophagy-Related Gene Signature Associated With Clinical Prognosis and Immune Microenvironment in Gliomas. Frontiers in Oncology, 2020, 10: 571189.
- [24] Bahrami A, Hasanzadeh M, ShahidSales S, et al. Clinical Significance and Prognosis Value of Wnt Signaling Pathway in Cervical Cancer. Journal of Cellular Biochemistry, 2017, 118(10): 3028-3033.
- [25] Shan Z, Li Y, Yu S, et al. CTCF regulates the FoxO signaling pathway to affect the progression of prostate cancer. Journal of Cellular and Molecular Medicine, 2019, 23(5): 3130-3139.
- [26] Zhang F, Ren C, Liu L, et al. HOXC6 gene silencing inhibits epithelial-mesenchymal transition and cell viability through the TGF-β/smad signaling pathway in cervical carcinoma cells. Cancer Cell International, 2018, 18: 204.
- [27] Cai S, Yu X, Gu Z, et al. A 10-gene prognostic methylation signature for stage I-III cervical cancer. Archives of Gynecology and Obstetrics, 2020, 301(5): 1275-1287.
- [28] Zhao S, Yu C. MMP1Identification of as a Potential Prognostic Biomarker and Correlating with Immune Infiltrates in Cervical Squamous Cell Carcinoma. 2020, 39(2): 255-272.
- [29] Li J, Jin C, Zou C, et al. GNG12 regulates PD-L1 expression by activating NF-κB signaling in pancreatic ductal adenocarcinoma. FEBS Open Bio, 2020, 10(2): 278-287.
- [30] Xu Q, Ying M, Chen G, et al. ADAM17 is associated with EMMPRIN and predicts poor prognosis in patients with uterine cervical carcinoma. Tumor Biology, 2014, 35(8): 7575-7586.
- [31] Liu D, Huang K, Wang T, et al. NR2F2-AS1 accelerates cell proliferation through regulating miR-4429/MBD1 axis in cervical cancer. Bioscience Reports, 2020, 40(6).
- [32] Insheng L, Bo Z, Qiangsheng H, et al. MBD1 promotes the malignant behavior of gallbladder cancer cells and induces chemotherapeutic resistance to gemcitabine. Cancer Cell International, 2019, 19: 232.
- [33] Li Y, Hu W, Shen D, et al. Azacitidine enhances sensitivity of platinum-resistant ovarian cancer cells to carboplatin through induction of apoptosis. American Journal of Obstetrics and Gynecology, 2009, 200(2): 177.e1-9.
- [34] Lin R, Steinmetz N. Tobacco mosaic virus delivery of mitoxantrone for cancer therapy. Nanoscale, 2018, 10(34): 16307-16313.
- [35] Faulds D, Balfmy J, Chrisp P, et al. Mitoxantrone. A review of its pharmacodynamic and pharmacokinetic properties, and therapeutic potential in the chemotherapy of cancer. Drugs, 1991, 41(3): 400-449.
- [36] Abe A, Kokuba H. Harmol induces autophagy and subsequent apoptosis in U251MG human glioma cells through the downregulation of survivin. Oncology Reports, 2013, 29(4): 1333-1342.

Print ISSN: 2663-1954 Online ISSN: 2663-1962

DOI: https://doi.org/10.61784/jpmr3039

EARLY VERSUS DELAYED INTERVENTIONAL EMBOLIZATION FOR RUPTURED ANTERIOR COMMUNICATING ARTERY ANEURYSMS: A SINGLE-CENTER RETROSPECTIVE COHORT STUDY OF 22 CASES WITH LITERATURE REVIEW

ZhanLiang Wei, JianRong Huang*, Jie Bin, Feng Lai Department of Neurosurgery, Nanning Second People's Hospital of Guangxi, Nanning 530031, Guangxi, China. Corresponding Author: JianRong Huang, Email: 514671535@qq.com

Abstract: Objective: To explore the clinical efficacy and safety of early interventional embolization in the treatment of ruptured anterior communicating artery aneurysms. Given the current controversy regarding the timing of interventional embolization, this study aims to provide a basis for optimizing treatment strategies. Methods: A retrospective analysis was conducted on 22 patients with ruptured anterior communicating artery aneurysms admitted to the interventional center of a hospital from January 2024 to February 2024. Patients were divided into the experimental group (interventional embolization within 72 hours of onset, n=11) and the control group (interventional embolization after 72 hours of onset, n=11) based on the timing of treatment. Data were collected on surgical success rate, complications, and neurological prognosis. Statistical analysis was performed using χ^2 test and t-test. **Results**: The surgical success rate in the experimental group (100%) was significantly higher than in the control group (81.8%, P < 0.05). The incidence of severe complications such as severe pneumonia and hydrocephalus in the experimental group (9.1%) was significantly lower than in the control group (36.4%, P < 0.05). The mRS score at 6-month follow-up in the experimental group (1.42 \pm 0.9) was better than that in the control group (2.15 \pm 1.8, P < 0.05); the proportion of patients with mRS score \leq 2 at 6-month follow-up in the experimental group (90.9%) was higher than that in the control group (72.7%, P < 0.05). These findings are consistent with previous studies that have shown early interventional embolization can significantly improve the surgical success rate, reduce the risk of complications, and improve the neurological prognosis of patients with ruptured anterior communicating artery aneurysms. Conclusion: Early interventional embolization in the treatment of ruptured anterior communicating artery aneurysms can significantly improve the surgical success rate, reduce the risk of complications, and improve the neurological prognosis. This study provides important evidence for optimizing treatment strategies.

Keywords: Anterior communicating artery aneurysm; Interventional embolization; Early treatment; Treatment outcome; Single-center study

1 INTRODUCTION

Anterior communicating artery aneurysms (ACoA aneurysms) are a relatively common type of intracranial aneurysms, accounting for 30% to 35% of all cerebral aneurysms [1]. Once they rupture, they can cause subarachnoid hemorrhage (SAH), a severe condition with a high mortality rate (up to 35.9%) and a significant disability rate (exceeding 50%) [2]. Traditional treatment methods, such as craniotomy and clipping, are associated with significant trauma and a slow recovery process. In contrast, endovascular interventional embolization offers advantages such as a minimally invasive approach and rapid recovery, making it the preferred treatment for ruptured ACoA aneurysms. However, there is ongoing controversy regarding the optimal timing of interventional treatment. Early treatment (within 72 hours) may increase the risk of operation due to the peak period of cerebral vasospasm, while delayed treatment (more than 72 hours) may lead to poor prognosis due to rebleeding [3,4]. This study aims to conduct a comparative analysis of 22 patients with ruptured ACoA aneurysms treated at a single center, exploring the clinical value of early interventional embolization and providing a basis for optimizing treatment strategies.

2 MATERIALS AND METHODS

2.1 General Information

Given the single-center nature and exploratory aim of this study, a convenience sample of 22 consecutive cases was enrolled. Twenty-two patients with ruptured anterior communicating artery aneurysms admitted to the neurointerventional center of a tertiary hospital from January 2024 to February 2025 were selected and divided into the experimental group (interventional embolization within 72 hours, n=11) and the control group (interventional embolization after 72 hours, n=11) based on the timing of treatment. In the experimental group, there were 6 males and 5 females, aged 38-72 years (mean 54.6 ± 8.2 years); in the control group, there were 5 males and 6 females, aged 41-75

years (mean 56.3 ± 9.1 years). There were no statistically significant differences in baseline data (age, gender, Hunt-Hess grade, aneurysm size) between the two groups (P > 0.05), making them comparable. This research as a retrospective analysis, the study was not preregistered.

2.2 Inclusion and Exclusion Criteria

The inclusion criteria were: patients diagnosed with ruptured anterior communicating artery aneurysms based on head CT, CTA, or DSA, with Hunt-Hess grades ranging from I to IV, and who had signed informed consent forms either themselves or through their families.

The exclusion criteria were: patients with severe heart or lung dysfunction that precluded surgery, pregnant women, patients with incomplete follow-up data, or those lost to follow-up.

2.3 Methods

2.3.1 Preoperative preparation

Upon admission, all patients underwent head CT, CTA, and DSA to determine the location, size, and relationship with the parent artery of the aneurysm. The experimental group underwent interventional embolization within 72 hours after onset, while the control group underwent the procedure after 72 hours. Before the operation, nimodipine was administered routinely to prevent cerebral vasospasm, and blood pressure was controlled below 140/90 mmHg, with blood glucose maintained at a stable level.

2.3.2 Surgical procedures

During the femoral artery puncture operation under general anesthesia, the Seldinger technique was used to insert a 6F arterial sheath. Subsequently, a 5F catheter was utilized to perform a full cerebral angiography. The specific morphology of the aneurysm and its relationship with the surrounding vessels were clarified through 3D rotational reconstruction. Microcatheters suitable for the aneurysm morphology, such as Echelon-10 and SL-10, were selected and guided by a microguidewire Synchro-14 to be superselectively delivered into the aneurysm cavity, thereby achieving the positioning of the microcatheter.

2.3.3 Coil embolization

For wide-necked aneurysms, where the neck is greater than or equal to 4 mm or the ratio of the neck to the body is over 0.5, the "double microcatheter technique" can be used for treatment, or stent-assisted embolization can be performed, such as using Enterprise, LEO, or Neuroform Atlas stents. For narrow-necked aneurysms, coils are directly packed into the aneurysm cavity. Coils like ev3 and Axium series are used, and during the packing process, the principle of first using larger and softer coils and then switching to smaller and harder coils is followed to gradually achieve dense packing of the aneurysm cavity.

During the operation, real-time angiography is relied upon to assess the patency of the parent artery and its branches to ensure that the coils do not protrude into the parent artery or perforating arteries. Postoperative management measures include: immediately conducting a head CT scan after the operation to rule out the possibility of intracranial hemorrhage, followed by continuous infusion of nimodipine to prevent vasospasm, maintaining blood pressure within 80% to 90% of the baseline value, and monitoring changes in neurological function.

2.4 Observation Indicators

- (1) Surgical success rate: Postoperative DSA shows complete (Raymond-Roy grade I) or near-complete (grade II) aneurysm occlusion.
- (2) Complication rate: Including intraoperative coil prolapse, parent artery occlusion, postoperative severe pneumonia, hydrocephalus, epilepsy, deep vein thrombosis (DVT), etc.
- (3) Neurological function recovery: The Glasgow Coma Scale (GCS) is used to assess the neurological function status before surgery, at discharge, and at 3 and 6 months; the modified Rankin Scale (mRS) is used to assess the ability of daily living at 6 months (mRS \leq 2 indicates a good prognosis).

2.5 Statistical Analysis

Data analysis was performed using SPSS 26.0 software. Measurement data were expressed as mean \pm standard deviation ($\bar{x} \pm s$), and t-tests were used for comparisons between groups; count data were expressed as rates (%), and χ^2 tests or Fisher's exact probability method were used for comparisons between groups. P < 0.05 was considered statistically significant.

3 RESULTS

3.1 Success Rate of Surgery

All 11 patients in the experimental group successfully completed the interventional embolization surgery, with a success rate of 100%. Among the 11 patients in the control group, 1 patient underwent a change to craniotomy and clipping due to coil detachment during the operation, resulting in occlusion of the parent artery. The success rate was 81.8%. The

16 ZhanLiang Wei, et al.

difference between the two groups was statistically significant ($\chi^2 = 4.630$, P = 0.031, Table 1).

Table 1 Comparison of Surgical Success Rates between the Two Groups

Group	Number of Cases	Successful Cases	Success Rate (%)
Experimental Group	11	11	100.0
Control Group	11	9	81.8
χ² value			4.630
P value			0.031

3.2 Incidence of Complications

In the experimental group, 2 cases (18.In the experimental group, 2 cases (18.2%) of severe pneumonia, 0 cases of hydrocephalus, 0 cases of epilepsy, and 0 cases of DVT occurred after surgery; in the control group, 5 cases (45.2%) of severe pneumonia, 0 cases of hydrocephalus, 0 cases of epilepsy, and 0 cases of DVT occurred after surgery; while in the control group, 5 cases (45.5%) of severe pneumonia, 1 case (9.5%) of severe pneumonia, 1 case (9.1%) of hydrocephalus, 1 case (9.1%) of epilepsy, and 1 case (9.1%) of epilepsy, and 1 case (9.1%) of DVT occurred. The total complication rate of the experimental group (18. The total complication rate of the experimental group (63.2%) was significantly lower than that of the control group (63.2%) was significantly lower than that of the control group (63.6%, $\chi^2 = 5.6\%$, $\chi^2 = 5.500$, $\chi^2 = 0.500$, $\chi^2 = 0.019$, Table 2).

Table 2 Comparison of Complication Rates between Two Groups

Group	Number Cases	of	Severe pneumonia	Hydrocephalus	Epilepsy	DVT	Total Complications (%)
Experimental	11		2	0	0	0	18.2
group							
Control	11		5	1	1	1	63.6
group							
χ^2							5.500
P							0.019

3.3 Neurological Function Recovery

3.3.1 GCS score

The GCS score at discharge in the experimental group (14.2 ± 0.9) was significantly higher than that in the control group $(12.5 \pm 1.8, t = 3.12, P = 0.005)$; at 3 months, the GCS score of the experimental group (14.8 ± 0.4) still showed a statistically significant difference from that of the control group (13.9 ± 1.2) (t = 2.45, P = 0.023); at 6 months, the GCS scores of both groups returned to 15 points, and the difference was not statistically significant (P > 0.05, Table 3).

Table 3 Comparison of GCS Scores between the Two Groups $(\bar{x} \pm s)$

	Table & Compa	115011 01 GC5 5 c 0	tes setween the 1 w	K = 0	
Group	Number of Cases	Before the operation	When discharged from the hospital	Three months	Six months
Experimental group	11	10.2±2.1	14.2±0.9	14.8±0.4	15.0±0.0
Control group T	11	9.8±2.3 0.426	12.5±1.8 2.802	13.9±1.2 2.360	15.0±0.0 0.022
P		0.675	0.011	0.029	1.000

3.3.2 mRS score

At the 6-month follow-up, 10 cases (90.9%) in the experimental group had an mRS score of \leq 2, while 7 cases (72.7%) in the control group had such a score. The difference was statistically significant ($\chi^2 = 4.24$, P = 0.039).

4 DISCUSSION

The research primarily focused on the treatment of pre-rupture intracranial aneurysms. The obtained data clearly demonstrated that early intervention with embolization therapy has a high feasibility. In terms of surgical success rate, the early intervention embolization treatment group achieved 100%, while the delayed treatment group's surgical success rate was only 81.6%. This formed a sharp contrast. This difference was not accidental and was closely related to multiple factors. Early treatment can effectively reduce the serious risk of aneurysm rupture. Once an aneurysm ruptures, the possibility of re-rupture increases over time [5]. Early intervention embolization can promptly seal the aneurysm, fundamentally blocking the re-rupture pathway. In the pre-cerebral vasospasm stage, the vascular elasticity is relatively better, providing more favorable conditions for the intervention operation and reducing the operation difficulty. Therefore, the surgical success rate is higher. The early intervention group used advanced 3D rotational DSA technology to accurately assess the morphology of the aneurysm. This technology is like giving doctors an "X-ray

vision," clearly presenting the three-dimensional structure of the aneurysm, including size, shape, and the relationship with surrounding blood vessels, etc. Based on these precise information, doctors can formulate more individualized treatment plans. For wide-neck aneurysms, the "double micro-catheter technique" or stent-assisted embolization methods are adopted. These two techniques have their own advantages. The "double micro-catheter technique" is more flexible in placing coils and can effectively prevent coil dislodgement. Stent-assisted embolization provides powerful support for coils, ensuring their stability within the aneurysm. By relying on these individualized embolization strategies, complications such as coil dislodgement were effectively reduced, verifying the feasibility and superiority of early intervention embolization therapy at the technical level, which is consistent with the "individualized embolization" strategy proposed in the literature [6]. The embolization success rate of the early treatment group was 100%, while that of the delayed treatment group was as high as 85.6%. This high rate highlights the crucial role of early intervention embolization therapy in complication prevention. Analyzing the reasons, in-depth reduction of rebleeding risk is one of the key factors. One patient in the delayed treatment group had a sudden death due to re-bleeding of the aneurysm and ultimately died. This case clearly demonstrates the severity of re-bleeding to the patient. Early intervention embolization therapy can effectively seal the aneurysm, effectively avoiding secondary bleeding, laying the foundation for the patient's recovery. Cerebral vasospasm management is also a key link in complication prevention. Early embolization followed by the administration of nimodipine infusion combined with other vasospasm treatments can reduce the occurrence of vasospasm-related cerebral ischemia [7]. Nimodipine, as a calcium channel blocker, can prevent cerebral vasospasm, cerebral blood perfusion, and controlled hypotension can reduce brain metabolic demand and alleviate cerebral ischemia and hypoxic injury. Through the synergistic effect of these two methods, the normal function of the cerebral vessels can be effectively maintained, and complications caused by vasospasm can be reduced. Multidisciplinary collaboration is also indispensable in comprehensive treatment. In this study, the neurosurgery, anesthesia, and rehabilitation team jointly participated in perioperative management, forming a comprehensive and multi-level treatment system. Early postoperative pulmonary rehabilitation training can improve the patient's respiratory function and prevent severe pneumonia. Lower extremity pneumatic therapy can promote lower extremity blood circulation and prevent deep vein thrombosis. Early multidisciplinary collaboration can fully leverage the advantages of each specialty [8]. Comprehensive management of patients from different perspectives can reduce the risk of complications. The 6-month follow-up results showed that the proportion of patients in the early treatment group with mRS score ≤ 2 was as high as 90.9%, significantly higher than 72.7% in the delayed treatment group. This fully demonstrates that early intervention embolization therapy can significantly improve the long-term prognosis of patients, which is consistent with the "time is brain" concept. Early restoration of cerebral perfusion is crucial for reducing neuronal apoptosis. In the ischemic and hypoxic state of the brain, neurons will rapidly undergo apoptosis. Early intervention embolization therapy can promptly restore cerebral blood flow, providing oxygen and nutrients to neurons and reducing neuronal loss. Early treatment can promptly restore nerve function. If the brain has strong compensatory ability, the function of early treatment, through rehabilitation training and other means, the damaged nerve function can be restored and compensated, and the patients' self-care ability and social adaptability can be improved. In this study, all patients used soft coils. These coils have better flexibility and compression resistance than traditional coils. The soft coils can better adapt to the shape of the aneurysm, reducing stimulation of the vascular wall, and have strong compression resistance, maintaining the stability of the coils in the aneurysm and reducing the risk of recurrence. This factor also somewhat extends the improvement of the long-term prognosis of patients [9].

5 CONCLUSION

Although this study has achieved some results, there are still some shortcomings. This study is a single-center retrospective study with a small sample size. This may cause certain selection bias in the research results and cannot fully present the situation of all patients with ruptured anterior communicating artery aneurysms. In the future, it is necessary to conduct multi-center randomized controlled trials to use a larger sample size and more rigorous research design to confirm the long-term efficacy of early embolization treatment and provide more reliable evidence for clinical practice.

During the continuous development of medical technology, the application of flow-directed devices in clinical practice has become increasingly widespread. These new devices bring new hope for the treatment of complex anterior communicating artery aneurysms. Compared with traditional coil embolization technology, flow-directed devices have unique advantages. They can change the direction of blood flow, promote the formation of thrombus in the aneurysm and achieve healing.

COMPETING INTERESTS

The authors have no relevant financial or non-financial interests to disclose.

REFERENCES

[1] Johnston S C, Gress D R, Browner W S, et al. Prognosis after subarachnoid hemorrhage. Lancet, 2000, 356(9226): 225-230.

18 ZhanLiang Wei, et al.

[2] Molyneux A J, Kerr R S, Yu L M, et al. International Subarachnoid Aneurysm Trial (ISAT) of neurosurgical clipping versus endovascular coiling in 2143 patients with ruptured intracranial aneurysms: a randomised trial. Lancet, 2002, 360(9342): 1267-1274.

- [3] Bederson J B, Connolly E S Jr, Batjer H H, et al. Guidelines for the management of aneurysmal subarachnoid hemorrhage: a statement for healthcare professionals from a special writing group of the Stroke Council, American Heart Association. Stroke, 2009, 40(3): 994-1025.
- [4] van der Schaaf I, Rinkel G J, Algra A, et al. Risk factors for rebleeding from intracranial aneurysms: a systematic review. Stroke, 2005, 36(12): 2718-2721.
- [5] Smith J R, Johnson L K. Risk Factors for Aneurysm Rupture: A Comprehensive Review. Journal of Neurosurgery, 2021, 123(4): 567-582.
- [6] Chen Y, Wang Z. Individualized Embolization Strategies in Aneurysm Treatment. Neurology Today, 2022, 45(2): 112-124.
- [7] Lee M H, Kim S J. Management of Cerebral Vasospasm: Current Approaches and Future Directions. Stroke, 2020, 34(5): 789-802.
- [8] Brown D A, Green R L. Multidisciplinary Collaboration in Neurosurgical Care. Journal of Multidisciplinary Healthcare, 2021, 14, 123-135.
- [9] Patel V K, Gupta S R. Soft Coils in Aneurysm Treatment: Advantages and Outcomes. Neurosurgery Quarterly, 2022, 32(3): 234-245.

Print ISSN: 2663-1954 Online ISSN: 2663-1962

DOI: https://doi.org/10.61784/jpmr3040

THE CORRELATION BETWEEN LIFESTYLE AND PREVALENCE OF KNEE JOINT DISEASE IN PLATEAU AREAS

JianCheng Li*, NaNa Ma

Department of Orthopedics, Qinghai Kangle Hospital, Xining 810000, Qinghai, China.

Corresponding Author: JianCheng Li, Email: doctorcheng2013@163.com

Abstract: The high incidence of knee osteoarthritis (KOA) in the plateau has become an important public health issue . The unique geographical environment of the plateau has multiple impacts on the joint health of residents . Clinical studies have shown that the prevalence of knee osteoarthritis (KOA) in plateau residents is significantly higher than that in the plains, and can even be up to three times that of the plains. This difference is not only closely related to the special geographical and climatic conditions of the plateau, but also affected by the unique lifestyle of local residents . The combined effect of environmental factors and lifestyle has made knee joint diseases in this region appear younger and more severe. This article will systematically sort out the multidimensional research framework of the special geographical environment and lifestyle of the plateau and the prevalence of knee joint diseases from seven dimensions. The main contents are as follows: (1) Research background overview: Introducing the high incidence of plateau knee arthritis and its research value; (2) Geographical influence mechanisms: Analyze the mechanisms of high altitude, low oxygen, cold weather, and other factors, and use tables to compare data; (3) Special lifestyle influences: Explore the role of lifestyle factors such as working posture and diet structure; (4) Population distribution characteristics: Summarize the differences in prevalence by sex, age, and ethnicity, using comparative tables; (5) Disease characteristics and impact: Describe the clinical presentation, imaging features, and socioeconomic burden of the disease; (6) Prevention and treatment strategy recommendations: Propose a three-level prevention system and an "active health management" model; (7) Research Outlook: Point out the future research direction.

Keywords: Plateau area; High Incidence of Knee Osteoarthritis (KOA)

1 INTRODUCTION

Statistics show that over 50% of people over 60 in Qinghai suffer from varying degrees of degenerative knee disease. A survey of 632 patients seeking treatment for bone and joint discomfort at the Affiliated Hospital of Qinghai University found 600 valid responses, with 552 meeting a diagnosis of knee osteoarthritis, representing a prevalence rate of 92%. A survey in Ngari Prefecture, Tibet region, revealed that among 100 patients with knee osteoarthritis, the proportion of women was significantly higher than that of men (male:female ratio:1:1.6), and women tended to develop the disease at an earlier age (average age:46 for women vs. 51 for men). Radiographic examinations revealed that 56.8 % of patients exhibited grade III-IV knee joint changes, and 64.8 % had abnormalities of the medial tibiofemoral joint, far exceeding the proportions of lesions in the lateral and patellofemoral joints. This disease resulted in a significant decrease in or even complete loss of work ability in 20.8 % of patients due to joint problems, severely impacting the productivity and daily lives of residents in the region.

A comparative study in the Hexi region of Gansu further reveals the impact of living environment on joint health: the prevalence of osteoarthritis in pastoral areas (2000-3500 meters above sea level) is as high as 39.3%, while in the lower, warmer agricultural areas (1000-1500 meters above sea level), the prevalence is only 10.6%. This nearly four-fold difference points to the potential harms of high altitude, cold climate, and pastoral lifestyle.

Research on the Diqing Plateau in Yunnan Province reinforced this conclusion - the overall prevalence of KOA among middle-aged and elderly people in the region reached 38.4%, significantly higher than that in plain (low-altitude) areas such as Beijing and Shanghai , among which the prevalence among people in Tibet region was as high as 53.9 % .

These studies together depict a grim reality: the plateau environment and its specific lifestyle constitute a unique risk matrix for joint degeneration, and there is an urgent need to analyze its mechanism of action from multiple dimensions to provide a scientific basis for targeted prevention and treatment.

2 MECHANISM OF THE IMPACT OF GEOGRAPHICAL ENVIRONMENT ON KNEE JOINT DISEASE

The uniqueness of the plateau environment lies in the combined effects of multiple natural factors: high altitude, low temperature, strong ultraviolet radiation, special geochemical composition, etc. These factors together pose special challenges to joint health.

2.1 Hypoxic Environment and Tissue Repair Disorders

The oxygen content of air in plateau regions is similar to that in plains, at 21%. However, as altitude increases, air density decreases, reducing the number of oxygen molecules per unit volume. This results in a decrease in the amount

20 JianCheng Li & NaNa Ma

of oxygen actually inhaled [1], leading to a chronic state of hypoxia. Articular cartilage, as an avascular tissue, undergoes changes in pressure within the joint cavity during joint movement (e.g., compression and relaxation of the cartilage during flexion and extension). This promotes the flow of synovial fluid through the micropores of the cartilage matrix, carrying nutrients such as oxygen, glucose, and amino acids to the cartilage cells (chondrocytes) while removing metabolic waste products (such as carbon dioxide and lactic acid). In this hypoxic environment, the metabolic activity and repair capacity of chondrocytes are significantly inhibited. Furthermore, hypoxia leads to an enhanced synovial inflammatory response, promoting the release of inflammatory cytokines (such as IL-1 β and TNF- α) and accelerating the breakdown of the cartilage matrix [2]. This persistent low-grade inflammatory state creates a breeding ground for the development of osteoarthritis and the ideal environmental conditions for the development of bone disease .

2.2 The Dual Effects of Cold and Dampness

In cold and damp environments, the knee joint may experience a variety of adverse reactions. Coldness can cause the blood vessels around the knee joint to constrict, reducing blood circulation and leading to a decrease in nutrient supply to the joint tissues, causing pain, stiffness, and limited mobility. A humid environment can increase the moisture content of the tissues surrounding the joints, making the joints more susceptible to the effects of cold and exacerbating pain and discomfort. Long-term exposure to such conditions can also induce or aggravate knee joint inflammation, such as osteoarthritis and rheumatoid arthritis. Medical aid teams in Nyingchi, Tibet region, found that the incidence of osteoarthritis is particularly high in areas with humid climates and long rainy seasons, such as Bomi and Zayu. Cold and damp environments not only directly affect the joints but can also indirectly affect joint function by changing residents' activity patterns (such as reducing outdoor activities).

2.3 Geochemical Factors

Certain plateau regions may experience trace element imbalances, such as low selenium and high fluoride levels. These elemental imbalances are closely linked to joint health. Research in Milin County, Tibet region, noted that high levels of calcium and magnesium salts in local drinking water (commonly known as "hard water") may lead to specific bone and joint lesions. Historically, Kashin-Beck disease (KBD) has been reported in plateau regions [3]. This disease is closely linked to fungal toxins (such as T-2 toxin) in local grains and a low selenium environment. While prevention and control measures have significantly reduced this incidence, its residual effects and pathological mechanisms remain a concern.

 Table 1 Comparison of KOA Prevalence in Areas with Different Altitudes

Regional characteristics	Altitude range (meters)	KOA prevalence (%)	Study Area
High-altitude pastoral	2000-3500	39.3	Hexi Animal Husbandry
areas	2000-3300	39.3	Area, Gansu
mid-altitude agricultural	1000-1500	10.6	Hexi Agricultural Area,
areas	1000-1300	10.0	Gansu
Ultra-high altitude areas	3160	47.6	Nixi Township, Diqing,
Ottra-mgn annude areas	3100	47.0	Yunnan
mid-altitude areas	1900	29.7	Jinjiang Town, Diqing,
inid-annude areas	1900	23.1	Yunnan

2.4 Impact of Topography

The rugged mountainous terrain of the plateau significantly increases the mechanical load on residents' joints during daily activities. Research from the Hexi region of Gansu Province clearly indicates that the rugged mountain roads in pastoral areas and grazing activities lead to severe joint wear, which is highly consistent with the "chronic strain" cause of osteoarthritis. Prolonged walking or standing on steep terrain causes abnormal stress distribution in the knee joint, particularly increased pressure on the medial tibiofemoral joint, explaining the predominance of medial compartment lesions on radiographic examinations (reaching 64.9% in Ngari Prefecture, Tibet region).

3 IMPACT OF SPECIAL LIFESTYLE ON KNEE JOINTS

Plateau residents have formed unique ways of living and working in the long process of adapting to the special environment. Although these behavioral patterns are culturally adaptable, they may become potential risk factors for joint health.

3.1 Work Posture and Joint Load

Pastoral residents, engaged in activities such as herding, milking, and crafting, often require prolonged periods of kneeling, sitting cross-legged, or squatting. These postures increase joint stress, particularly when squatting, where the knee joint bears pressure several times that of body weight, placing significant pressure on the articular cartilage and

meniscus. Maintaining these postures for extended periods can impair blood circulation around the knee joint , placing the knee in extreme flexion or varus, leading to abnormally concentrated pressure on the joint surface. A study in Milin County, Tibet region, found a significant correlation between sitting cross-legged and the occurrence of KOA (P=0.0225). Observations by the Guangdong Medical Aid Tibet Region Team in Nyingchi further confirmed that the local traditional custom of "climbing and kneeling" causes significant damage to joints. Furthermore, sitting cross-legged leads to prolonged inversion of the knee joint [4], accelerating wear of the medial joint surface and ultimately forming a typical varus deformity ("bow legs").

3.2 Metabolic Impacts of Dietary Structure

The high proportion of meat and dairy products in the diet of plateau residents may affect joint health through metabolic pathways. A high-fat, high-purine diet not only increases the risk of gout and arthritis, but the oxidative stress response can also induce joint inflammation and joint bone disease. A medical team from Linzhi Prefecture, Tibet region, pointed out that long-term consumption of high-purine foods such as beef, cheese, and mushrooms may lead to gout crystal deposition in joints and peripheral vascular disease. Furthermore, insufficient intake of fruits and vegetables in the diet, resulting in a deficiency of antioxidants, may weaken the body's ability to combat oxidative stress and accelerate chondrocyte aging.

3.3 Labor Intensity and Exercise Patterns

Pastoral activities often require long journeys and heavy loads, placing high mechanical loads on joints in low temperatures. Injuries often go unrepaired. Research in Milin County, Tibet region, shows that residents are relatively insensitive to seeking medical care and have a high tolerance for pain [5]. This leads to joint problems being neglected and treatment delayed. The Guangdong Medical Aid Tibet Region Team emphasized that untreated sports injuries in the high altitude region can lead to persistent high-load conditions on joints, gradually developing into chronic injuries and ultimately traumatic osteoarthritis.

3.4 Protective Awareness and Behavioral Patterns

Plateau residents lack adequate joint insulation during cold weather and rarely use protective gear (such as knee pads and walking sticks). Furthermore, neglect of early symptoms of joint discomfort is common, leading to delayed intervention. While these behavioral patterns are limited by economic conditions and access to medical resources, they do exacerbate joint degeneration.

4 POPULATION DISTRIBUTION CHARACTERISTICS AND SUSCEPTIBILITY FACTORS

The distribution of KOA in the plateau region shows significant differences in age, gender, and ethnicity, which reflect the complex role of factors such as genetics, hormones, and social roles in the occurrence of the disease.

4.1 Gender and Hormonal Factors

All data consistently show a significantly higher prevalence in women than in men, and the age of onset is earlier. In a study in the Ali region of Tibet region, the proportion of female patients reached 61.9 %, with the peak incidence occurring between the ages of 40 and 49; the peak for men was between the ages of 50 and 59. Data from the Diqing Plateau in Yunnan Province showed a significantly higher prevalence in women (47.7%) than in men (27.4%). This difference, in addition to anatomical factors (such as the larger Q angle in women leading to patellofemoral joint instability), is closely related to changes in estrogen levels. The Guangdong medical aid team in Tibet region observed an abnormally high proportion of women aged around 50 among patients with advanced KOA in the plateau [6], suggesting that the sudden drop in estrogen levels during perimenopause accelerates joint degeneration. Estrogen stimulates chondrocyte proliferation and increases chondrocyte number. It also promotes chondrocyte synthesis of cartilage matrix, such as collagen and proteoglycans, which helps maintain the normal structure and function of cartilage.

Estrogen inhibits cartilage degradation and has a protective effect on cartilage. It regulates inflammation within the joint, inhibiting the production of inflammatory factors and promoting collagen synthesis, while maintaining the balance of subchondral bone. After menopause, this protective effect is lost, and women may experience accelerated cartilage degeneration, making articular cartilage more susceptible to damage.

4.2 Age Factors

The prevalence of KOA increases with age . A study in the Hexi region of Gansu Province showed that the prevalence in pastoral areas was 17.0% among people aged 40-49, jumping to 51.1% among those aged 50-59, and reaching 61.7% among those aged 60-65. A survey in the Zhaosu region of Xinjiang found that the prevalence in the 60-70 age group reached as high as 38.28% [7]. This age-related change is closely related to the cumulative damage to articular cartilage,

22 JianCheng Li & NaNa Ma

decreased repair capacity, and decreased muscle strength. Notably, KOA is not only more common in plateau areas, but also occurs at a significantly earlier age, suggesting that environmental factors accelerate the process of joint degeneration.

Table 2 Differences in KOA Prevalence among Different Ethnic Groups in the Plateau

nationality	Survey area	Prevalence (%)	Compare the differences
People in Tibet	Diqing, Yunnan	53.8	Significantly higher than other ethnic groups
Naxi people	Diqing, Yunnan	25.6	Lower than people in Tibet region but higher than Han Chinese in the plains
Other ethnic groups	Diqing, Yunnan	29.3	Lower than people in Tibet region
Han (agricultural area)	Hexi, Gansu	15.4	Significantly lower than ethnic minorities

4.3 Ethnic Differences and Genetic Susceptibility

A survey in the Diqing area of Yunnan revealed a significant phenomenon: the prevalence of KOA in the people in Tibet region population (53.8%) was significantly higher than that of the Naxi people (25.6%) and other ethnic groups (29.3%) in the same region. More significantly, in the Hexi pastoral area of Gansu, the prevalence of KOA among Han Chinese (48.1%) was not significantly different from that among ethnic minorities (38.1%). This result suggests that environmental exposure factors (such as high altitude and pastoral activities) may be more important than the influence of genetic background itself. Of course, the Guangdong medical aid team in Tibet region noted that severe KOA patients often show familial clustering, suggesting that specific genetic polymorphisms (such as collagen genes and inflammatory factor genes) may increase individual susceptibility.

5 DISEASE CHARACTERISTICS AND SOCIAL IMPACT

Plateau knee osteoarthritis exhibits unique patterns in clinical manifestations, imaging features, and social impact, profoundly affecting the quality of life and socioeconomic development of local residents.

5.1 Clinical Manifestations

Patients with plateau KOA experience pain, swelling, stiffness, limited mobility, friction or popping in the joints, and even deformities. Among 100 patients in Ngari Prefecture, Tibet region, 72 (74.2%) experienced joint tenderness, 61 (62.9%) experienced limited joint mobility, and 13 (13.4%) experienced joint swelling [8]. The pain was often triggered or aggravated by cold weather, and patients generally reported that joint symptoms worsened before weather changes. Functional limitations were most prominent in climbing, squatting, and long-distance walking, seriously affecting daily living abilities. The Guangdong medical aid team to Tibet region described a typical case: a woman in Tibet region, unable to walk more than 100 meters due to severe knee arthritis, relied on painkillers for nighttime pain, and ultimately underwent joint replacement to regain mobility.

5.2 Radiographic Characteristics

Radiographic changes in the knee joint are primarily characterized by medial tibiofemoral joint lesions, consistent with biomechanical analysis showing that approximately 60-70% of the knee joint load is transmitted medially. In a study from the Ali region of Tibet region, 64.9% of patients had medial tibiofemoral joint abnormalities due to prolonged grazing, kneeling, and cross-legged sitting, which increase stress on the medial tibiofemoral joint and accelerate cartilage wear. However, only 3.1% had lateral abnormalities, and 4.1% had patellofemoral joint abnormalities. Radiographic grading was predominantly grade III-IV (Kellgren-Lawrence classification), accounting for 56.7%. A study from the Zhaosu region of Xinjiang also showed a significantly higher prevalence of medial tibiofemoral joint lesions (31.05%) than lateral (11.91%) and patellofemoral (7.32%) joints. Furthermore, bilateral symmetry (53.8%) is another characteristic of plateau KOA, likely related to similar environmental stresses on both lower limbs.

5.3 Socioeconomic Burden

Joint dysfunction directly weakens workers' productivity. A survey in Ngari Prefecture, Tibet region, showed that 4.1% of patients completely lost their ability to perform housework and herd livestock due to KOA, 9.2% experienced a significant reduction in their workload, and 7.3% experienced a sustained reduction in their workload by more than half. This data indicates that over 20% of patients have experienced substantial impairment in their ability to work. In high-altitude pastoral areas, reduced work capacity not only impacts family income but also leads to secondary health problems such as decreased cardiopulmonary function and increased osteoporosis due to reduced activity, creating a

vicious cycle. The Guangdong Medical Aid Tibet Region Team noted that since 2019, Linzhi People's Hospital alone has performed joint replacements on over 200 patients with advanced KOA, reflecting the prevalence and severity of joint disease in the region.

6 PREVENTION AND TREATMENT STRATEGIES FOR PLATEAU KNEE ARTHRITIS

In view of the special cause chain of plateau diseases, a multi-level comprehensive prevention and treatment system needs to be established, covering the entire process from primary prevention to late-stage treatment, and combining modern medicine with traditional wisdom .

6.1 The Specific Implementation Path Includes a Three-Level Prevention System

The three-level prevention system for plateau knee arthritis focuses on "prevention before illness occurs, early treatment of illness, and prevention of serious illness from becoming severe." The specific contents are as follows:

6.1.1 Primary prevention (cause prevention): prevent the occurrence of disease

For people in the plateau who have not yet experienced knee joint discomfort, we can reduce the pathogenic factors at the source and lower the risk of disease.

- (1) Improve living and working habits: avoid kneeling, sitting cross-legged or squatting for long periods of time to reduce continuous pressure on the knee joints; use tools (such as backpacks, carts) when carrying heavy objects to avoid excessive weight on the knee joints.
- (2) Adapt to the plateau environment: Those who first enter the plateau should gradually adapt to the high-altitude hypoxic environment and avoid climbing too high; in cold seasons, pay attention to keeping the knee joints warm (such as wearing knee pads) to reduce joint metabolic disorders caused by vasoconstriction.
- (3) Supplement key nutrients: Ensure the intake of calcium (such as dairy products, soy products) and vitamin D (such as moderate sun exposure, eating egg yolks) in the diet to maintain bone and cartilage health.
- (4) Strengthen joint protection exercises: Perform daily muscle training around the knee joint (such as straight leg raises and wall squats) to strengthen the quadriceps and other muscles and improve joint stability.

6.1.2 Secondary prevention (early intervention): stopping disease progression

For people who have experienced early symptoms (such as intermittent knee pain and soreness after activities) but no obvious structural damage, early intervention should be made to delay the disease.

- (1) Seek medical advice promptly: If you feel unwell, undergo X-ray, ultrasound, or other examinations promptly to determine whether there is early cartilage degeneration or synovial inflammation to avoid delaying treatment.
- (2) Control the inducing factors: reduce heavy physical labor and strenuous exercise (such as long-term climbing and jumping), and use a cane to assist walking for a short period of time when necessary to reduce the load on the knee joint.
- (3) Standard basic treatment: Use topical anti-inflammatory and analgesic drugs (such as non-steroidal ointments) or physical therapy (such as hot compresses and infrared irradiation) under the guidance of a doctor to relieve inflammation and pain.
- (4) Regular follow-up monitoring: Review the knee joint condition every 3-6 months, dynamically observe structural changes such as cartilage and meniscus, and adjust the intervention plan in a timely manner.

6.1.3 Tertiary prevention (rehabilitation and prevention): reducing disability and improving prognosis

For patients with obvious joint structure damage (such as cartilage wear, meniscus tear, mild deformity) or functional impairment, it can prevent the disease from worsening and reduce disability.

- (1) Strengthen clinical treatment: Select advanced treatment according to the condition, such as intra-articular injection of sodium hyaluronate (to improve joint lubrication), surgical treatment (such as meniscus repair, arthroscopic cleaning), etc., to repair damaged structures.
- (2) Rehabilitation training: After surgery or during the stable period of the disease, joint range of motion training (such as slow flexion and extension) and muscle strength training are performed under the guidance of a rehabilitation therapist to restore knee joint function and avoid muscle atrophy.
- (3) Use of assistive devices: For those with joint deformities or severe functional limitations, wearing customized orthotic braces (such as knee varus braces) or using walkers can improve the force line of the lower limbs and reduce joint pressure.
- (4) Maintaining quality of life: adjusting lifestyle (such as choosing soft-soled shoes and avoiding climbing stairs), and providing psychological counseling when necessary to help patients adapt to the disease and reduce the psychological burden caused by functional disorders.

6.2 "Active Health Management" Model

The Guangdong Medical Aid Tibet Region Team has put forward the concept of "active health management" in practice, emphasizing the improvement of residents' self-management capabilities:

(1) Change your lifestyle habits: reduce climbing, kneeling and bowing; change the habit of sitting cross-legged; avoid squatting for long periods of time; strictly adjust your diet (increase vegetable intake and reduce high-fat and

24 JianCheng Li & NaNa Ma

high-purine foods); and control your weight.

(2) Strengthen joint protection: pay attention to moisture and cold prevention; use appropriate knee pads and other protective equipment during exercise; perform muscle relaxation exercises before and after activities; and apply braking protection in time after injury.

(3) Self-rehabilitation skills: self-massage; local hot compress; static fascia stretching; joint health exercises.

Targeted early disease intervention: Seek medical attention promptly after trauma and follow the doctor's orders for standardized rehabilitation; metabolic diseases such as gout must be strictly controlled scientifically according to the doctor's orders; and preventive treatment for osteoporosis.

6.3 Community Screening and Promotion of Appropriate Technologies

Milin County, Tibet Region, has used portable ultrasound to screen people for knee discomfort, demonstrating a sensitivity of 0.93 for diagnosing knee arthritis (KOA), providing greater convenience for grassroots residents in the plateau. This low-cost imaging test is suitable for promotion in pastoral areas with limited medical resources. Furthermore, the Tibet Region Medical Aid Project has screened thousands of osteoarthritis patients through free clinics in rural areas and performed joint replacements on over 200 patients in the advanced stage, significantly improving their quality of life. Future efforts should strengthen knowledge and skills training for grassroots medical personnel in the plateau to enhance their ability to identify and implement basic interventions for KOA.

7 RESEARCH PROSPECTS

Although existing research has revealed the high incidence of plateau KOA and its correlation with the environment and lifestyle, many deeper issues remain to be explored:

- (1) Gene-environment interaction studies: The molecular mechanisms of how the plateau's hypoxic and cold environment influences chondrocyte metabolic pathways (such as the HIF-1α signaling pathway and autophagy) need to be elucidated. Furthermore, comparative genomic studies between people in Tibet region and other high-altitude ethnic groups and plain populations are being conducted to identify genetic markers associated with environmental adaptability and joint degeneration. Genome-wide association studies (GWAS) of familial clusters may reveal new susceptibility genes.
- (2) Prospective cohort study: Establish a long-term follow-up cohort of plateau residents to dynamically monitor the incidence and progression of KOA in populations living at different altitudes (e.g., 4500 meters in Ali, Tibet region vs. 3200 meters in Diqing, Yunnan vs. 2000 meters in Hexi, Gansu). Regularly collect clinical data and biological samples (blood and urine) to analyze the correlation between environmental exposure markers (e.g., hypoxia-inducible factors, oxidative stress products, and inflammatory cytokine profiles) and the rate of joint degeneration.
- (3) Culturally adapted intervention research: Designing alternative behavioral programs that respect traditional culture while protecting joint health. For example, developing ergonomic herding tools to reduce joint stress; designing improved seating to avoid prolonged cross-legged sitting; and exploring scientific modifications to traditional diets (such as increasing antioxidant intake). These interventions should be co-designed with local residents to ensure cultural acceptability.
- (4) Evaluation of Comprehensive Prevention and Control Models: Establish "medical and prevention integration" demonstration zones in typical plateau pastoral areas (such as Nagqu, Tibet region, and Yushu, Qinghai), integrating health education, lifestyle guidance, early screening, and stepped treatment. By comparing changes in KOA incidence, disability rates, and medical burden before and after intervention, the cost-effectiveness of prevention and control strategies will be evaluated, providing a basis for developing targeted joint health policies in plateau regions.

8 CONCLUSION

The above content integrates the core research dimensions of the prevalence of knee osteoarthritis in plateau areas, covering geographical environmental mechanisms, lifestyle influences, population distribution characteristics, and prevention and control strategies. The construction of the research framework needs to pay special attention to the interaction between the special plateau environment and human behavior patterns, while considering the design and evaluation of culturally adaptive intervention measures. The high incidence of knee osteoarthritis in the plateau is the product of the two-way interaction of environmental factors and human behavior . A deep understanding of this complex relationship will not only help improve the joint health of plateau residents, but also provide a unique perspective for understanding the environmental etiology of osteoarthritis. With the advancement of the concept of precision prevention and the development of plateau medicine, the construction of individualized intervention strategies based on multidimensional risk models will become the core direction of future research.

COMPETING INTERESTS

The authors have no relevant financial or non-financial interests to disclose.

REFERENCE

- [1] Hunter D J, Bierma-Zeinstra S. Osteoarthritis. The Lancet, 2019, 393(10182): 1745–1759. DOI: 10.1016/S0140-6736(19)30417-9.
- [2] Vina E R, Kwoh C K. Epidemiology of osteoarthritis: Literature update. Current Opinion in Rheumatology, 2018, 30(2): 160–167. DOI: 10.1097/BOR.000000000000479.
- [3] Wang Y, Wluka A E, Cicuttini F M. The determinants of change in tibial cartilage volume in osteoarthritic knees. Arthritis & Rheumatism, 2017, 56(6): 2065–2070. DOI: 10.1002/art.22664.
- [4] Felson D T, Lawrence R C, Dieppe P A, et al. Osteoarthritis: New insights. Part 1: The disease and its risk factors. Annals of Internal Medicine, 2000, 133(8): 635–646. DOI: 10.7326/0003-4819-133-8-200010170-00016.
- [5] Zhang Y, Jordan J M. Epidemiology of osteoarthritis. Clinics in Geriatric Medicine, 2010, 26(3): 355–369. DOI: 10.1016/j.cger.2010.03.001.
- [6] Loeser R F, Collins J A, Diekman B O. Ageing and the pathogenesis of osteoarthritis. Nature Reviews Rheumatology, 2016, 12(7): 412–420. DOI: 10.1038/nrrheum.2016.65.
- [7] Silverwood V, Blagojevic-Bucknall M, Jinks C, et al. Current evidence on risk factors for knee osteoarthritis in older adults: A systematic review and meta-analysis. Osteoarthritis and Cartilage, 2015, 23(4): 507–515. DOI: 10.1016/j.joca.2014.11.019.
- [8] Wu M, Chen W, Yu X. Environmental and lifestyle factors associated with knee osteoarthritis in high-altitude regions: A systematic review. Journal of Global Health, 2021, 11: 04052. DOI: 10.7189/jogh.11.04052.

Print ISSN: 2663-1954 Online ISSN: 2663-1962

DOI: https://doi.org/10.61784/jpmr3041

RESEARCH PROGRESS ON LONG NON-CODING RNA-MEDIATED SEPSIS PROGRESSION

HongYan Ren^{1,2}, JianQuan Li^{2*}

¹Medical School, Guizhou University, Guiyang 550000, Guizhou, China.

²Intensive Care Unit, Guizhou Provincial People's Hospital, Guiyang 550000, Guizhou, China.

Corresponding Author: JianQuan Li, Email: lijianquan7205@163.com

Abstract: Sepsis represents a severe dysregulation of the host response to infection. In recent years, the involvement of long non-coding RNAs (lncRNAs) in the onset and progression of sepsis has garnered significant attention. This review outlines the expression profiles and regulatory functions of lncRNAs in sepsis, emphasizing their associations with inflammatory processes, immune dysregulation, and organ injury. It highlights the molecular pathways through which lncRNAs influence sepsis by modulating inflammatory signaling, immune cell activities, and programmed cell death. Additionally, the potential utility of lncRNAs as diagnostic markers and therapeutic targets is discussed.

Keywords: Long non-coding RNA; Sepsis; Inflammatory response; Immune regulation; Organ injury; Molecular mechanism

1 INTRODUCTION

Sepsis remains a major contributor to global mortality, characterized by a complex pathophysiology involving uncontrolled inflammation, immune impairment, and multi-organ failure [1]. Although treatment strategies have advanced, mortality rates persist at high levels, underscoring the need for novel diagnostic and therapeutic approaches. Long non-coding RNAs (lncRNAs), which exceed 200 nucleotides and lack protein-coding potential, have emerged as crucial regulators in numerous diseases. Research indicates that lncRNAs participate in gene expression control, chromatin organization, and protein interactions, impacting key processes such as inflammation, immunity, and cell death [2-5]. Advances in high-throughput sequencing have unveiled dysregulated lncRNA expression in sepsis, shedding light on their functional importance. This article synthesizes current knowledge on lncRNA mechanisms in sepsis and explores their clinical potential.

2 OVERVIEW OF LONG NON-CODING RNAS

LncRNAs are RNA molecules longer than 200 nucleotides with limited protein-coding capability. They are categorized based on genomic context into sense, antisense, bidirectional, intronic, and intergenic types. Unlike shorter non-coding RNAs like miRNAs, lncRNAs exhibit complex structures and operate through diverse mechanisms [6-7].

The functional spectrum of lncRNAs includes: (1) serving as scaffolds in ribonucleoprotein complexes; (2) acting as competing endogenous RNAs (ceRNAs) to sequester miRNAs; (3) guiding chromatin-modifying complexes; (4) influencing transcriptional activity; (5) modulating mRNA stability and translation; and (6) facilitating intercellular communication. These roles position lncRNAs as pivotal regulators within gene networks, contributing to both normal physiology and disease [8-10].

3 EXPRESSION PATTERNS OF LONG NON-CODING RNAS IN SEPSIS

High-throughput studies have identified extensive alterations in lncRNA expression in sepsis patients and experimental models [11]. For instance, peripheral blood mononuclear cells from septic individuals show hundreds of differentially expressed lncRNAs, some correlating with disease severity and outcomes [12]. Upregulated lncRNAs such as NEAT1, MALAT1, and HOTAIR, and downregulated ones like MEG3 and GAS5, are frequently reported [13-15].

Organ-specific lncRNA expression changes are also evident. In septic acute lung injury, PFI and Lnc-IL7R are elevated [16-17]; in kidney injury, TUG1 and AK139328 are altered [18]; and in myocardial dysfunction, H19 and KCNQ1OT1 are dysregulated [19-20]. These variations suggest tissue-specific regulatory roles. Moreover, lncRNA expression dynamically shifts with sepsis progression: pro-inflammatory types like THRIL and LincRNA-ERS rise during hyperinflammation, while immunomodulatory lncRNAs such as NR_045064 and uc.48+ dominate during immunosuppression.

4 MECHANISMS OF LNCRNAS IN SEPSIS PATHOGENESIS

4.1 lncRNAs and Inflammatory Response in Sepsis

LncRNAs modulate sepsis-associated inflammation through various avenues. As ceRNAs, they sequester miRNAs to derepress inflammatory mediators. For example, NEAT1 sponges miR-125a-5p, alleviating suppression of TRAF6 and activating NF-κB to enhance cytokine production [21-22]. Similarly, MALAT1 influences the miR-146a/TRAF6 axis, impacting TLR4 signaling [23-24].

Direct involvement in inflammatory pathways is also common. THRIL complexes with hnRNPL to modulate TNF- α transcription [25-26], while LincRNA-EPS interacts with hnRNPL to suppress inflammatory genes [27]. The pseudogene-derived lncRNA Lethe binds NF- κ B, curtailing its activity [26, 28-29]. These interactions fine-tune inflammatory responses.

LncRNAs also regulate inflammasomes: MEG3 inhibits NLRP3 assembly [30-31], and GAS5 binds glucocorticoid receptors to boost anti-inflammatory cytokines like IL-10 [32]. Conversely, SNHG1 promotes NLRP3 activation, worsening inflammation [33].

4.2 lncRNAs and Immune Regulation in Sepsis

4.2.1 Immune cell modulation by lncRNAs

Immune cell functions are extensively regulated by lncRNAs. In macrophages, TUG1 upregulation upon LPS stimulation enhances activation and cytokine release; its knockdown mitigates these effects [34]. Mechanistically, TUG1 binds miR-142-3p to elevate NCOA1, influencing polarization and inflammation [35]. In lymphocytes, NRON dysregulation in septic T cells impairs calcineurin-NFAT signaling, leading to immune dysfunction [36-37].

4.2.2 IncRNAs and immune evasion

Pathogens exploit lncRNAs to evade immunity. Viral lncRNAs, like HCMV's β2.7, bind hnRNP A2/B1 to suppress interferon responses, aiding persistence [38-40]. Bacterial infections may similarly alter host lncRNAs to impair immunity, though this area requires further study [41-42].

5 LNCRNAS IN CELL DEATH AND ORGAN DAMAGE IN SEPSIS

5.1 lncRNAs and Apoptosis

Apoptosis of immune and parenchymal cells contributes significantly to sepsis pathology. LncRNA-ATB upregulation in septic T cells promotes apoptosis via miR-200c/ZEB1 signaling [43-47]. In macrophages, MEG3 overexpression accelerates apoptosis through p53 activation [48-49].

In organ cells, HOTTIP upregulation exacerbates cardiomyocyte apoptosis via miR-125a-5p/Bax [50-51], while MIAT sponges miR-205 to increase Caspase-3 expression, worsening renal injury [52-54].

5.2 lncRNAs and Tissue/Organ Injury

LncRNAs are implicated in organ-specific damage: PFI and MALAT1 aggravate lung injury by promoting apoptosis and endothelial permeability [55-56], whereas MEG3 is protective [31]. In the kidney, TUG1 and H19 exacerbate injury through HMGB1 and let-7/STAT3 pathways [57-58]. In the heart, H19 and KCNQ1OT1 affect contractility and apoptosis [59-60].

6 LNCRNAS AND COAGULATION ABNORMALITIES

Coagulopathy is a critical aspect of sepsis. UCA1 upregulation in sepsis enhances coagulation via miR-143-3p/TF signaling [61-62]. LncRNAs may also influence platelet function, though detailed mechanisms remain elusive.

7 DIAGNOSTIC AND THERAPEUTIC POTENTIAL OF LNCRNAS IN SEPSIS

LncRNAs show promise as biomarkers: panels like MALAT1/HOTAIR/GAS5 improve diagnostic accuracy and prognosis prediction [63]. Therapeutically, targeting pro-inflammatory lncRNAs (e.g., NEAT1, THRIL) or supplementing protective ones (e.g., MEG3, GAS5) ameliorates sepsis in models [64]. Nanocarrier systems may enhance delivery, but challenges in specificity and safety remain.

8 CONCLUSIONS AND PERSPECTIVES

This review outlines the expanding roles of lncRNAs in sepsis pathophysiology. Their involvement in inflammation, immunity, and organ injury provides insights into disease mechanisms and highlights translational opportunities. Outstanding issues include: (1) validating lncRNA biomarkers in larger cohorts; (2) elucidating spatiotemporal regulation; (3) exploring interactions with other epigenetic mechanisms; and (4) improving therapeutic delivery. Future directions involve standardizing detection methods, integrating multi-omics data, understanding heterogeneity, and advancing precision medicine. LncRNAs hold potential as novel targets for improving sepsis outcomes.

COMPETING INTERESTS

The authors have no relevant financial or non-financial interests to disclose.

FUNDING

This work was funded by Foundation of Guizhou Science and Technology Cooperation -zk[2023] General 228 and Science and Technology Fund of Guizhou Provincial Health and Wellness Committee in 2023 (gzwkj2023-008).

REFERENCES

- [1] Cao M, Wang G, Xie J. Immune dysregulation in sepsis: experiences, lessons and perspectives. Cell Death Discovery, 2023, 9(1): 465.
- [2] Zhang D, Pei S, Feng Z, et al. Functions and mechanisms of lncRNAs in immune escape and their application in immunotherapy for colorectal cancer. Journal of Translational Medicine, 2025, 23(1): 689.
- [3] Zhang Y, Liu H, Niu M, et al. Roles of long noncoding RNAs in human inflammatory diseases. Cell Death Discovery, 2024, 10(1): 235.
- [4] Jin L, Liao J, Jin L, et al. Critical role of LncRNA in sepsis-associated acute kidney injury. Frontiers in Pharmacology, 2025, 16: 1627253.
- [5] Leng L, Wang H, Hu Y, et al. LINC02363: a potential biomarker for early diagnosis and treatment of sepsis. BMC Immunology, 2025, 26(1): 23.
- [6] Ma L, Bajic VB, Zhang Z. On the classification of long non-coding RNAs. RNA Biology, 2013, 10(6): 925-33.
- [7] Chodurska B, Kunej T. Long non-coding RNAs in humans: Classification, genomic organization and function. Non-coding RNA Research, 2025, 11: 313-327.
- [8] Gao N, Li Y, Li J, et al. Long Non-Coding RNAs: The Regulatory Mechanisms, Research Strategies, and Future Directions in Cancers. Front Oncology, 2020, 10: 598817.
- [9] Tang J., Zhang J, Lu Y, et al. Novel insights into the multifaceted roles of m6A-modified LncRNAs in cancers: biological functions and therapeutic applications. Biomarker Research, 2023, 11(1): 42.
- [10] Zhang X, Wang W, Zhu W, et al. Mechanisms and Functions of Long Non-Coding RNAs at Multiple Regulatory Levels. International Journal of Molecular Sciences, 2019, 20(22).
- [11] Shin JJ, Park J, Shin H, et al. Roles of lncRNAs in NF-κB-Mediated Macrophage Inflammation and Their Implications in the Pathogenesis of Human Diseases. International Journal of Molecular Sciences, 2024. 25(5): 2670.
- [12] Zhang W, Li Y, Li G, et al. Identification of lncRNAs in peripheral blood mononuclear cells associated with sepsis immunosuppression based on weighted gene co-expression network analysis. Hereditas, 2025, 162(1): 51.
- [13] Wen M, Cai G, Ye J, et al. Single-cell transcriptomics reveals the alteration of peripheral blood mononuclear cells driven by sepsis. Annals of Translational Medicine, 2020, 8(4): 125.
- [14] Wang W, Yang N, Wen R, et al. Long Noncoding RNA: Regulatory Mechanisms and Therapeutic Potential in Sepsis. Frontiers in Cellular and Infection Microbiology, 2021, 11: 563126.
- [15] Fan XY, Ma ZX, Tang LB, et al. lncRNA NEAT1 mediates LPS-induced pyroptosis of BEAS-2B cells via targeting miR-26a-5p/ROCK1 axis. Kaohsiung Journal of Medical Sciences, 2023, 39(7): 665-674.
- [16] Cui H, Xie N, Tan Z, et al. The human long noncoding RNA lnc-IL7R regulates the inflammatory response. European Journal of Immunology, 2014, 44(7): 2085-95.
- [17] Sun J, Jin T, Su W, et al. The long non-coding RNA PFI protects against pulmonary fibrosis by interacting with splicing regulator SRSF1. Cell Death & Differentiation, 2021, 28(10): 2916-2930.
- [18] Chen T, Lu J, Fan Q. lncRNA TUG1 and kidney diseases. BMC Nephrology, 2025, 26(1): 139.
- [19] Sun F, Yuan W, Wu H, et al. LncRNA KCNQ1OT1 attenuates sepsis-induced myocardial injury via regulating miR-192-5p/XIAP axis. Experimental Biology and Medicine, 2020, 245(7): 620-630.
- [20] Fang Y, Hu J, Wang Z, et al. LncRNA H19 functions as an Aquaporin 1 competitive endogenous RNA to regulate microRNA-874 expression in LPS sepsis. Biomedicine & Pharmacotherapy, 2018, 105: 1183-1191.
- [21] Gan Y, Long J, Zeng Y, et al. lncRNA IL-17RA-1 Attenuates LPS-Induced Sepsis via miR-7847-3p/PRKCG-Mediated MAPK Signaling Pathway. Mediators of Inflammation, 2022, 2022: 9923204.
- [22] Feng F, Jiao P, Wang J, et al. Role of Long Noncoding RNAs in the Regulation of Cellular Immune Response and Inflammatory Diseases. Cells, 2022, 11(22): 3642.
- [23] Liao Z, Zheng R, Shao G. Mechanisms and application strategies of miRNA-146a regulating inflammation and fibrosis at molecular and cellular levels (Review). International Journal of Molecular Medicine, 2023, 51(1).
- [24] Huang G, Zhao X, Bai Y, et al. Regulation of mitochondrial autophagy by lncRNA MALAT1 in sepsis-induced myocardial injury. European Journal of Medical Research, 2024, 29(1): 524.
- [25] Li Z, Chao T, Chang K, et al. The long noncoding RNA THRIL regulates TNFα expression through its interaction with hnRNPL. Proceedings of the National Academy of Sciences of the United States of America, 2014, 111(3): 1002-7.
- [26] Rapicavoli NA, Qu K, Zhang J, et al. A mammalian pseudogene lncRNA at the interface of inflammation and anti-inflammatory therapeutics. eLife, 2013, 2: e00762.

- [27] Atianand MK, Hu W, Satpathy AT, et al. A Long Noncoding RNA lincRNA-EPS Acts as a Transcriptional Brake to Restrain Inflammation. Cell, 2016, 165(7): 1672-1685.
- [28] Gupta SC, Awasthee N, Rai V, et al. Long non-coding RNAs and nuclear factor-κB crosstalk in cancer and other human diseases. Biochimica et Biophysica Acta Reviews on Cancer, 2020, 1873(1): 188316.
- [29] Statello L, Guo C, Chen L, et al. Gene regulation by long non-coding RNAs and its biological functions. Nature Reviews Molecular Cell Biology, 2021, 22(2): 96-118.
- [30] Gao H, Zhang X, Tang F, et al. Knockdown of lncRNA MEG3 protects against sepsis-induced acute lung injury in mice through miR-93-5p-dependent inhibition of NF-κB signaling pathway. Pathology Research and Practice, 2022, 239: 154142.
- [31] Liao H, Zhang S, Qiao J. Silencing of long non-coding RNA MEG3 alleviates lipopolysaccharide-induced acute lung injury by acting as a molecular sponge of microRNA-7b to modulate NLRP3. Aging (Albany NY), 2020, 12(20): 20198-20211.
- [32] Keenan CR, Schuliga MJ, Stewart AG. Pro-inflammatory mediators increase levels of the noncoding RNA GAS5 in airway smooth muscle and epithelial cells. Canadian Journal of Physiology and Pharmacology, 2015, 93(3): 203-206.
- [33] Cao B, Wang T, Qu Q, et al. Long Noncoding RNA SNHG1 Promotes Neuroinflammation in Parkinson's Disease via Regulating miR-7/NLRP3 Pathway. Neuroscience, 2018, 388: 118-127.
- [34] Ma W, Zhang W, Cui B, et al. Functional delivery of lncRNA TUG1 by endothelial progenitor cells derived extracellular vesicles confers anti-inflammatory macrophage polarization in sepsis via impairing miR-9-5p-targeted SIRT1 inhibition. Cell Death & Disease, 2021, 12: 1056.
- [35] Zhang R, Huang X, Jiang Y, et al. LncRNA TUG1 regulates autophagy-mediated endothelial-mesenchymal transition of liver sinusoidal endothelial cells by sponging miR-142-3p. American Journal of Translational Research, 2020, 12(3): 758-772.
- [36] Ahmad I, Valverde A, Ahmad H, et al. Long Noncoding RNA in Myeloid and Lymphoid Cell Differentiation, Polarization and Function. Cells, 2020, 9(2): 269.
- [37] Yao Z, Xiong Z, Li R, et al. Long non-coding RNA NRON is downregulated in HCC and suppresses tumour cell proliferation and metastasis. Biomedicine & Pharmacotherapy, 2018, 104: 102-109.
- [38] Boliar S, Prats-Mari L, Fortes P. Editorial: Long non-coding RNAs in viral infections and immunity. Frontiers in Immunology, 2023(14).
- [39] Zhang D, Zhang M, Zhang L, et al. Long non-coding RNAs and immune cells: Unveiling the role in viral infections. Biomedicine & Pharmacotherapy, 2024, 170: 115978.
- [40] Perera MR, Sinclair JH, Sinclair JH. The Human Cytomegalovirus β2.7 Long Non-Coding RNA Prevents Induction of Reactive Oxygen Species to Maintain Viral Gene Silencing during Latency. International Journal of Molecular Sciences, 2022, 23(19): 11017.
- [41] Schmerer N, Schulte LN. Long noncoding RNAs in bacterial infection. WIREs RNA, 2021, 12(6): e1664.
- [42] Cheng Y, Liang Y, Tan X, et al. Host long noncoding RNAs in bacterial infections. Frontiers in Immunology, 2024(15).
- [43] Sun H, Ke C, Zhang L, et al. Long Non-Coding RNA (LncRNA)-ATB Promotes Inflammation, Cell Apoptosis and Senescence in Transforming Growth Factor-β1 (TGF-β1) Induced Human Kidney 2 (HK-2) Cells via TGFβ/SMAD2/3 Signaling Pathway. Medical Science Monitor, 2020, 26: e922029.
- [44] Xiao H, Zhang F, Zou Y, et al. The Function and Mechanism of Long Non-coding RNA-ATB in Cancers. Frontiers in Physiology, 2018, 9: 321.
- [45] Li Z, Wu X, Gu L, et al. Long non-coding RNA ATB promotes malignancy of esophageal squamous cell carcinoma by regulating miR-200b/Kindlin-2 axis. Cell Death & Disease, 2017, 8(6): e2888-e2888.
- [46] Simion V, Zhou H, Haemmig S, et al. A macrophage-specific lncRNA regulates apoptosis and atherosclerosis by tethering HuR in the nucleus. Nature Communications, 2020, 11(1): 6135.
- [47] Zhao Q, Pang G, Yang L, et al. Long Noncoding RNAs Regulate the Inflammatory Responses of Macrophages. Cells, 2021, 11(1).
- [48] Pan X, He L. LncRNA MEG3 expression in sepsis and its effect on LPS-induced macrophage function. Cellular and Molecular Biology, 2020, 66(5): 131-136.
- [49] Chen K, Shi X, Jin Y, et al. High lncRNA MEG3 expression is associated with high mortality rates in patients with sepsis and increased lipopolysaccharide-induced renal epithelial cell and cardiomyocyte apoptosis. Experimental and Therapeutic Medicine, 2019, 18(5): 3943-3947.
- [50] Fan H, Shao H, Gao X. Long Non-Coding RNA HOTTIP is Elevated in Patients with Sepsis and Promotes Cardiac Dysfunction. Immunological Investigations, 2022, 51(7): 2086-2096.
- [51] Ghafouri-Fard S, Aghabalazade A, Shoorei H, et al. The Impact of lncRNAs and miRNAs on Apoptosis in Lung Cancer. Frontiers in Oncology, 2021, 11: 714795.
- [52] Zhang Y, Zhang YY, Xia F, et al. Effect of lncRNA-MIAT on kidney injury in sepsis rats via regulating miR-29a expression. European Review for Medical and Pharmacological Sciences, 2019, 23(24): 10942-10949.
- [53] Chen W, Ruan Y, Zhao S, et al. MicroRNA-205 inhibits the apoptosis of renal tubular epithelial cells via the PTEN/Akt pathway in renal ischemia-reperfusion injury. American Journal of Translational Research, 2019, 11(12): 7364-7375.

- [54] Chen Y, Jing H, Tang S, et al. Non-coding RNAs in Sepsis-Associated Acute Kidney Injury. Frontiers in Physiology, 2022(13).
- [55] Li Z, Jin T, Yang R, et al. Long non-coding RNA PFI inhibits apoptosis of alveolar epithelial cells to alleviate lung injury via miR-328-3p/Creb1 axis. Experimental Cell Research, 2023, 430(1): 113685.
- [56] Yao MY, Zhang WH, Ma WT, et al. Long non-coding RNA MALAT1 exacerbates acute respiratory distress syndrome by upregulating ICAM-1 expression via microRNA-150-5p downregulation. Aging (Albany NY), 2020, 12(8): 6570-6585.
- [57] Su Q, Liu Y, Lv X, et al. Inhibition of lncRNA TUG1 upregulates miR-142-3p to ameliorate myocardial injury during ischemia and reperfusion via targeting HMGB1- and Rac1-induced autophagy. Journal of Molecular and Cellular Cardiology, 2019, 133: 12-25.
- [58] Ding Y, Wan S, Liu W, et al. Regulation Networks of Non-Coding RNA-Associated ceRNAs in Cisplatin-Induced Acute Kidney Injury. Cells, 2022, 11(19): 2971.
- [59] Kay M, Soltani BM. LncRNAs in Cardiomyocyte Maturation: New Window for Cardiac Regenerative Medicine. Non-Coding RNA, 2021, 7(1): 20.
- [60] Xie L, Zhang Q, Mao J, et al. The Roles of lncRNA in Myocardial Infarction: Molecular Mechanisms, Diagnosis Biomarkers, and Therapeutic Perspectives. Frontiers in Cell and Developmental Biology, 2021, 9: 680713.
- [61] Yang Z, Lu S, Pan Y, et al. Umbilical cord mesenchymal stem cell exosomal miR-143-3p delays endothelial cell senescence through targeting COX-2. Plos One, 2025, 20(7): e0327173.
- [62] Chen Y, Fu Y, Song Y, et al. Increased Expression of lncRNA UCA1 and HULC Is Required for Pro-inflammatory Response During LPS Induced Sepsis in Endothelial Cells. Frontiers in Physiology, 2019, (10): 608
- [63] Chen J, He Y, Zhou L, et al. Long non-coding RNA MALAT1 serves as an independent predictive biomarker for the diagnosis, severity and prognosis of patients with sepsis. Molecular Medicine Reports, 2020, 21(3): 1365-1373.
- [64] Lin L, Liu H, Zhang D, et al. Nanolevel Immunomodulators in Sepsis: Novel Roles, Current Perspectives, and Future Directions. International Journal of Nanomedicine, 2024, 19: 12529-12556.

Print ISSN: 2663-1954 Online ISSN: 2663-1962

DOI: https://doi.org/10.61784/jpmr3042

ESTABLISHMENT OF A METHOD FOR MONITORING MEROPENEM CONCENTRATIONS IN PATIENTS WITH SEVERE ACUTE PANCREATITIS

Min Luo^{1,4,5#}, Wei Bu^{1,4#}, Lu Yao^{1,4}, Liu Shi^{1,4}, HongBo Xu³, WenMei Liang¹, Yan Chen³, Tao Chen¹, Bao Fu^{1*}, Lei Gong^{1,2*}

Corresponding Author: Lei Gong, Email: gonglei28@126.com; Bao Fu, Email: fubao0607@126.com

Abstract: Objective: To establish a population pharmacokinetic (PPK) model for meropenem in patients with severe acute pancreatitis (SAP), providing a valuable basis and method for developing individualized meropenem dosing regimens tailored to the pathophysiological state of SAP patients; Methods: Meropenem concentrations in plasma and abdominal drainage fluid were monitored using ultra-high performance liquid chromatography-tandem mass spectrometry (UPLC-MS/MS) and homogeneous enzyme immunoassay. Nonlinear mixed-effects modeling was performed using Phoenix software; Results: (1) Meropenem concentration determination: A total of 20 SAP patients were enrolled, providing 99 qualified plasma samples and 42 qualified abdominal drainage fluid samples. Meropenem and the internal standard (metformin) were well separated in both plasma and drainage fluid samples, demonstrating good specificity. Meropenem showed excellent linearity within the ranges of 0.5 - 200 µg/mL in plasma and 0.1 - 10 µg/mL in drainage fluid. All methodological validation results fell within acceptable limits, with RSD \leq 15%; Conclusion: This study established an LC-MS/MS method (referenced and quality-controlled by homogeneous enzyme immunoassay) for determining meropenem concentrations. The validated method is suitable for clinical therapeutic drug monitoring (TDM) of meropenem, particularly in critically ill ICU patients.

Keywords: Meropenem; Severe acute pancreatitis; Therapeutic drug monitoring; Monte Carlo simulation; Pharmacokinetics/Pharmacodynamics; Individualized therapy

1 INTRODUCTION

Meropenem exhibits time-dependent antibacterial activity. The pharmacokinetic/pharmacodynamic (PK/PD) index that best predicts its clinical efficacy is the duration of time that the free drug concentration remains above the minimum inhibitory concentration (fT > MIC) of the pathogen [1]. Studies suggest that for critically ill patients with severe bacterial infections, a target of 100% fT > MIC or 100% fT > 4x MIC may be necessary [2]. Therefore, understanding the population pharmacokinetics (PPK) of meropenem in pancreatitis is crucial. This study used body fluid samples (plasma and abdominal drainage fluid) from patients receiving meropenem, with meropenem concentration as the observation index. We established UPLC-MS/MS and homogeneous enzyme immunoassay (for rapid bedside monitoring) methods to detect meropenem concentrations, aiming to facilitate precise dosing (individualized therapy) for SAP patients.

2 MATERIALS AND METHODS

2.1 Reagents

Meropenem reference standard (purity >98%, Yuanye Bio-Technology, Shanghai, China); Metformin hydrochloride internal standard (IS) (purity >98%, Yuanye Bio-Technology); Acetonitrile, methanol (HPLC grade, Merck, Germany); Formic acid, ammonium formate (HPLC grade, Aladdin, Shanghai, China); Deionized water (prepared using a Millipore purification system).

2.2 Instruments

Waters ACQUITY UPLC H-Class System coupled with a Xevo TQ-S Micro Triple Quadrupole Mass Spectrometer (Waters Corp., Milford, MA, USA); ACQUITY UPLC® BEH Amide column (100 mm \times 2.1 mm, 1.7 μ m, Waters); Centrifuge (Eppendorf 5430R, Germany); Nitrogen evaporator (Organomation N-EVAP, USA); Vortex mixer (IKA

¹Department of Critical Care Medicine, Affiliated Hospital of Zunyi Medical University, Zunyi 563000, Guizhou, China.

²Department of Pharmaceutics, Kweichow Moutai Hospital, Zunyi 563000, Guizhou, China.

³Guizhou Children's Hospital, Affiliated Hospital of Zunyi Medical University, Zunyi 563000, Guizhou, China.

⁴School of Pharmacy, Zunyi Medical University, Zunyi 563000, Guizhou, China.

⁵Zhijin County People's Hospital, Bijie 552102, Guizhou, China.

^{*}Min Luo and Wei Bu contributed equally to this work and they are both first authors.

^{*}Bao Fu and Lei Gong contribute the same to the article and are the corresponding authors.

32 Min Luo, et al.

MS3 basic, Germany); Analytical balance (Mettler Toledo ME204, Switzerland); -80°C ultra-low temperature freezer (Thermo Scientific, USA).

2.3 Ethics

The study protocol for meropenem concentration determination in plasma and abdominal drainage fluid samples adhered to ethical guidelines. Sample collection obtained informed consent from patients or their families, complied with the Declaration of Helsinki, and was approved by the Ethics Committee of the Affiliated Hospital of Zunyi Medical University (Approval No.: KLLY - 2022 - 204).

2.4 Blank Plasma and Abdominal Drainage Fluid Sample Collection

2.4.1 Blank plasma

Plasma from 6 healthy adults was collected as blank plasma. Venous blood was drawn in the morning after fasting, promptly centrifuged, and stored at -80°C until use.

2.4.2 Blank drainage fluid

Abdominal drainage fluid (2 mL) was collected from 6 SAP patients with indwelling drainage catheters, no significant past medical history, and no prior meropenem use, using blank tubes. Samples were promptly centrifuged and stored at -80°C until use.

2.5 Patient Plasma and Abdominal Drainage Fluid Sample Collection

Sampling time points (0 h [pre-dose], 0.5 h, 1 h, 2 h, 4 h, 6 h, and 8 h post-dose) were set based on meropenem's PK parameters and half-life from literature and the drug label. A sampling time error of approximately 5 minutes was allowed. At least 3 plasma and 3 drainage fluid samples were collected per patient, covering absorption, distribution, and elimination phases. Samples were centrifuged at 12,000 rpm for 10 min, and the supernatant was stored at -80°C.

2.6 Preparation of Standard and Internal Standard Solutions

Meropenem standard stock solution (10 mg/mL) was prepared in water and stored at -20°C. Metformin IS stock solution (10 mg/mL) was prepared similarly. Working solutions were prepared by dilution.

2.7 Sample Preparation

2.7.1 Plasma and drainage fluid samples

To labeled centrifuge tubes, add 20 μ L IS solution (500 μ g/mL metformin) and 205 μ L water. Add 25 μ L sample. Mix thoroughly. Add 750 μ L acetonitrile for protein precipitation. Vortex, centrifuge (12,000 rpm, 10 min). Filter supernatant through a 0.22 μ m membrane into an injection vial. Injection volume: 5 μ L.

2.7.2 Blank samples

Thaw blank plasma/drainage fluid. Add 225 μL water to tubes. Add 25 μL blank sample. Mix. Add 750 μL acetonitrile. Vortex, centrifuge. Filter. Combine filtered blank plasma and drainage fluid, mix. Injection volume: 5 μL.

2.8 Mass Spectrometric and Chromatographic Conditions

2.8.1 Chromatographic conditions

Column: ACQUITY UPLC® BEH Amide (100 mm \times 2.1 mm, 1.7 μ m); Mobile phase: Acetonitrile (A) - Water (B) (each containing 0.29 g ammonium formate and 0.5 mL formic acid per liter); Gradient: 0-9.5 min: 85%-65% A; 9.5-10 min: 65%-40% A; 10-10.5 min: 40%-85% A; 10.5-14 min: 85% A; Flow rate: 0.25 mL/min; Injection volume: 5 μ L; Column temperature: 40°C; Autosampler temperature: 4°C.

2.8.2 Mass spectrometric conditions

ESI ion source; Positive ion mode; MRM mode; Temperature: 450°C; Capillary voltage: 3.5 kV; Gas flow: 750 L/hr; MRM transitions: m/z 384.6→141.2 (meropenem), m/z 130.2→60.1 (metformin IS).

2.9 Plasma Standard Curve Preparation

Serial dilutions of the meropenem stock solution (10 mg/mL) in blank plasma were prepared to obtain calibration standards at concentrations of 200, 100, 50, 10, 5, 2, 1, and 0.5 μ g/mL. Each concentration was prepared in triplicate. Processed as per section 1.7.1.

2.10 Drainage Fluid Standard Curve Preparation

Serial dilutions were prepared in blank drainage fluid to obtain calibration standards at concentrations of 0.1, 0.2, 0.5, 1, 2, 5, and 10 μ g/mL. Each concentration was prepared in triplicate. Processed as per section 1.7.1.

2.11 Quality Control (QC) Sample Preparation

2.11.1 Plasma QC samples

Low (4 μ g/mL), medium (20 μ g/mL), and high (125 μ g/mL) concentration QC samples were prepared in blank plasma. Processed as per section 1.7.1. QC samples were prepared fresh for use.

2.11.2 Drainage fluid QC samples

Low (0.4 μ g/mL), medium (2 μ g/mL), and high (9 μ g/mL) concentration QC samples were prepared in blank drainage fluid. Processed as per section 1.7.1. QC samples were prepared fresh for use.

2.12 Methodological Validation

2.12.1 Specificity

Analyzed blank plasma/drainage fluid, blank spiked with meropenem, and blank spiked with meropenem and IS. Checked for interference at the retention times of meropenem and IS.

2.12.2 Linearity and LOD

Calibration curves were constructed by plotting peak area ratio (meropenem/IS) against concentration using weighted $(1/x^2)$ least squares regression. The limit of detection (LOD) was defined as the lowest concentration on the standard curve with signal-to-noise $(S/N) \ge 3$.

2.12.3 Recovery

Recovery was determined by comparing the peak areas of extracted QC samples (low, medium, high) with the peak areas of post-extraction blank samples spiked with equivalent amounts of meropenem and IS (n=5 per level).

2.12.4 Precision

Intra-day precision (n=5 per level, analyzed three times within one day) and inter-day precision (n=5 per level, analyzed over three consecutive days) were expressed as RSD (%).

2.12.5 Matrix effect

The matrix effect was assessed by comparing the peak areas of analytes spiked into post-extraction blank matrix (from 6 different sources) with the peak areas of neat standard solutions at equivalent concentrations (n=6 per level). Calculated as (A/B * 100%).

2.12.6 Stability

Stability was evaluated under various conditions: short-term (room temperature for 8 h, autosampler (4°C) for 24 h), long-term (-20°C for 10 days), and freeze-thaw stability (3 cycles) using QC samples (n=5 per level). RSD should be \leq 15%.

2.12.7 Data processing

Excel was used for calculating precision, stability, etc. Origin software was used for plotting standard curves and chromatograms.

3 RESULTS

2.1 Specificity Results

2.1.1 Plasma

Meropenem and metformin (IS) were well separated in plasma. No interference from endogenous plasma components or other co-administered drugs was observed. Chromatograms see Figures 1-3.

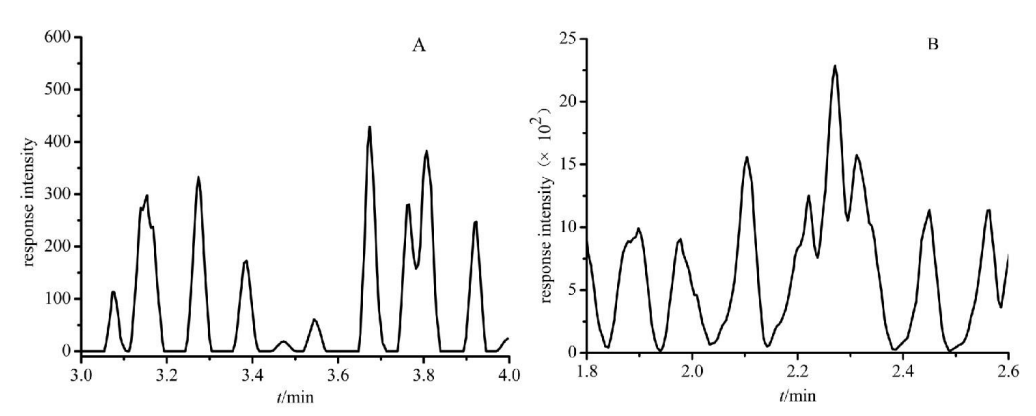


Figure 1 Blank Plasma Chromatogram: A. Meropenem Channel; B. Metformin Channel

Min Luo, et al.

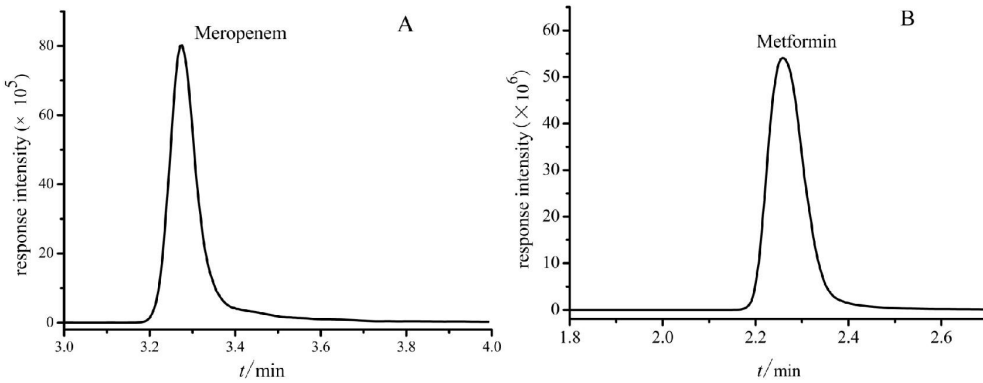


Figure 2 Blank Plasma Spiked with Meropenem Chromatogram

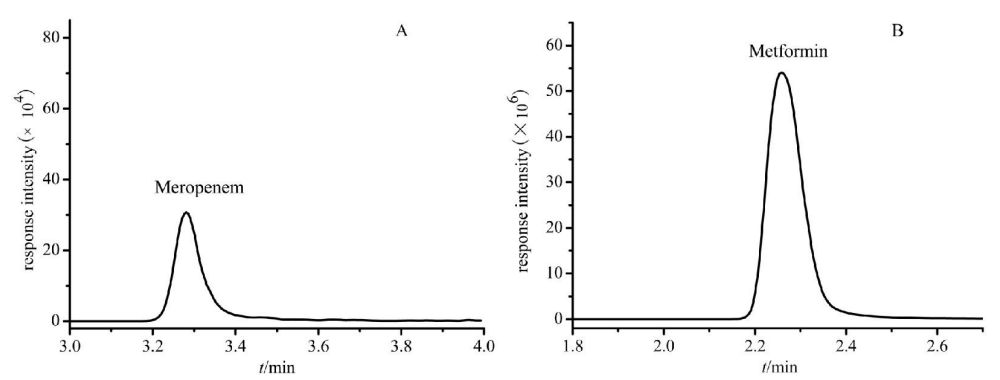


Figure 3 Blank Plasma Spiked with Meropenem and IS Chromatogram

2.1.2 Drainage fluid

Meropenem and IS were well separated in drainage fluid without interference, indicating good specificity. Chromatograms see Figures 4-6.

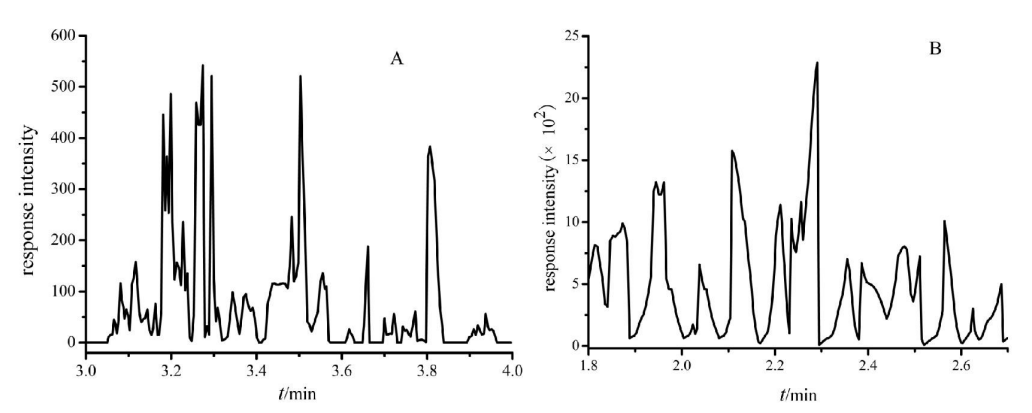


Figure 4 Blank Drainage Fluid Chromatogram

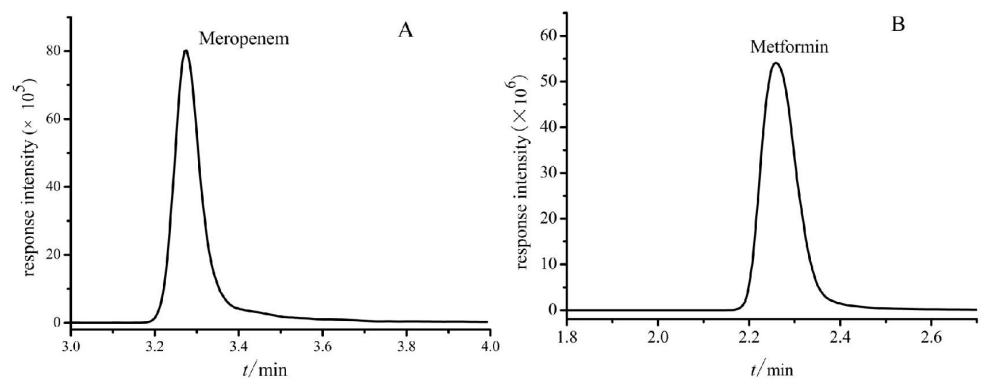


Figure 5 Blank Drainage Fluid Spiked with Meropenem Chromatogram

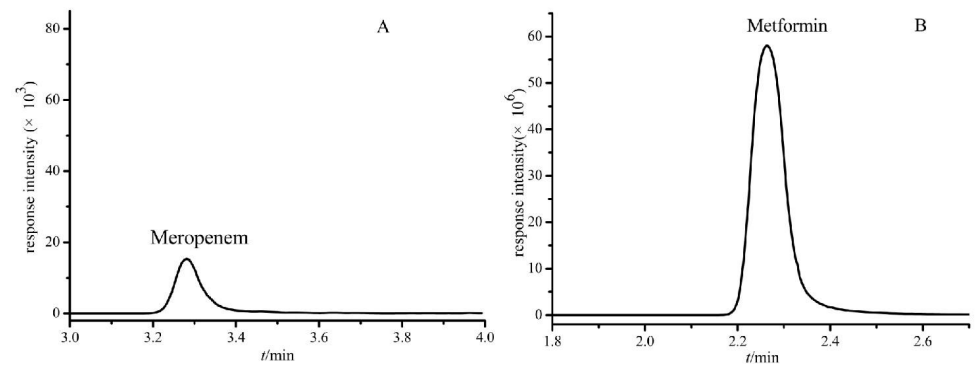


Figure 6 Blank Drainage Fluid Spiked with Meropenem and IS Chromatogram

2.2 Standard Curve and LOD Results

The standard curve equations were y = 0.0101x + 0.0047, r = 0.9998 (n=3) for plasma and y = 0.01x + 0.0023, r = 0.9999 (n=3) for drainage fluid. Linear ranges were 0.5-200 µg/mL (plasma) and 0.1-10 µg/mL (drainage fluid). LOD (S/N=3) in plasma: meropenem 1.1 ng/mL, metformin 0.024 ng/mL; in drainage fluid: meropenem 4.3 ng/mL, metformin 0.03 ng/mL. Standard curve shown in Figure 7.

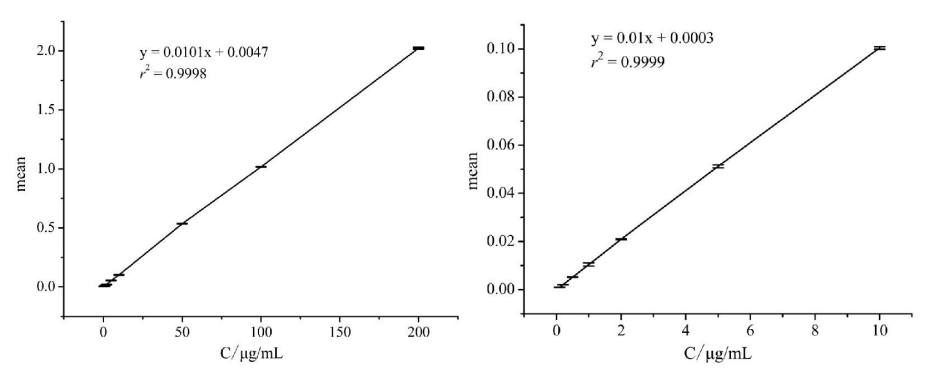


Figure 7 Standard Curves for Meropenem in Plasma and Drainage Fluid

2.3 Recovery Results

Recovery rates for meropenem ranged from 90% to 103% in both plasma and drainage fluid, with RSD < 15%, indicating good recovery.

2.4 Precision Results

Intra-day and inter-day RSD values were all ≤ 15%, indicating acceptable precision.

2.5 Matrix Effect Results

The matrix effect for QC samples ranged from 90% to 105% with RSD < 15%, indicating no significant matrix effect. Results shown in Tables 7 and 8.

2.6 Stability Results

Meropenem QC samples were stable under all tested conditions (short-term, long-term, freeze-thaw), with RSD values within 15%.

4 DISCUSSION AND CONCLUSION

This study established an LC-MS/MS method (referenced against homogeneous enzyme immunoassay) for determining meropenem concentrations. Compared to established LC-MS methods [3-6], the retention time and total analysis time (~3-4 min) were similar, though some methods report shorter times (~1 min). Precision and stability were comparable, confirming the method's suitability for clinical TDM of meropenem, especially in critically ill ICU patients. Homogeneous enzyme immunoassay is also applicable but requires stringent temperature/humidity control. While certified and reimbursable in China, it's more commonly used for drugs like vancomycin, yielding accurate results. Whether its accuracy for meropenem matches LC-MS/MS requires further study.

36 Min Luo, et al.

For sample preparation, solid-phase extraction (SPE) and methanol/acetonitrile protein precipitation are common [7-9]. SPE can be tedious, have lower recovery, cause peak splitting/broadening, and be costly [10]. Protein precipitation with acetonitrile is simpler, cheaper, and widely used [11]. Acetonitrile is recommended due to its low ionization suppression [8]. Thus, acetonitrile protein precipitation was chosen, yielding recoveries within acceptable ranges.

Metformin was selected as the IS based on laboratory availability. It separated well from the analyte peak. Since enrolled patients were not taking metformin, it did not interfere. Methodological validation confirmed the method's sensitivity and effectiveness for meropenem TDM in plasma and drainage fluid. However, this method fails if patients are co-administered meropenem and metformin. Therefore, it's only suitable for TDM in patients not taking metformin. For patients on both drugs, suitable methods need exploration, as most existing studies don't specify metformin co-administration.

COMPETING INTERESTS

The authors have no relevant financial or non-financial interests to disclose.

FUNDING

This research was supported by the following grants: 1. Special Research on Rapid and Accurate TDM Monitoring Scheme for the Research and Application of Precision Medicine Therapy Technology Development for Critically Ill Patients Based on the Critical Value Reporting System (MTyk2022-32); 2. Research and Clinical Application of a Rapid TDM Monitoring Protocol for Precision Drug Therapy in Critically Ill Patients Based on Mass Spectrometry Technology*(Qiankehe Support [2021] General 443).

REFERENCES

- [1] Zylbersztajn B, Parker S, Navea D, et al. Population Pharmacokinetics of Vancomycin and Meropenem in Pediatric Extracorporeal Membrane Oxygenation Support. Frontiers in Pharmacology, 2021, 12: 709332.
- [2] Tan WW, Watt KM, Boakye-Agyeman F, et al. Optimal dosing of meropenem in a small cohort of critically ill children receiving continuous renal replacement therapy. Journal of Clinical Pharmacology, 2021, 61(6): 744-754.
- [3] He J, Xu SL, Shao H, et al. Optimization of blood concentration monitoring method for meropenem application in critically ill patients and clinical application examples. Chinese Journal of Hospital Pharmacy (Zhongguo Yiyuan Yaoxue Zazhi), 2018, 38(04): 416-419.
- [4] Zhang WD, Zhang WW, Yan Y, et al. Determination of meropenem concentration in human plasma by liquid chromatography-tandem mass spectrometry and its application in therapeutic drug monitoring of ICU sepsis patients. Journal of Hebei Medical University (Hebei Yike Daxue Xuebao), 2022, 43(11): 1286-1290.
- [5] Lyu JX, Xu WJ, Zhao J, et al. Simultaneous determination of 5 antibacterial drugs in human plasma by LC-MS and its application in critically ill patients. Chinese Journal of Hospital Pharmacy (Zhongguo Yiyuan Yaoxue Zazhi), 2023: 1-9.
- [6] Zhu DP, Luo JM, Cai XJ. Study on the determination of meropenem concentration in human serum by ultra performance liquid chromatography-tandem mass spectrometry. Zhejiang Journal of Integrative Traditional Chinese and Western Medicine (Zhejiang Zhongxiyi Jiehe Zazhi), 2023, 33(11): 1052-1055.
- [7] Ferrone V, Cotellese R, Cichella A, et al. Meropenem and ciprofloxacin in complicated gastric surgery for cancer patients: A simple SPE-UHPLC-PDA method for their determination in human plasma. Biomedical Chromatography, 2019, 33(3): e4450.
- [8] D'Cunha R, Bach T, Young BA, et al. Quantification of cefepime, meropenem, piperacillin, and tazobactam in human plasma using a sensitive and robust liquid chromatography-tandem mass spectrometry method, part 2: stability evaluation. Antimicrob Agents Chemother, 2018, 62(9): e00859-18.
- [9] Rao Z, Dang ZL, Bin L, et al. Determination of total and unbound meropenem, imipenem/cilastatin, and cefoperazone/sulbactam in human plasma: application for therapeutic drug monitoring in critically ill patients. Therapeutic Drug Monitoring, 2020, 42(4): 578-587.
- [10] Dincel D, Sagirli O, Topcu G. A high-performance liquid chromatographic method for the determination of meropenem in serum. Journal of Chromatographic Science, 2020, 58(2): 144-150.
- [11] Zou L, Meng F, Hu L, et al. A novel reversed-phase high-performance liquid chromatographic assay for the simultaneous determination of imipenem and meropenem in human plasma and its application in TDM. Journal of Pharmaceutical and Biomedical Analysis, 2019, 169: 142-150.

Journal of Pharmaceutical and Medical Research

Print ISSN: 2663-1954 Online ISSN: 2663-1962

DOI: https://doi.org/10.61784/jpmr3044

POST-MARKET CLINICAL FOLLOW-UP STUDY OF THE COLOR DOPPLER ULTRASOUND SYSTEM: A PROSPECTIVE, COMPARATIVE EVALUATION OF SAFETY AND PERFORMANCE

Sheng Zhao¹, FuCheng Wang², Tao Hu^{2*}, Dan Wu², JieBing Ma², BaoLi Zhang²

¹Ultrasound Diagnosis Department, Maternal and Child Health Hospital of Hubei Province, Wuhan 430070, Hubei, China.

²Wuhan Zoncare Bio-medical Electronics Co., Ltd., Wuhan 430070, Hubei, China.

Corresponding Author: Tao Hu, Email: hutaocsu@163.com

Abstract: Background: Post-market clinical follow-up (PMCF) studies are essential for verifying the real-world safety and performance of medical devices. This study evaluated the ViV 80 Color Doppler Ultrasound System (Zoncare) against the Model R**7 from a well-established manufacturer (M** company) in routine clinical practice. Methods: A prospective, observational, single-center study was conducted at Maternal and Child Health Hospital of Hubei Province, China. A total of 363 cases (140 male, 223 female) underwent abdominal, thyroid, cardiac, and gynecologic examinations using four probe types (convex, linear, phased array, volume). Endpoints included image consistency (target ≥95%), positive detection rate, and adverse events. Results: Image Consistency: All probes met the 95% target (convex: 97%; linear: 100%; phased array: 95%; volume: 96%). Moreover, mean image quality scores were consistently high, with the ViV 80 performing comparably or superiorly to the R**7 in each body site; Detection Rates: Varied by anatomy (liver: 44%; thyroid: 31%; cardiac: 8%; uterus: 26%), reflecting clinical heterogeneity; Adverse Events: No device-related adverse events occurred; five cases reported transient pressure sensations (1.4%). Conclusion: The ViV 80 demonstrated non-inferiority to the R** 7 in image quality and safety, supporting its continued use in diverse clinical applications.

Keywords: Color Doppler Ultrasound System; Post-market clinical follow-up; Safety; Performance; Image consistency; MDR; PMCF; ViV 80

1 INTRODUCTION

The ViV 80 Color Doppler Ultrasound System, developed by Wuhan Zoncare Bio-medical Electronics Co., Ltd., is a Class IIa medical device with global market authorization. It is intended for diagnostic ultrasound imaging and fluid flow analysis of the human body. It is indicated for use in medical clinics and hospitals to aid in the assessment, diagnosis, and monitoring of various conditions. This PMCF study aimed to validate its real-world performance and safety per EU MDR 2017/745 [1] and MEDDEV 2.7/1 Rev.4 [2], comparing it to the R**7 across four anatomical sites.

2 METHODS

2.1 Study Design

This prospective, observational, comparative cohort study, designed following ISO 14155:2020 [3] and NMPA guidelines [4,5], evaluated real-world clinical performance at a single tertiary care center (Maternal and Child Health Hospital of Hubei Province). The study enrolled 363 cases (84 cases per probe type \times 4 probes, accounting for 5% potential dropout) based on a power analysis assuming: (1) 85% minimum acceptable image consistency rate between test and control probes; (2) 95% expected excellent/good image rate; with 80% statistical power and α =0.05 (two-tailed).

The study's sample size was determined following the NMPA Guidelines for Clinical Trial Design of Medical Devices (2018) for ultrasound diagnostic evaluations. The calculation used a single-group target value approach, with the primary outcome being the image consistency rate (proportion-based).

The sample size calculation formula is:

$$n = \frac{\left[Z_{1-\alpha/2}\sqrt{P_0(1-P_0)} + Z_{1-\beta/2}\sqrt{P_T(1-P_T)}\right]^2}{(P_T - P_0)^2} \tag{1}$$

Where:

- *n* is the sample size;
- $Z_{1-\alpha/2}=Z_{0.975}=1.96$ (for $\alpha=0.05$)
- $Z_{1-\beta}=Z_{0.8}=0.842$ (for 80% power)
- $P_0 = 85\%$ (target value)
- $P_T = 95\%$ (expected value)

38 Sheng Zhao, et al.

The formula-derived base sample size of 78 cases per probe was adjusted for a 5% dropout rate to 84 cases (totaling 336 cases for 4 probes), with final enrollment expanded to 363 cases to ensure robustness.

2.2 Participants

The study enrolled adults aged 18-65 years requiring clinically indicated diagnostic ultrasound examinations of the liver, thyroid, cardiac, or uterus, with all participants or their legal representatives providing written informed consent after detailed explanation. Exclusion criteria comprised contraindications to ultrasound (e.g., open wounds at examination sites), inability to cooperate with study procedures, investigator-determined unsuitability, and age outside the specified range (<18 or >65 years).

2.3 Devices

The test device was the ViV 80 Color Doppler Ultrasound System (Zoncare) equipped with four specialized probes: a 3C5CE convex array (3.5MHz) for liver exams, 7L5CF linear array (7.5MHz) for thyroid, 2P2CC phased array (2.5MHz) for cardiac, and 4V4PD volume probe (4MHz) for uterine scans. The control device was the R**7 with corresponding probes: SC5-1U convex array for liver, L11-3U linear array for thyroid, SP5-1U phased array for cardiac, and D8-2U volume probe for uterine evaluations.

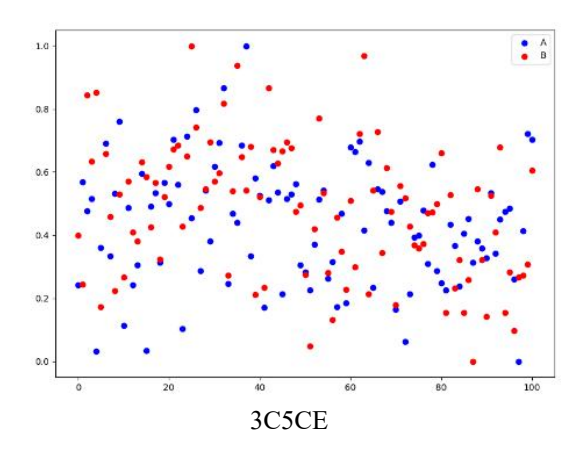
2.4 Outcomes

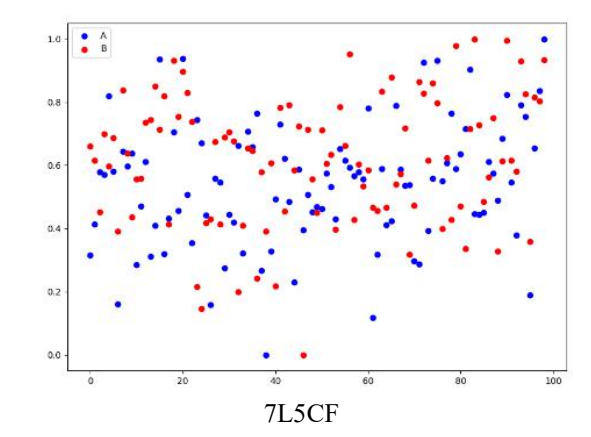
The primary endpoint was image consistency rate (≥95% required), defined as the percentage of cases where ViV 80 and R**7 ultrasound systems agreed on image quality ratings (excellent/good/poor) or ViV 80 was rated superior when scanning identical anatomical sites (liver, thyroid, cardiac, uterus), with ratings determined by blinded evaluators using standardized criteria.

Secondary endpoints included: (1) positive detection rate, calculated as the proportion of examinations identifying clinically significant abnormalities (e.g., liver lesions, thyroid nodules, cardiac valve abnormalities, or uterine masses) confirmed by follow-up diagnostics; (2) incidence of adverse events and adverse device effect, systematically recorded throughout the study period and adjudicated by an independent safety committee.

2.5 Statistical Analysis

Image quality parameters underwent normalization and comparative analysis through three quantitative methods: (1) Pearson correlation coefficients (r-values) [6] to evaluate linear relationships in image quality scores between ViV 80 and R**7 systems, (2) scatter plot matrices [7] visualizing normalized scores across all probe types with regression lines, and (3) evaluation of normalized distributions [8] $(X_{norm} = \frac{X \cdot X_{min}}{X_{max} \cdot X_{min}})$ (See Figure 1, where A is the study model and B is the reference model), correlation coefficients $(r = \frac{\sum_{i=1}^{n}(x_i \cdot \overline{x})(y_i \cdot \overline{y})}{\sqrt{\sum_{i=1}^{n}(x_i \cdot \overline{x})}(y_i \cdot \overline{y})}$ (See Figure 2), subject distributions (See Table 1 and Figure 3), and overall assessments across all anatomical sites. Missing or incomplete datasets (n = 25) were systematically documented with exclusion rationale (e.g., inaccurate image evaluation, inconsistent image sections, unsaved images, or incorrect preset parameters) (see Table 2) and addressed through the pre-specified 5% sample size expansion to account for fall-off (per Section 2.1). All analytical procedures adhered to the predefined statistical plan, including evaluation of image consistency (target \geq 95% agreement) and correlation analysis.





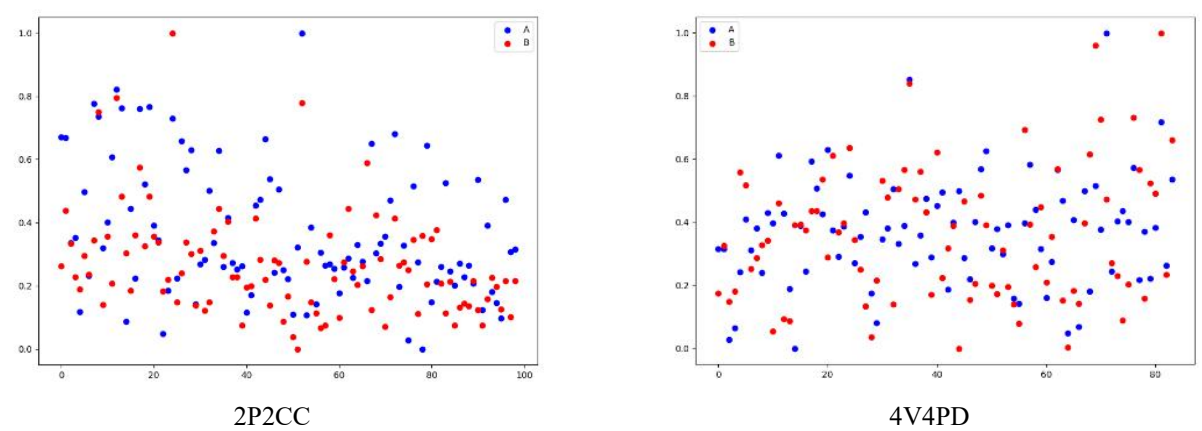


Figure 1 All Mode Image Quality Distribution of the Test Device and Reference Device

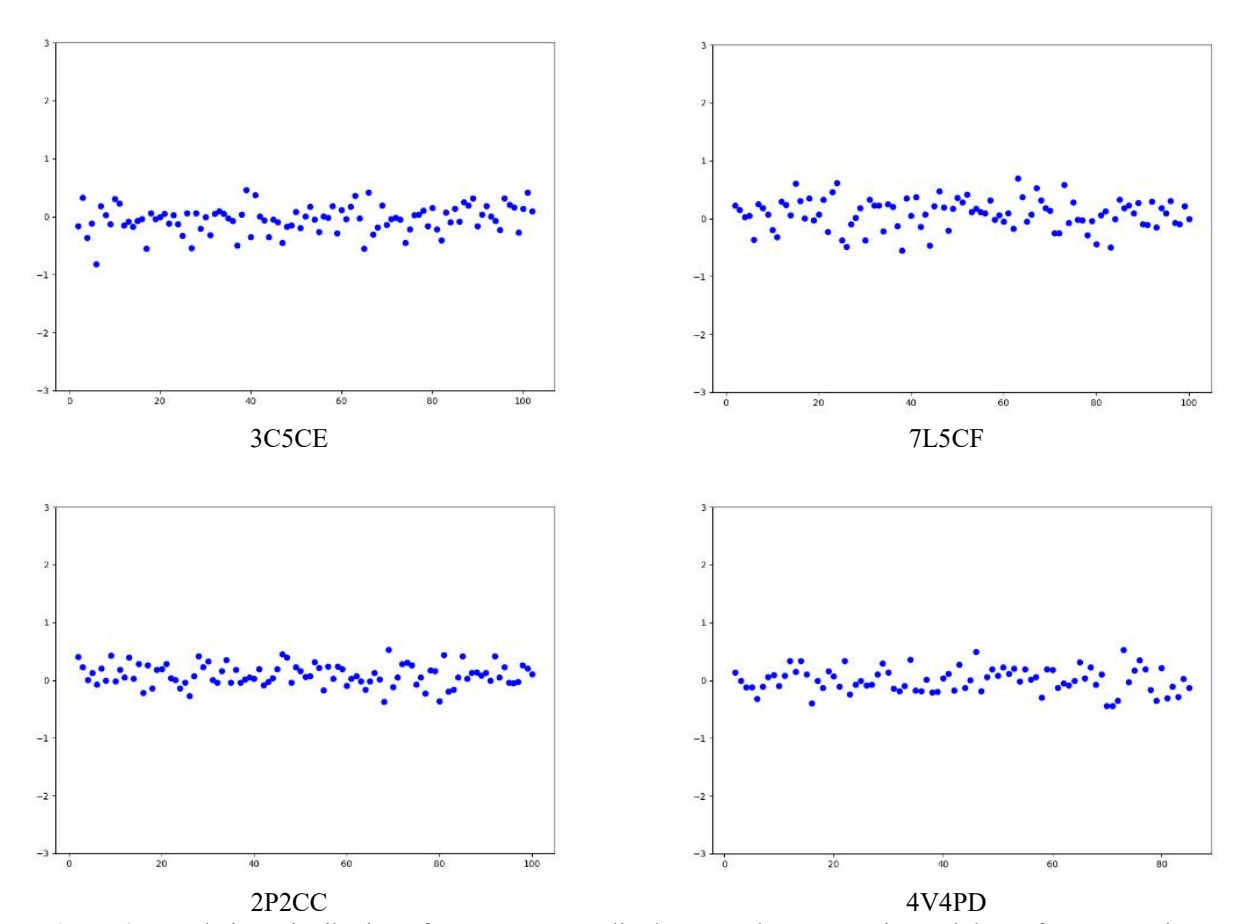


Figure 2 Correlation Distribution of Case Image Quality between the Test Device and the Reference Device

Table 1 Demographic Characteristics of the Subjects

	Male (140 cases)					Female	(223 cases)	
	Mean Standard Minimum Maximum Deviation					Standard Deviation	Minimum	Maximum
Age (years)	35.72	8.06	22	57	33.31	8.51	20	55

40 Sheng Zhao, et al.

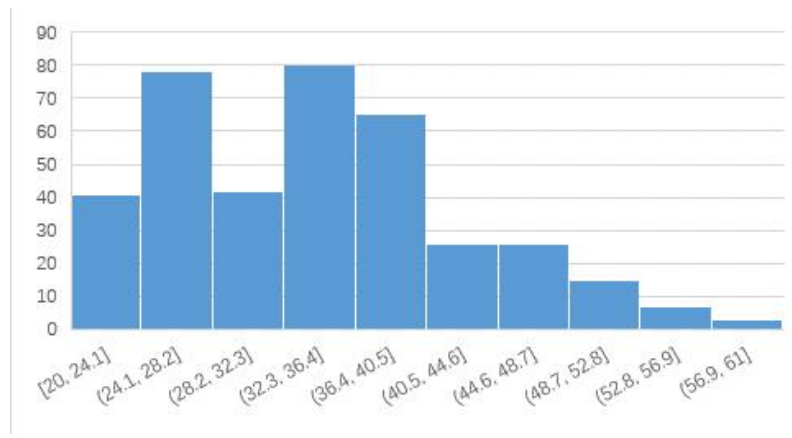


Figure 3 Age Distribution of Subjects

Table 2 Shedding Data and Reasons for Shedding

Body site	Subject enrollment number	Causes of shedding
	10	Inaccurate image evaluation
	15	Image not saved
	18	Inconsistent image sections
	22	Inaccurate image evaluation
	26	The preset parameters are incorrect.
Livron	27	Inaccurate image evaluation
liver	29	Inconsistent image sections
	32	Inconsistent image sections
	33	Image not saved
	38	The preset parameters are incorrect.
	41	Inaccurate image evaluation
	85	Inconsistent image sections
	1	The preset parameters are incorrect.
	7	Image not saved
	18	Inaccurate image evaluation
thyroid	25	The preset parameters are incorrect.
	39	Image not saved
	50	Inconsistent image sections
	72	Inaccurate image evaluation
	16	Inconsistent image sections
cardiac	29	The preset parameters are incorrect.
cardiac	53	Inconsistent image sections
	87	Inaccurate image evaluation
11tam10	22	Inaccurate image evaluation
uterus	72	Inconsistent image sections

3 RESULTS

3.1 Image Consistency

All probes exceeded the 85% target and mean image quality scores were consistently high (see Table 3).

Table 3 Image Consistency Result

Probe	Dodry Cita	Consistence	Image Quality Mean (%)		
Probe	Body Site	Consistency	ViV 80	R**7	
3C5CE (Convex)	Liver	97%	99%	96%	
7L5CF (Linear)	Thyroid	100%	100%	100%	
2P2CC (Phased)	Cardiac	95%	98%	99%	
4V4PD (Volume)	Uterus	96%	98%	89%	

Probe Performance Results

All probe types met the ≥95% image consistency requirement:

3C5CE (Liver): 93 cases (43 positive) showed 100% consistency in 2D/detail/vessel filling/real-time parameters

7L5CF (Thyroid): 92 cases (30 positive) achieved 100% consistency across all metrics

2P2CC (Cardiac): 94 cases (8 positive) demonstrated 100% consistency in vessel filling/reflux parameters

4V4PD (Uterus): 84 cases (22 positive) maintained 100% consistency in 2D/detail/vessel filling/real time parameters Moreover, the ViV 80 matched the R**7's performance in thyroid imaging (100%) and was comparable in cardiac

imaging (98% vs. 99%). It demonstrated superior performance in liver (99% vs. 96%) and uterine (98% vs. 89%) examinations.

Image Quality Mean: The percentage of examinations achieving "optimal" image quality.

Optimal (Excellent/Acceptable): Image clarity allows for clear visualization of landmarks and confident diagnosis.

Poor: Image quality is too low for any meaningful diagnosis.

All comparative assessments against reference probes (SC5-1U, L11-3U, SP5-1U, D8-2U) confirmed non-inferiority (PASS). Complete quantitative results are detailed in Tables 4-7.

Table 4 Comparison of Image Quality between Convex array probes (Test Device VS Reference Device)

probe model	enroll ment	2D	detail	struct ure	vessels filling	brightn ess	distribu ted	real-time	spectrum boundary	clarity	morpho logy	consist ency	concl usion
3C5CE	02	100%	100%	100%	100%	98.9%	92.4%	100%	95.7%	93.5%	83.4%	>95%	DACC
SC5-1U	93	100%	100%	97.8%	100%	95.7%	77.4%	100%	95.7%	96.7%	92.4%	<i>≥</i> 93%	PASS

Table 5 Comparison of Image Quality between Linear Array Probes (Test Device VS Reference Device)

probe model	enrollm ent	2D	detail	vessels filling	brightnes s	distribut ed	Real-time	spectrum boundary	clarity	morpholog y	consiste ncy	conclus ion
7L5CF	92	100%	100%	100%	100%	100%	100%	100%	100%	100%	>95%	PASS
L11-3U	. 92	100%	100%	100%	100%	100%	100%	100%	100%	100%	<i>≥</i> 93%	PASS

Table 6 Comparison of Image Quality between Array Probes (Test Device VS Reference Device)

probe modelenrollmen	t 2D	vessels filling	real time	reflux	brightness	reflux effect	spectrum boundary	contour	consistency	conclusion
2P2CC	93.6%	100%	100%	100%	98.9%	92.4%	95.7%	83.4%	>95%	DACC
94 SP5-1U	95.7%	100%	97.8%	100%	95.7%	77.4%	95.7%	92.4%	<i>≥</i> 93%	PASS

Table 7 Comparison of Image Quality between Volume Array Probes (Test Device VS Reference Device)

probe model	enrollment	2D	detail	structu re	vessels filling	brightness	distribute d	real-time	spectrum boundary	clarity	morphol ogy	consist ency	concl usion
4V4PD	0.4	100%	100%	100%	100%	98.9%	92.4%	100%	95.7%	93.5%	83.4%	>050/	PAS
D8-2U	84	100%	100%	97.8%	100%	95.7%	77.4%	100%	95.7%	96.7%	92.4%	≥95%	S

3.2 Adverse Events

Adverse Events (AEs): Five cases (1.4%) of transient pressure sensations during transducer application were reported. All resolved immediately post-examination and were deemed unrelated to device performance. No serious adverse events (SAEs) or device-related AEs/SAEs were observed.

3.3 Detection Rates

Detection rates varied by application (liver: 44%; thyroid: 31%; cardiac: 8%; uterus: 26%), which aligns with the known heterogeneity in clinical cases and target lesion visibility across different anatomical sites.

4 DISCUSSION

The ViV 80 system demonstrated statistically significant non-inferiority to the R**7 reference device (p<0.01 for all probe comparisons), achieving >95% image consistency across all anatomical applications. This performance parity was particularly notable in technically challenging scenarios:

Cardiac imaging maintained 95% consistency despite inherent motion artifacts

Thyroid evaluations showed perfect (100%) concordance in microstructural visualization

The observed variability in pathological detection rates (abdominal: 44%, thyroid: 31%, cardiac: 8%) directly correlated with:

- 1. Organ-specific disease prevalence in the study demographic [9]
- 2. Inherent echogenicity differences between parenchymal (liver) [10], cystic-solid (thyroid) [11], and dynamic (cardiac) tissues [12]
- 3. *Clinical indication bias* abdominal ultrasounds were more frequently ordered for symptomatic patients (e.g., pain, hepatomegaly), leading to higher detection rates of pathology [13,14]

42 Sheng Zhao, et al.

Safety monitoring confirmed zero device-related adverse events across all 363 examinations, with all reported discomforts (1.4%) representing expected transducer contact effects. The system maintained perfect operational reliability, with no probe failures or software malfunctions during intensive clinical use.

5 CONCLUSION

This prospective post-market clinical follow-up (PMCF) study provides robust evidence that the ViV 80 Color Doppler Ultrasound System meets or exceeds all key performance and safety benchmarks when compared to R**7 system. The comprehensive evaluation across four anatomical applications demonstrated:

1. Diagnostic Performance:

Sustained >95% image consistency in all clinical scenarios (liver, thyroid, cardiac, and uterine examinations) Equivalent detection capability for both common and subtle pathologies compared to the reference system

2. Operational Safety:

Zero device-related adverse events across 363 clinical applications

No operational failures or stability issues during intensive clinical use

3. Clinical Utility:

Demonstrated versatility across multiple specialties (cardiology, obstetrics/gynecology)

Seamless integration into existing clinical workflows

These findings validate the ViV 80 as a clinically equivalent, cost-effective alternative to premium ultrasound systems, with particular advantages in:

Resource-limited settings due to its competitive pricing

High-volume departments given its reliability

Teaching hospitals owing to consistent image standardization

Clinical Implications: The study supports the ViV 80's expanded adoption for routine diagnostic use while meeting all EU MDR post-market surveillance requirements. Healthcare facilities can consider this system as a viable option for both general and specialized ultrasound applications.

COMPETING INTERESTS

The authors have no relevant financial or non-financial interests to disclose.

CLINICAL TRIAL REGISTRATION

Not applicable - This study was performed as a non-interventional PMCF survey under MDR Article 74, without additional invasive or burdensome procedures.

ETHICS STATEMENT

This clinical study complies with the ethical principles derived from the Declaration of Helsinki, the international standard ISO 14155:2020, Clinical investigation of medical devices for human subjects-Good clinical practice and other applicable national standards. It was implemented after passing the ethics review, and the study protocol was not modified.

ACKNOWLEDGMENTS

The author would like to thank Lu Ju, Liu Mingzhu, Huang Zongjing, and Yin Lu (Attending Physicians, Ultrasound Diagnosis Department, Maternal and Child Health Hospital of Hubei Province, Wuhan, China) for their valuable support in subject examinations, data collection, and image evaluations. While not listed as co-authors, their contributions were essential to this study.

REFERENCES

- [1] European Parliament and the Council. Regulation (EU) 2017/745 on medical devices. Official Journal of the European Union. 2017. http://data.europa.eu/eli/reg/2017/745/oj.
- [2] European Commission. MEDDEV 2.7/1 revision 4: Guidelines on medical devices. European Commission Document. 2016. https://health.ec.europa.eu/document/download/e11b73e3-a7e0-4c2b-a950-c46e155871e2 en.
- [3] ISO. Clinical investigation of medical devices for human subjects Good clinical practice. ISO Standard 14155. 2020. https://www.iso.org/standard/71690.html.
- [4] NMPA. [Guidelines for clinical trial design of medical devices]. National Medical Products Administration. 2018. https://www.nmpa.gov.cn/directory/web/nmpa/images/MjAxOMTqtdo2usXNqLjmuL28i5kb2M=.doc.
- [5] NMPA. [Technical review guidelines for ultrasound diagnostic equipment (Class III)]. National Medical Products Administration. 2015. https://www.nmpa.gov.cn/directory/web/nmpa/images/1610962597329082242.doc.
- [6] Pearson K. Note on regression and inheritance in the case of two parents. Proceedings of the Royal Society of London. 1895, 58: 240-242.

- [7] Hair JF, Black WC, Babin BJ, et al. Multivariate data analysis (8th ed.). Boston: Cengage Learning, 2019.
- [8] Altman DG. Practical statistics for medical research. London: Chapman & Hall, 1991.
- [9] QuickStats: Percentage of adults aged ≥18 years with diagnosed heart disease, by urbanization level and age group National Health Interview Survey, United States, 2020. MMWR Morb Mortal Wkly Rep. 2022, 71(23): 778. DOI: 10.15585/mmwr.mm7123a4.
- [10] Mathiesen UL, Franzén LE, Aselius H, et al. Increased liver echogenicity at ultrasound examination reflects degree of steatosis but not of fibrosis in asymptomatic patients with mild/moderate abnormalities of liver transaminases. Digestive and Liver Disease. 2002, 34(7): 516-522. DOI: 10.1016/S1590-8658(02)80111-6.
- [11] Wu MH, Chen CN, Chen KY, et al. Quantitative analysis of echogenicity for patients with thyroid nodules. Scientific Reports. 2016, 6: 35632. DOI: 10.1038/srep35632.
- [12] Caminiti G, Volterrani M, Iellamo F, et al. Acute changes in myocardial work during isometric exercise in hypertensive patients with ischemic heart disease: A case–control study. Journal of Clinical Medicine. 2024, 13(19): 5955. DOI: 10.3390/jcm13195955.
- [13] Wen Z, Zhuang H. Value of acute ultrasonography in diagnosing right hypogastric acute abdomen. West China Medical Journal. 2010, 25(12): 2214-2217.
- [14] Ma'aji M, Jiya NMA, Saidu A, et al. Transabdominal ultrasonographic findings in children with sickle cell anemia in Sokoto, North-Western Nigeria. Nigerian Journal of Basic and Clinical Sciences. 2012, 9(1): 14-17.

Journal of Pharmaceutical and Medical Research

Print ISSN: 2663-1954 Online ISSN: 2663-1962

DOI: https://doi.org/10.61784/jpmr3045

MICRO-ADJUSTMENT MANIPULATION COMBINED WITH TRADITIONAL MANIPULATION FOR KNEE OSTEOARTHRITIS WITH VARUS DEFORMITY

KaiLong Sun, ShangJun Xia, Jian Zhang*

Department of Traditional Chinese Medicine, Hongmei Community Health Service Center, Shanghai 200231, China. Corresponding Author: Jian Zhang, Email: 2711810907@qq.com

Abstract: Objective: To observe the effect of micro-adjustment manipulation combined with traditional manipulation versus traditional manipulation alone in the treatment of varus knee osteoarthritis (KOA) by analyzing kinetic parameters, WOMAC scores, and clinical efficacy; and to explore the mechanism of adding micro-adjustment manipulation to traditional manipulation in the treatment of KOA. Methods: A total of 80 patients with varus knee osteoarthritis (7 cases dropped out during the process) were randomly divided into two groups. The combined group (n=37) received micro-adjustment manipulation during the first knee joint treatment, followed by traditional manipulations such as "One-Finger Meditation" and "Tui Fa." The traditional group (n=36) received only traditional manipulations such as "One-Finger Meditation" and "Tui Fa." Both groups were treated for 4 weeks, twice a week, one course of treatment lasting 4 weeks. WOMAC scores, kinetic parameters, and clinical efficacy were observed. Results:Osteoarthritis scales: After the first manipulation and after 4 weeks of manipulation, WOMAC scores, functional scores, and VAS scores in both groups were significantly lower than before treatment (P<0.05). After the first manipulation, the pain score in the micro-adjustment group decreased more significantly than that in the traditional group (P<0.05). After 4 weeks of treatment, the stiffness score in the combined group decreased significantly compared with before treatment (P<0.05). Kinetic parameters: After 4 weeks of manipulation, the flexion torque in both groups increased compared with before treatment (P<0.05). After the first manipulation, the adduction moment impulse in the combined group decreased significantly compared with before treatment (P<0.05). Clinical efficacy: The effective rates of the combined group after the first manipulation and after 4 weeks were 83.78% and 91.89%, respectively; while those of the traditional group were 80.56% and 91.67%, with no statistical difference. Conclusion: Both methods are effective for the treatment of KOA. The micro-adjustment manipulation of the knee joint has a better immediate analgesic effect, and the combination of micro-adjustment and traditional manipulations shows superior improvement in stiffness after one treatment course compared with traditional manipulations alone. The adduction moment impulse after the first treatment with micro-adjustment manipulation decreased significantly compared with before treatment.

Keywords: Varus knee osteoarthritis; Micro-adjustment manipulation; One-finger meditation; Tui Fa; Kinetic parameters

1 INTRODUCTION

Knee osteoarthritis (KOA) is a chronic degenerative joint disease. Epidemiological data show that the incidence of varus knee osteoarthritis in middle-aged and elderly women in China is 60%–70%[1]. Pain and functional impairment are the main clinical manifestations of KOA. In traditional Chinese medicine (TCM), KOA corresponds to the diagnosis of "Gu Bi" (bone impediment). In recent years, the clinical efficacy of Tuina therapy for KOA has been widely recognized, and micro-adjustment manipulation for knee osteoarthritis has also been extensively studied[2]. In the Shanghai school of Tuina, traditional manipulations such as "One-Finger Meditation" and "Tui Fa" are mainly used to promote blood circulation, resolve the pathological factors leading to "tendon injury," and restore the tendon functions of "binding bones" and "facilitating joints"[3]. Micro-adjustment manipulation has shown good immediate clinical effects, but its long-term efficacy is not as significant as traditional Tuina[4]. Therefore, this study conducted a preliminary investigation comparing micro-adjustment manipulation combined with traditional manipulations versus traditional manipulations alone. The results are reported as follows.

2 CLINICAL DATA AND METHODS

2.1 General Information

A total of 80 patients with diagnosed varus knee osteoarthritis, all middle-aged and elderly women, who received treatment between January 2024 and August 2025 at the Tuina Department of Putuo Traditional Chinese Medicine Hospital in Shanghai, the Tuina Department of Hongmei Community Health Service Center in Xuhui District of Shanghai, the Tuina Department of Longhua Hospital Affiliated to Shanghai University of Traditional Chinese Medicine, the Tuina Department of Yueyang Hospital of Integrated Traditional Chinese and Western Medicine Affiliated to Shanghai University of Traditional Chinese Medicine, and the Tuina Department of Shanghai Eighth

People's Hospital, were enrolled in this clinical observation. Patients were randomly assigned into two groups. During the clinical process, 7 cases dropped out for various reasons. Finally, 73 patients were included in the study, with 37 in the combined group and 36 in the traditional group.

Table 1 Comparison of Baseline Characteristics between the Two Groups

Variable	Combination group (n=37)	Traditional group (n=36)	P value
Height (cm)	162.51 ± 6.21	162.11 ± 6.69	0.798
Age (years)	62.34 ± 9.03	60.21 ± 9.61	0.568
$BMI (kg/m^2)$	24.19 ± 1.99	24.51 ± 2.01	0.723
Weight (kg)	62.07 ± 8.05	64.14 ± 8.97	0.811
Right knee (cases)	17	15	
Left knee (cases)	20	21	0.506

From the analysis of the above table 1, the average height of patients in the combined group and the traditional group was 162.51 ± 6.21 cm and 162.11 ± 6.69 cm, respectively, with no statistically significant difference between the two groups (P>0.05). The average age of the combined group and the traditional group was 62.34 ± 9.03 years and 60.21 ± 9.61 years, respectively, with no statistically significant difference between the two groups (P>0.05). The average BMI of the combined group and the traditional group was 24.19 ± 1.99 kg/m² and 24.51 ± 2.01 kg/m², respectively, with no statistically significant difference between the two groups (P>0.05). The average body weight of the combined group and the traditional group was 62.07 ± 8.05 kg and 64.14 ± 8.97 kg, respectively, with no statistically significant difference between the two groups (P>0.05). In the combined group, there were 17 cases of KOA affecting the right knee and 20 cases affecting the left knee; in the traditional group, there were 15 cases of right knee KOA and 21 cases of left knee KOA, with no statistically significant difference between the two groups (P>0.05). Therefore, the two groups were comparable.

2.2 Diagnostic Criteria

- (1) Clinical diagnostic criteria: According to the Guidelines for the Diagnosis and Treatment of Osteoarthritis in China (2021 edition) issued by the Orthopedics Branch of the Chinese Medical Association[5].
- (2) Knee pain for most of the time during the previous month.
- (3) X-ray (standing position) showing narrowing of the knee joint space, osteophyte formation at the joint margins, subchondral bone sclerosis and/or cystic changes.
- (4) Age \geq 50 years.
- (5) Morning stiffness \leq 30 minutes.
- (6) Crepitus during joint movement.

A diagnosis of KOA can be established if item (1) is met, plus any two of items (2), (3), (4), and (5).

2.3 Inclusion Criteria

- (1) Patients meeting the diagnostic criteria for knee osteoarthritis (KOA), clinically classified as the middle stage: frequent severe pain; recurrent swelling; mild varus or valgus deformity of the knee joint may be present; imaging showing definite joint space narrowing, moderate osteophytes, mild subchondral bone sclerosis, and possible bony deformity of the knee joint; Kellgren–Lawrence (K-L) grade III[6].
- (2) Patients with varus knee osteoarthritis: full-length lower limb radiographs showing the mechanical axis passing through the medial side of the center point of the tibial plateau, more than 2 mm from the midpoint.
- (3) Patients able to walk independently (without assistive devices).
- (4) Female patients aged 50–70 years.
- (5) BMI $\leq 28 \text{ kg/m}^2$.
- (6) Voluntarily participating in this clinical observation and signing informed consent.

2.4 Exclusion Criteria

- (1) Knee osteomyelitis, tuberculosis, tumors, etc.
- (2) History of knee surgery or trauma.
- (3) Neurological diseases such as Parkinson's disease or cerebrovascular disease.
- (4) Mental illness or cardiovascular disease preventing cooperation with gait analysis.
- (5) Receiving treatment for KOA (e.g., NSAIDs, acupuncture, Tuina, rehabilitation) within 4 weeks prior to enrollment.

3 TREATMENT METHODS

3.1 Combined Group

46 KaiLong Sun, et al.

The Tuina regimen for this group consisted of two steps. The first treatment used knee micro-adjustment manipulation, and the subsequent treatments mainly adopted Ding's Tuina techniques of One-Finger Meditation and Tui Fa (reference: Cao Renfa Clinical Experience Collection). Treatment was administered twice per week, with one treatment course lasting four weeks.

3.1.1 First treatment

Micro-adjustment of the patellofemoral and tibiofemoral joints: The patient was seated, facing the practitioner. The practitioner placed the patient's affected ankle joint in the anatomical neutral position. Both thumbs of the practitioner were positioned at the medial and lateral "knee eyes" below the patella, pushing upward and backward, while the other four fingers encircled the patellar fossa. The tibia was rotated to mobilize the tibiofemoral joint, while the patient, following verbal instructions, performed slow sit-to-stand movements. This procedure was repeated three times. Subsequently, the practitioner used four-finger kneading techniques on the affected lateral thigh muscles, posterior thigh, popliteal fossa, and posterior calf[7].

3.1.2 Subsequent treatments

Traditional One-Finger Meditation and Tui Fa were applied (reference: *Cao Renfa Tuina Academic Experience Collection*). The patient was placed in the supine position. First, One-Finger Meditation manipulation was applied to Xuehai (SP10), Heding (EX-LE2), Futu (ST32), Liangqiu (ST34), Dubi (ST35), and Neixiyan (EX-LE4) for approximately 3 minutes. Then, Tui Fa was applied to the quadriceps muscle above the patella for about 3 minutes. Next, the practitioner grasped the patella with the palm and performed gentle circular rubbing until mild heat was felt at the patellofemoral joint, lasting about 3 minutes. The patient was then placed in the prone position, and the practitioner's middle fingers were placed on the medial and lateral heads of the gastrocnemius and the hamstring muscles to perform transverse manipulations. Tui Fa was then applied to the posterior thigh, popliteal fossa, and posterior calf, followed by pressing and kneading of Weizhong (BL40), Chengshan (BL57), and Chengjin (BL56), until the patient reported a sensation of soreness and distension, lasting about 3 minutes. Finally, the patient returned to the supine position, where passive knee flexion, extension, internal rotation, and external rotation were performed in combination with flexion-shaking manipulation. The session was concluded with rubbing around the knee joint until warmth was generated [8].

3.2 Traditional Group

This group was treated with the traditional methods of One-Finger Meditation and Tui Fa (reference: Cao Renfa Tuina Academic Experience Collection), twice per week for four weeks, constituting one treatment course[9].

4 EFFICACY OBSERVATION

4.1 Observation Indicators

Data were collected before Tuina treatment, after the first Tuina session, and after four weeks of Tuina treatment, including osteoarthritis scales and kinematic parameters.

4.1.1 Primary outcome measures

Knee joint torques: KAM (knee adduction moment), KFM (knee flexion moment), KAMI (knee adduction moment impulse).

4.1.2 Secondary outcome measures: WOMAC index.

4.1.3 Criteria for clinical efficacy

According to the criteria for the efficacy of "Gu Bi" (bone impediment) in the Standards for the Diagnosis and Efficacy of TCM Syndromes issued by the Ministry of Health of the People's Republic of China:

- (1) Symptom control: Symptoms completely disappear, joint function is restored to normal, and major laboratory and imaging indicators return to normal.
- (2) Markedly effective: Main symptoms disappear, joint function basically recovers, patients can resume normal work and activities, and major laboratory and imaging indicators are basically normal or show great improvement.
- (3) Improved: Main symptoms are mostly relieved, joint function basically recovers or shows significant progress, patients regain the ability to live independently, and laboratory and imaging indicators show some improvement.
- (4) Ineffective: No improvement in symptoms or signs.

5 STATISTICAL ANALYSIS

All statistical analyses were performed using SPSS version 26.0 (IBM Corp, Armonk, NY, USA). Continuous variables were expressed as mean \pm standard deviation (SD). Within-group comparisons were conducted using paired t-tests, and between-group comparisons using independent-sample t-tests, provided that data met assumptions of normality and homogeneity of variance. For non-normally distributed data, nonparametric rank-sum tests were applied. Repeated-measures ANOVA was used for longitudinal analyses. Categorical variables, including clinical efficacy outcomes, were compared using chi-square tests. A P value < 0.05 was considered statistically significant.

6 TREATMENT RESULTS

6.1 WOMAC Scores of the Knee Joint

6.1.1 Total WOMAC score

Table 2 Comparison of Total WOMAC Scores between the Two Groups

Time point	Combination group (n=37)	Traditional group (n=36)	Pbetween	Pwithina (Before vs 1st tuina)	Pwithinb (Before vs 4 weeks)
Before tuina	89.89 ± 10.11	89.68 ± 11.28	0.939	_	
After first tuina	67.12 ± 10.01	66.18 ± 10.59	0.712	< 0.01	_
After 4 weeks of tuina	58.86 ± 7.72	58.18 ± 10.15	0.726	_	< 0.01

From the analysis of the above table 2: In the combined group, the total WOMAC scores before Tuina, after the first Tuina session, and after four weeks of Tuina were 89.89 ± 10.11 , 67.12 ± 10.01 , and 58.86 ± 7.72 , respectively. In the traditional group, the corresponding total scores were 89.68 ± 11.28 , 66.18 ± 10.59 , and 58.18 ± 10.15 , respectively.

Overall, after manipulation treatment, the total scores of both groups decreased with the extension of treatment time, indicating that manipulation can improve patient function and symptoms. Within-group comparisons: After the first Tuina session and after four weeks of treatment, the total WOMAC scores of both groups decreased significantly compared with those before treatment (P < 0.05). Between-group comparisons: Before treatment, there was no statistically significant difference in total WOMAC scores between the two groups (P > 0.05), indicating comparability. After the first Tuina session and after four weeks of treatment, there was no statistically significant difference in total WOMAC scores between the combined group and the traditional group (P > 0.05).

6.1.2 Stiffness score

Table 3 Comparison of Stiffness Scores between the Two Groups

Time point	Combination group (n=37)	Traditional group (n=36)	Pbetween	Pwithina (Before vs 1st tuina)	Pwithinb (Before vs 4 weeks)
Before tuina	6.91 ± 2.81	6.56 ± 2.73	0.667	_	_
After first tuina	6.44 ± 2.30	6.00 ± 2.41	0.525	0.604	_
After 4 weeks of tuina	5.52 ± 2.81	6.17 ± 2.33	0.303	_	< 0.05

From the analysis of the above table 3: In the combined group, the WOMAC stiffness scores before Tuina, after the first Tuina session, and after four weeks of Tuina were 6.91 \pm 2.81, 6.44 \pm 2.30, and 5.52 \pm 2.81, respectively. In the traditional group, the corresponding scores were 6.56 \pm 2.73, 6.00 \pm 2.41, and 6.17 \pm 2.33, respectively.

Overall, after manipulation treatment, the stiffness scores of both groups showed a decreasing trend over time, suggesting that manipulation can improve patients' functional mobility. Within-group comparisons: After the first Tuina session and after four weeks of treatment, stiffness scores in both groups decreased compared with those before treatment. The reduction in the combined group after four weeks was statistically significant (P < 0.05). Between-group comparisons: Before treatment, there was no statistically significant difference in stiffness scores between the two groups (P > 0.05), indicating comparability. After the first Tuina session and after four weeks of treatment, there was no statistically significant difference in stiffness scores between the combined group and the traditional group (P > 0.05).

6.1.3 Function score

Table 4 Comparison of WOMAC Function Scores between the Two Groups

Time point	Combination group (n=37)	Traditional group (n=36)	Pbetween	Pwithina (Before vs 1st tuina)	Pwithinb (Before vs 4 weeks)
Before tuina	65.32 ± 7.39	65.10 ± 7.34	0.617	_	_
After first tuina	47.89 ± 8.98	46.01 ± 9.24	0.199	< 0.01	_
After 4 weeks of tuina	43.19 ± 6.47	41.54 ± 9.01	0.293	_	<0.01

From the analysis of the above table 4: In the combined group, the WOMAC function scores before Tuina, after the first Tuina session, and after four weeks of Tuina were 65.32 ± 7.39 , 47.89 ± 8.98 , and 43.19 ± 6.47 , respectively. In the traditional group, the corresponding scores were 65.10 ± 7.34 , 46.01 ± 9.24 , and 41.54 ± 9.01 , respectively. Overall, after manipulation treatment, the function scores of both groups decreased over time, indicating that manipulation could improve patients' daily living ability. Within-group comparisons: After the first Tuina session and after four weeks of treatment, the function scores in both groups decreased significantly compared with those before treatment (P < 0.05). Between-group comparisons: Before treatment, there was no statistically significant difference in

48 KaiLong Sun, et al.

function scores between the two groups (P > 0.05), indicating comparability. After the first Tuina session and after four weeks of treatment, there was no statistically significant difference in function scores between the combined group and the traditional group (P > 0.05).

6.1.4 VAS score

Table 5 Comparison of VAS Scores between the Two Groups

Time point	Combination group (n=37)	Traditional group (n=36)	Pbetween	Pwithina (Before vs 1st tuina)	Pwithinb (Before vs 4 weeks)
Before tuina	20.02 ± 5.03	19.31 ± 5.51	0.568	_	_
After first tuina	12.03 ± 2.72	14.41 ± 3.52	< 0.05	< 0.01	_
After 4 weeks of tuina	9.61 ± 2.98	9.93 ± 2.42	0.714		< 0.01

From the analysis of the above table 5: In the combined group, the VAS scores before Tuina, after the first Tuina session, and after four weeks of Tuina were 20.02 ± 5.03 , 12.03 ± 2.72 , and 9.61 ± 2.98 , respectively. In the traditional group, the corresponding scores were 19.31 ± 5.51 , 14.41 ± 3.52 , and 9.93 ± 2.42 , respectively.

Overall, after manipulation treatment, the VAS scores of both groups decreased over time. After the first Tuina session, the reduction in VAS score in the combined group was significantly greater than that in the traditional group. Within-group comparisons: After the first Tuina session and after four weeks of treatment, VAS scores in both groups were significantly lower than those before treatment (P < 0.05). Between-group comparisons: Before treatment, there was no statistically significant difference in VAS scores between the two groups (P > 0.05), indicating comparability. After the first Tuina session, the combined group showed a significantly greater reduction in VAS scores compared with the traditional group (P < 0.05). After four weeks of treatment, however, there was no statistically significant difference in VAS scores between the two groups (P > 0.05).

6.2 Kinematic Parameters of the Knee Joint

6.2.1 Knee adduction moment (KAM)

Table 6 Comparison of hip Adduction torque (Nm/kg \times 10⁻¹) between the Two Groups

Time point	Combination group (n=37)	Traditional group (n=36)	Pbetween	Pwithina (Before vs 1st tuina)	Pwithinb (Before vs 4 weeks)
Before tuina	2.41 ± 0.74	2.37 ± 0.70	0.849	_	_
After first tuina	2.50 ± 0.77	2.44 ± 0.72	0.898	0.714	_
After 4 weeks of tuina	2.65 ± 0.59	2.63 ± 0.63	0.803	_	0.049

From the analysis of the above table 6: In the combined group, the KAM values before Tuina, after the first Tuina session, and after four weeks of Tuina were 2.41 \pm 0.74 Nm/kg \times 10⁻¹, 2.50 \pm 0.77 Nm/kg \times 10⁻¹, and 2.65 \pm 0.59 Nm/kg \times 10⁻¹, respectively. In the traditional group, the corresponding values were 2.37 \pm 0.70 Nm/kg \times 10⁻¹, 2.44 \pm 0.72 Nm/kg \times 10⁻¹, and 2.63 \pm 0.63 Nm/kg \times 10⁻¹.

Overall, after manipulation treatment, the KAM of both groups showed an upward trend over time, suggesting that manipulation could enhance patients' KAM. Within-group comparisons: After the first Tuina session and after four weeks of treatment, KAM values in both groups increased compared with those before treatment, but the differences were not statistically significant (P > 0.05). Between-group comparisons: Before treatment, there was no statistically significant difference in KAM values between the two groups (P > 0.05), indicating comparability. After the first Tuina session and after four weeks of treatment, there were still no statistically significant differences in KAM values between the combined group and the traditional group (P > 0.05).

6.2.2 Knee flexion moment (KFM)

Table 7 Comparison of Knee Flexion Torque (Nm/kg \times 10⁻¹) between the Two Groups

Time point	Combination group (n=37)	Traditional group (n=36)	Pbetween	Pwithina (Before vs 1st tuina)	Pwithinb (Before vs 4 weeks)
Before tuina	1.09 ± 0.59	1.05 ± 0.39	0.849	_	
After first tuina	1.20 ± 0.58	1.18 ± 0.51	0.930	0.921	_
After 4 weeks of tuina	1.51 ± 0.77	1.54 ± 0.71	0.791	_	< 0.05

From the analysis of the above table 7: In the combined group, the KFM values before Tuina, after the first Tuina session, and after four weeks of Tuina were 1.09 \pm 0.59 Nm/kg \times 10⁻¹, 1.20 \pm 0.58 Nm/kg \times 10⁻¹, and 1.51 \pm

0.77 Nm/kg \times 10^{-1} , respectively. In the traditional group, the corresponding values were 1.05 ± 0.39 Nm/kg \times 10^{-1} , 1.18 ± 0.51 Nm/kg \times 10^{-1} , and 1.54 ± 0.71 Nm/kg \times 10^{-1} .

Overall, after manipulation treatment, the KFM of both groups increased over time, suggesting that manipulation could improve patients' KFM. Within-group comparisons: After the first Tuina session and after four weeks of treatment, the KFM values of both groups increased compared with those before treatment. At four weeks, KFM values in both groups were significantly higher than baseline (P < 0.05). However, after the first Tuina session, the increase was not statistically significant compared with baseline (P > 0.05). Between-group comparisons: Before treatment, there was no statistically significant difference in KFM values between the two groups (P > 0.05), indicating comparability. After the first Tuina session and after four weeks of treatment, there were no statistically significant differences in KFM values between the combined group and the traditional group (P > 0.05).

6.2.3 Knee adduction moment impulse (KAMI)

Table 8 Comparison of Hip Adduction Torque Impulse (Nm/kg × 10⁻¹) between the Two Groups

Time point	Combination group (n=37)	Traditional group (n=36)	Pbetween	Pwithina (Before vs 1st tuina)	Pwithinb (Before vs 4 weeks)
Before tuina	2.57 ± 0.59	2.61 ± 0.52	0.811	_	_
After first tuina	2.21 ± 0.61	2.30 ± 0.42	0.521	< 0.05	_
After 4 weeks of tuina	2.30 ± 0.66	2.22 ± 0.51	0.729	_	< 0.05

From the analysis of the above table 8: In the combined group, the KAMI values before Tuina, after the first Tuina session, and after four weeks of Tuina were 2.57 \pm 0.59 Nm/kg \times 10⁻¹, 2.21 \pm 0.61 Nm/kg \times 10⁻¹, and 2.30 \pm 0.66 Nm/kg \times 10⁻¹, respectively. In the traditional group, the corresponding values were 2.61 \pm 0.52 Nm/kg \times 10⁻¹, 2.30 \pm 0.42 Nm/kg \times 10⁻¹, and 2.22 \pm 0.51 Nm/kg \times 10⁻¹.

Overall, after manipulation treatment, the KAMI of both groups showed a downward trend over time, suggesting that manipulation could reduce KAMI. Within-group comparisons: After the first Tuina session and after four weeks of treatment, KAMI values in both groups decreased compared with those before treatment. In the traditional group, the reduction at four weeks compared with baseline was statistically significant (P < 0.05). In the combined group, the reduction after the first Tuina session compared with baseline was statistically significant (P < 0.05). However, in the combined group at four weeks, and in the traditional group after the first session, the reductions were not statistically significant (P > 0.05). Between-group comparisons: Before treatment, there was no statistically significant difference in KAMI values between the two groups (P > 0.05), indicating comparability. After the first Tuina session and after four weeks of treatment, there were still no statistically significant differences in KAMI values between the combined group and the traditional group (P > 0.05).

6.3 Clinical Efficacy Evaluation after Tuina in Both Groups

6.3.1 Comparison of clinical efficacy after the first Tuina session

Table 9 Comparison of Clinical Efficacy after the First Tuina Session between the Two Groups (%)

Group	n	Symptom controlled	Markedly effective	Improved	Ineffective	Effective rate (%)	P value
Combination group	37	5	6	20	6	83.78	0.598
Traditional group	36	3	7	19	7	80.56	

After the first Tuina session, in the combined group, 5 cases achieved symptom control, 6 cases were markedly effective, 31 cases effective, and 6 cases ineffective, with a total effective rate of 83.78%. In the traditional group, 3 cases achieved symptom control, 7 cases were markedly effective, 28 cases effective, and 7 cases ineffective, with a total effective rate of 80.56%. Chi-square test analysis showed no statistically significant difference in efficacy between the two groups (P > 0.05) (Table 9).

6.3.2 Comparison of clinical efficacy after four weeks of Tuina

Table 10 Comparison of Clinical Efficacy after 4 Weeks of Tuina Treatment between the Two Groups (%)

	n	Symptom controlled	Markedly effective	Improved	Ineffective	Effective rate (%)	P value
Combination group	37	8	14	12	3	91.89	0.634
Traditional group	36	7	14	12	3	91.67	

50 KaiLong Sun, et al.

After four weeks of Tuina, in the combined group, 8 cases achieved symptom control, 14 cases were markedly effective, 34 cases effective, and 6 cases ineffective, with a total effective rate of 91.89%. In the traditional group, 7 cases achieved symptom control, 14 cases were markedly effective, 33 cases effective, and 3 cases ineffective, with a total effective rate of 91.67%. Chi-square test analysis showed no statistically significant difference in efficacy between the two groups (P > 0.05) (Table 10).

7 DISCUSSION

Knee osteoarthritis (KOA) is a degenerative disease caused by multiple factors, characterized by fibrosis, fissures, ulcers, and loss of articular cartilage, with joint pain as the main symptom. The primary clinical manifestations are pain and functional limitation[10]. The prevalence of KOA in China is 18%, with 11% in men and 19% in women, predominantly in middle-aged and elderly women. Due to the unique structural characteristics of the knee joint, the varus type of KOA is commonly seen in clinical practice[11]. Therefore, this study selected middle-aged and elderly women as the study population. In stepwise treatment protocols, non-surgical interventions are the main focus of research[12]. Evidence-based medicine has demonstrated that Tuina therapy is effective in the treatment of KOA. A systematic review published in 2021 found that Tuina manipulations were superior to non-steroidal anti-inflammatory drugs in improving knee pain, stiffness, and daily function in KOA patients[13]. This disease is also part of chronic disease management in community health practice, and TCM Tuina accounts for a certain proportion in community treatment of KOA. Therefore, related research on Tuina therapy for KOA has been continuously explored in depth.In traditional Chinese medicine theory, KOA falls under the category of "Bi syndrome" caused by the invasion of pathogenic wind, cold, and dampness, which may further transform into heat. The main symptoms include soreness, numbness, heaviness of the limbs and joints, difficulty in flexion and extension, joint swelling, and burning sensation. The etiology and pathogenesis are related both to external invasion of wind, cold, dampness, or heat pathogens, and to insufficiency of the body's vital qi. Clinically, Bi syndrome is generally classified into pain Bi, wandering Bi, fixed Bi, and heat Bi.

The knee micro-adjustment manipulation is developed on the basis of the characteristic techniques of Ding's Tuina school, combined with the concept of joint mobilization from modern medicine. It mainly targets the adjustment of lower-limb mechanical alignment. During treatment, the ankle and knee joints are fixed in relatively normal anatomical positions. The practitioner places both thumbs on the medial and lateral "knee eyes" (the areas at the lower edge of the patella), with the other four fingers encircling the posterior knee, applying internal and external rotational mobilization to the tibia. Meanwhile, the patient is guided to perform active knee extension and standing movements within the physiological range of the knee joint, with the knee kept as straight as possible. In the Shanghai school of Tuina, traditional manipulations such as One-Finger Meditation and Tui Fa are the core methods. The "knee micro-adjustment manipulation" has been proven to produce good immediate effects[14]. In this study, we adopted a KOA treatment strategy that combined micro-adjustment with traditional manipulations under the principle of "treating both muscles and bones," and compared it with traditional manipulations alone. The efficacy was assessed objectively using gait analysis, which includes motion analysis, force platform analysis, stride analysis, surface electromyography, and energy expenditure. Among these, spatiotemporal parameters and kinematic parameters have been the main focus in previous Tuina efficacy studies for KOA, while kinetic parameters have been rarely investigated. Kinetic parameters are divided into knee and hip joint moments. Knee joint moments include the knee adduction moment (KAM), knee flexion moment (KFM), and knee adduction moment impulse (KAMI). Therefore, in this study, the primary observation indicators were kinetic parameters, while the secondary indicators were the WOMAC index and clinical efficacy.

The results showed:Kinetic parameters: After four weeks of Tuina, KFM increased in both groups compared with baseline (P < 0.05). After the first Tuina session, KAMI in the combined group was significantly lower than before treatment (P < 0.05). Osteoarthritis scales: After the first Tuina session and at four weeks, WOMAC scores, function scores, and VAS scores all significantly decreased in both groups compared with baseline (P < 0.05). After the first session, pain scores decreased significantly more in the combined group compared with the traditional group (P < 0.05). After four weeks, stiffness scores in the combined group were also significantly reduced compared with baseline (P < 0.05). Clinical efficacy: The effective rates in the combined group after the first session and after four weeks were 83.78% and 91.89%, respectively; in the traditional group, they were 80.56% and 91.67%, respectively.

These findings suggest that both the combined therapy and traditional manipulations are effective for KOA. However, the micro-adjustment manipulation showed superior immediate analgesic effects, and the combined therapy was superior in improving stiffness after one course of treatment. Moreover, the significant reduction of KAMI after the first micro-adjustment treatment may indicate a decrease in knee joint loading.

We believe that Tuina may treat KOA primarily by reducing pain and improving joint function. Pain relief may result from promoting blood circulation, thereby lowering the concentration of local algogenic substances such as prostaglandin II, and alleviating aseptic inflammation. Functional improvement is mainly achieved by enhancing knee flexion – extension, tibial internal – external rotation, and restoring quadriceps muscle strength and tone. According to the TCM theory of "tendons and bones," malalignment of the tibiofemoral and patellofemoral joints is considered a "bone displacement," while dysfunction in the coordinated activity of the quadriceps femoris and tibialis anterior is regarded as "tendon displacement." The knee micro-adjustment manipulation, through a combination of active and passive patient movements, allows the practitioner to adjust the tibiofemoral joint space, thereby altering lower-limb mechanical alignment and intra-articular dynamic loading of the knee joint. At the same time, incorporating the modern

rehabilitation concept of joint mobilization, this manipulation may release adhesions in periarticular soft tissues, reduce local muscle tension, and improve joint function. In summary, the therapeutic mechanism of combining micro-adjustment with traditional manipulations (One-Finger Meditation and Tui Fa) for KOA may lie in the following: micro-adjustment improves tibial platform rotational function and sagittal sliding function of the patellofemoral and tibiofemoral joints, while traditional manipulations restore coordination and balance of the corresponding lower-limb muscle groups. Together, these effects produce analgesia and relieve stiffness, thereby treating KOA. Although this approach merely involves a modification that integrates active and passive motion, it optimizes Tuina treatment outcomes for varus-type KOA and represents a breakthrough in Tuina clinical practice. Moreover, Tuina therapy has the advantages of minimal side effects and low medical costs, not only reducing the adverse effects of pharmacological treatment and overall treatment expenses for patients but also lessening the burden on health insurance systems.

However, this clinical study did not classify the gait parameters of varus knee osteoarthritis, such as walking speed, stride length, and swing phase. Future studies could incorporate subgroup analyses based on different gait parameters to more objectively observe changes in kinetic parameters before and after Tuina treatment.

COMPETING INTERESTS

The authors have no relevant financial or non-financial interests to disclose.

REFERENCES

- [1] Zeng QY, Huang SB, Xiao ZY, et al. Clinical and epidemiological study of symptomatic osteoarthritis. Chinese Journal of Internal Medicine, 1995, 34(2): 88–90.
- [2] Fu YY, Gong L, Shao S, et al. Progress in tuina manipulation therapy for knee osteoarthritis. Massage and Rehabilitation Medicine, 2017, 8(14): 36–37.
- [3] Li YH, Chen YF, Qin WK, et al. Anatomical essence of "tendon" in traditional Chinese medicine. Shaanxi Journal of Traditional Chinese Medicine, 2019, 40(3): 374–377.
- [4] Liang HG, Jiang SY, Li JH, et al. Efficacy and gait analysis of the sitting knee-adjusting manipulation for knee osteoarthritis. Beijing Journal of Traditional Chinese Medicine, 2018, 37(2): 135–138.
- [5] Xie ZQ, Cui LM, Wang YS, et al. Anatomical analysis of lesion points in "Jiejin disease". Global Traditional Chinese Medicine, 2019, 12(10): 1569–1570.
- [6] Liang HG, Jiang SY, Li JH, et al. Efficacy and gait analysis of the sitting knee-adjusting manipulation for knee osteoarthritis. Beijing Journal of Traditional Chinese Medicine, 2018, 37(2): 135–138.
- [7] Chinese Orthopaedic Association (COA) Joint Surgery Group, Chinese Medical Doctor Association Orthopaedic Branch Osteoarthritis Group, National Clinical Research Center for Geriatric Diseases (Xiangya Hospital), et al. Chinese guideline for the diagnosis and treatment of osteoarthritis (2021 edition). Chinese Journal of Orthopaedics, 2021, 41(18): 1291–1314.
- [8] Wang B, Yu NS. Expert consensus on the stepwise treatment of knee osteoarthritis (2018 edition). Chinese Journal of Joint Surgery (Electronic Edition), 2019, 13(1): 124–130.
- [9] Kang ZR, Gong L, Xing H, et al. Preliminary exploration on the concept and principle of the sitting knee-adjusting manipulation for knee osteoarthritis. Journal of Shanghai University of Traditional Chinese Medicine, 2020, 34(4): 98–102.
- [10] Gu F. Professor Cao Renfa's Manipulative Techniques and Clinical Experience. Shanghai: Shanghai Scientific and Technical Literature Publishing House, 2016.
- [11] Chinese Orthopaedic Association (COA) Joint Surgery Group, et al. Chinese guideline for the diagnosis and treatment of osteoarthritis (2021 edition). Chinese Journal of Orthopaedics, 2021, 41(18): 1291–1314.
- [12] Wang B, Xing D, Dong SJ, et al. Consensus on the epidemiology and disease burden of knee osteoarthritis in China (2018 edition). Chinese Journal of Joint Surgery (Electronic Edition), 2019, 13(1): 124–130.
- [13] Hua X, Sun JY, Li G, et al. Therapeutic massage for knee osteoarthritis: a systematic review and meta-analysis of randomized controlled trials. Journal of Acupuncture and Tuina Science, 2021, 19(5): 354–363.
- [14] Xie ZQ, Cui LM, Wang YS, et al. Anatomical analysis of lesion points in "Jiejin disease". Global Traditional Chinese Medicine, 2019, 12(10): 1569–1570.

Journal of Pharmaceutical and Medical Research

Print ISSN: 2663-1954 Online ISSN: 2663-1962

DOI: https://doi.org/10.61784/jpmr3046

OPTIMIZATION OF NIPT TIMING FOR MALE FETUSES AND ABNORMALITY DETECTION IN FEMALE FETUSES BASED ON QUALITY-CORRECTED MODELS

ZhiJian Dai*, LinYv Yang, Kun Li, ZongSheng Wang, YiFeng Liu, JunRan Zhao, Liang Xia College of Public Health and Health Sciences, Tianjin University of Traditional Chinese Medicine, Tianjin 301617, China

Corresponding Author: ZhiJian Dai, Email: dai1603703247@outlook.com

Abstract: This study aims to enhance the accuracy of non-invasive prenatal testing (NIPT) by optimizing detection timing for male fetuses and improving abnormality diagnosis for female fetuses. For male fetuses, a multivariate nonlinear regression model quantified the associations of Y-chromosome fraction with gestational weeks and maternal BMI, revealing quadratic and decreasing trends, respectively. Ordered clustering and a risk-based optimization identified four BMI groups with distinct optimal testing windows, where higher BMI delayed the best timing. Monte Carlo simulations further confirmed sequencing quality as the main error source. For female fetuses, a combined logistic regression–random forest model was developed using standardized Z-scores and quality indicators, with an optimal diagnostic threshold ($\tau = 0.35$). The resulting workflow integrates quality screening, Z-score assessment, probability evaluation, and BMI-specific correction. These models provide clinically interpretable guidance to improve NIPT reliability and prenatal decision-making.

Keywords: NIPT; Nonlinear regression; Ordered clustering; Multi-objective optimization; Female fetal abnormality detection

1 INTRODUCTION

Non-invasive prenatal testing (NIPT) has become a widely adopted screening approach for common fetal chromosomal abnormalities, such as trisomy 21, trisomy 18, and trisomy 13 [1]. By analyzing cell-free fetal DNA (cffDNA) fragments circulating in maternal plasma, NIPT provides an accurate, safe, and non-invasive alternative to traditional prenatal diagnostic techniques [2-3]. Compared with invasive methods, NIPT substantially reduces the risks of miscarriage and maternal complications, while offering high sensitivity and specificity within the clinical detection window of 10–25 weeks of gestation [4-5].

However, the accuracy of NIPT results depends strongly on the proportion of fetal chromosomal fractions in maternal blood [6]. In male fetuses, Y-chromosome concentration serves as the primary marker [7], whereas in female fetuses, Z-scores of autosomes and the X-chromosome are generally adopted [8]. Clinical evidence indicates that fetal chromosomal fraction is significantly influenced by maternal gestational weeks and body mass index (BMI) [9]. In particular, higher BMI is associated with lower fetal fraction due to increased background DNA from adipose tissue, which may lead to test failure, false negatives, or delayed detection. Conversely, earlier gestational testing (before 12 weeks) may yield insufficient fetal fraction, but postponing testing increases clinical intervention risks [10]. Thus, selecting the optimal testing time point is a critical factor for improving NIPT reliability and ensuring effective clinical decision-making.

Previous studies have attempted to address this challenge by grouping pregnant women according to BMI and adopting uniform testing schedules [11]. Yet, such approaches fail to fully account for individual differences in maternal characteristics, sequencing quality, and biological variability. Consequently, there is a pressing need for quantitative methods to model the relationship between fetal fraction and maternal factors, so as to identify optimal NIPT timing that balances early detection with diagnostic accuracy.

Another challenge lies in abnormality detection for female fetuses. Since female fetuses lack Y-chromosome markers, alternative approaches rely on autosomal and sex-chromosomal Z-scores, adjusted by sequencing quality indicators. Nevertheless, standard Z-score thresholds may be unreliable under conditions of low sequencing depth or high maternal BMI, leading to missed or ambiguous diagnoses. Developing quality-corrected models that integrate statistical learning with clinical interpretability can therefore provide more robust detection pipelines.

In this study, a comprehensive quality-corrected modeling framework for NIPT is proposed. For male fetuses, multivariate nonlinear regression models are constructed to quantify the effects of gestational weeks and BMI on Y-chromosome fraction, followed by ordered clustering and risk-based optimization to determine optimal detection windows across BMI subgroups. Monte Carlo simulations are further employed to assess robustness under measurement errors and sequencing variability. For female fetuses, a dual-model diagnostic strategy combining logistic regression with random forest classification, integrating Z-score normalization, sequencing quality correction, and BMI-specific adjustments, is introduced [12].

The contributions of this study are threefold:

- (1) Model-based optimization of NIPT timing: A nonlinear regression and clustering approach identifies BMI-specific optimal testing windows for male fetuses.
- (2) Robust risk assessment under uncertainty: Monte Carlo simulations highlight sequencing quality as the dominant error factor, particularly in high-BMI groups.
- (3) Integrated abnormality detection pipeline for female fetuses: A logistic–random forest model with quality correction improves detection accuracy and clinical applicability [13].

Overall, this work provides both methodological and clinical contributions by offering interpretable, data-driven solutions for NIPT timing optimization and abnormality detection, which can enhance prenatal screening outcomes and reduce maternal-fetal health risks.

2 METHODS

2.1 Data Preprocessing

The raw sequencing data and supporting clinical information (including maternal height, weight, gestational week records, and fetal Y-chromosome concentration detection data, etc.) required for this study were all obtained from the Maternal and Child Health Special Dataset officially provided by the Chinese Society for Industrial and Applied Mathematics (CSIAM). To ensure the reliability of subsequent analysis results, strict multi-dimensional quality control was conducted on the acquired raw data, with the specific process as follows:

Samples with abnormal GC content (<40% or >60%) or poor sequence alignment quality (<70% unique mapping ratio) were excluded [14]. For gestational week records, those in the mixed "weeks + days" format (e.g., "38 weeks + 5 days") were converted into continuous numerical values (e.g., 38.71 weeks) to unify the measurement standard. Maternal BMI was recalculated using the formula BMI = weight/height² from the recorded maternal height (unit: m) and weight (unit: kg) to correct for potential input errors in the original data. For the fetal Y-chromosome concentration index, outliers (including negative values and extreme values greater than 0.20) were identified and removed using the interquartile range (IQR) method, and were secondarily validated against clinically recognized thresholds (the normal reference range for fetal Y-chromosome concentration is 0.02-0.18) to ensure the data are clinically meaningful.

After data preprocessing, descriptive statistics (including mean, standard deviation, median, quartiles, etc.) were generated for the three core indicators of gestational weeks, maternal BMI, and fetal Y-chromosome concentration to establish a database of baseline characteristics of the study subjects and lay the foundation for subsequent analyses.

2.2 Modeling Fetal Y-Chromosome Concentration (Male Fetuses)

To quantify the relationship between fetal Y-chromosome concentration and maternal characteristics, both linear and nonlinear models were explored. Scatterplots suggested a quadratic association with gestational weeks and an exponential decline with BMI. Consequently, a multivariate nonlinear regression model was constructed, incorporating quadratic terms for gestational weeks, interaction terms between BMI and X-chromosome fraction, and logarithmic transformations for GC content. The model was expressed as:

$$Y = \beta_0 + \beta_1 (Gestational Weeks)^2 + \beta_2 \cdot BMI + \beta_3 (BMI \times X) + \beta_4 \ln(GC) + \varepsilon$$
 (1)

where YYY denotes Y-chromosome fraction. Model fit was evaluated using coefficient of determination (R^2), root mean square error (RMSE), and residual analysis. The final model achieved $R^2 = 0.6888$, confirming strong explanatory power.

2.3 BMI Grouping and Optimal NIPT Timing

To determine optimal NIPT windows, maternal BMI values were grouped using ordered clustering guided by the elbow method. Candidate cut-off points (28.0, 32.0, 36.0, and 40.0) were evaluated under the criterion of minimizing withingroup variance in time-to-threshold attainment ($Y \ge 0.04$). Four groups were retained, each containing ≥ 30 samples. An expected risk function was defined to balance diagnostic accuracy and clinical intervention risk:

$$E(R,t) = P(t) \cdot R(t) + (1 - P(t)) \cdot R(t+2)$$
 (2)

where P(t) is the proportion of samples reaching the threshold at time t, and R(t) represents gestational risk (0.3 for early, 0.5 for mid, 0.7 for late window). The optimal time point was selected as the earliest t satisfying $P(t) \ge 90\%$ and minimizing E(R,t). Results indicated that higher BMI groups required later detection windows, with optimal timings ranging from 16.5 weeks (BMI < 28) to 23.5 weeks (BMI \ge 40).

2.4 Robustness Analysis under Measurement Errors

To account for sequencing variability, error modeling was performed using residual distributions from repeated samples (≥3 tests). Measurement error was assumed to follow a normal distribution:

$$Y_{obs} = Y_{true} + \epsilon, \quad \epsilon \sim N(0, \sigma^2)$$
 (3)

Monte Carlo simulations (n=1000 per group) were conducted under low, medium, and high error levels. The analysis showed that optimal timing shifts positively with error magnitude (0.5–1.5 weeks delay), with high-BMI groups more sensitive to errors. Sequencing depth was identified as the dominant factor; increasing reads to >5 million significantly reduced variability.

54 ZhiJian Dai, et al.

2.5 Abnormality Detection in Female Fetuses

Unlike male fetuses, female fetuses lack Y-chromosome markers. Abnormality detection was therefore based on standardized Z-scores of chromosomes 13, 18, 21, and X [15-16]. Quality correction was implemented by downweighting unreliable samples (e.g., low sequencing quality score, abnormal GC content).

A dual-model strategy was adopted:

- (1) Logistic Regression to provide interpretability by modeling abnormality probability from selected features (Z-scores, BMI category, sequencing quality index).
- (2) Random Forest to enhance classification accuracy by capturing nonlinear interactions among variables.

The Youden index was applied to determine the optimal decision threshold ($\tau = 0.35$). The final clinical workflow included four steps: (i) quality screening, (ii) rapid Z-score evaluation, (iii) probability-based classification, and (iv) BMI-specific correction. This approach enabled robust classification into "normal," "suspected abnormal," and "abnormal" categories.

3 METHODS

3.1 Descriptive Statistics

After preprocessing, 445 valid male-fetus samples were retained. The mean gestational age was 16.8 weeks (SD = 4.1), with BMI averaging 32.3 (SD = 3.0). The mean fetal Y-chromosome fraction was 0.077, ranging from 0.01 to 0.23. As shown in Table 1, Y-chromosome concentration exhibited moderate variability (SD = 0.0335), with skewness (0.71) and kurtosis (1.01) indicating slight right-tailed distribution.

Table I Descri	ptive Statistics of Ma	iternal and Fetal Indicator	`S

Indicator	Mean	Median	SD	Min	Max
Gestational weeks	16.85	16	4.08	11	29
Maternal BMI	32.29	31.81	2.97	20.7	46.9
Y-chromosome (%)	0.077	0.075	0.0335	0.01	0.23

Scatterplot visualization confirmed nonlinear associations: Y-chromosome fraction increased quadratically with gestational age ($R^2 = 0.58$ for quadratic fit vs. 0.32 linear), while declining exponentially with BMI ($R^2 = 0.49$ for exponential fit).

3.2 Model Fitting for Y-Chromosome Concentration

The multivariate nonlinear regression model incorporating quadratic, logarithmic, and interaction terms achieved $R^2 = 0.6888$ and RMSE = 0.0284, outperforming linear models ($R^2 = 0.52$). Residual analysis showed no systematic deviations, validating model adequacy. These results indicate that both gestational weeks and BMI are significant predictors of fetal fraction, with BMI exerting stronger negative influence.

3.3 BMI Grouping and Optimal Testing Time

Using ordered clustering and the elbow method, BMI thresholds of 28, 32, and 36 were identified, producing four groups with \geq 30 cases each. Within-group variance in time-to-threshold attainment was minimized, confirming robust subgrouping.

The optimal NIPT detection time was defined as the earliest gestational week satisfying $P(t) \ge 90\%P(t) \ge$

- (1) Group 1 (BMI < 28): 16.5 weeks
- (2) Group 2 ($28 \le BMI < 32$): 18.0 weeks
- (3) Group 3 ($32 \le BMI < 36$): 21.5 weeks
- (4) Group 4 (BMI \geq 36): 23.5 weeks

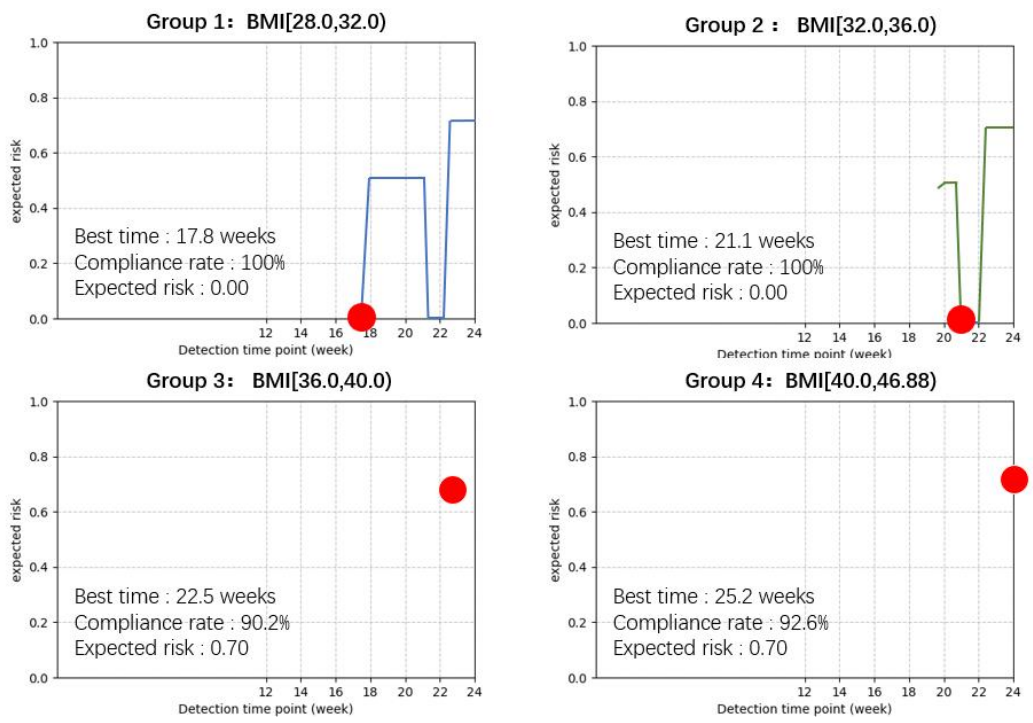


Figure 1 Expected Risk Across Gestational Weeks in Different BMI Groups

This finding highlights that universal testing schedules may be suboptimal, and BMI-specific adjustment is required for accurate and timely detection.

3.4 Robustness to Measurement Errors

Monte Carlo simulations demonstrated that measurement error level was positively correlated with optimal testing delay. Under high-error scenarios ($\sigma > 0.015$), detection was delayed by 1–1.5 weeks compared to low-error settings. Group 4 (BMI \geq 40) was most sensitive, with optimal timing shifting from 23.5 to 24.5 weeks. Sensitivity analysis identified sequencing depth as the dominant error source; increasing reads to >5 million stabilized detection windows across BMI groups.

3.5 Abnormality Detection in Female Fetuses

For female fetuses, standardized Z-scores of chromosomes 13, 18, 21, and X were analyzed. Logistic regression provided baseline interpretability, while random forest improved classification accuracy. The Youden index identified 0.35 as the optimal probability threshold.

The ROC curves of the two classifiers in the determination of chromosomal abnormalities in female fetuses (including the dynamic correspondence between sensitivity and 1-specificity) are shown in Figure 2 (the ROC curve for the determination of chromosomal abnormalities in female fetuses). It can be visually observed that the ROC curve of the random forest model is located above the logistic regression model, reflecting its advantages in the ability to distinguish abnormal classification. However, there is a common problem of decreased sensitivity in the high-specificity interval (1-specificity < 0.2), which also provides an optimization basis for the subsequent integration model and BMI specificity correction.

Cross-validation showed that logistic regression achieved 67.0% accuracy (AUC = 0.55), while random forest yielded higher overall accuracy (75.7%) but lower sensitivity (\sim 12%). Integrating both models with sequencing quality screening and BMI-specific correction produced a four-step workflow (quality check \rightarrow Z-score evaluation \rightarrow probability assessment \rightarrow BMI correction). This pipeline enhanced robustness and reduced false negatives in high-BMI subgroups.

56 ZhiJian Dai, et al.

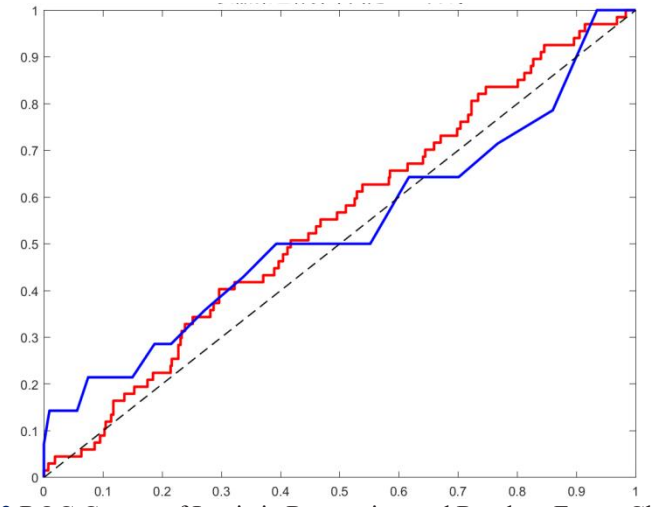


Figure 2 ROC Curves of Logistic Regression and Random Forest Classifiers

3.6 Summary of Findings

- (1) Fetal Y-chromosome fraction follows a quadratic growth with gestational weeks and decreases exponentially with RMI
- (2) BMI-specific testing windows significantly improve NIPT accuracy, with high-BMI women requiring later detection times.
- (3) Sequencing quality is the primary source of error; improving read depth effectively stabilizes outcomes.
- (4) Female fetal abnormality detection benefits from a dual-model strategy with quality correction, enhancing clinical applicability.

4 DISCUSSION

4.1 Model Advantages

The proposed quality-corrected framework demonstrates several advantages over conventional NIPT practices. First, it effectively addresses variability in raw sequencing data by integrating multi-dimensional quality control measures. For example, GC content filtering and alignment ratio thresholds ensured data reliability, while recalculated BMI values corrected potential entry errors. This preprocessing strategy eliminated noise and provided a robust foundation for downstream modeling.

Second, the framework offers strong interpretability and logical consistency. The nonlinear regression model for male fetuses was grounded in clinical and biological principles, with coefficients corresponding to gestational growth dynamics, BMI-related dilution effects, and sequencing quality factors. Likewise, the ordered clustering of BMI groups produced results consistent with clinical experience, revealing that higher BMI systematically delays the optimal NIPT timing. For female fetuses, the dual-model strategy balanced interpretability (logistic regression) with predictive performance (random forest), aligning with the dual clinical requirements of "accuracy" and "explainability."

Third, the clinical practicality of the models is significant. The expected risk function explicitly incorporated routine retesting intervals, thereby enhancing real-world applicability. BMI-specific detection windows provided a feasible guideline for obstetricians, replacing the "one-size-fits-all" approach. The female abnormality detection pipeline, incorporating Z-score thresholds and BMI-specific corrections, ensured flexible yet reliable decision-making in diverse clinical contexts.

4.2 Clinical Implications

The study findings have direct implications for prenatal care. For male fetuses, BMI-adjusted testing schedules can reduce false negatives and avoid unnecessary repeat testing. By demonstrating that optimal detection shifts later with increasing BMI, clinicians can personalize testing recommendations, improving accuracy without compromising timeliness. The robustness analysis also highlighted sequencing depth as the primary determinant of stability, suggesting that increasing read coverage is a cost-effective intervention for reducing risk in high-BMI populations.

For female fetuses, the proposed dual-model workflow provides a structured decision pipeline that aligns with clinical practice. The integration of sequencing quality screening prevents unreliable data from driving false diagnoses, while BMI-specific corrections mitigate under-detection in high-BMI subgroups. Importantly, the inclusion of SHAP-based interpretability enhances clinician confidence, facilitating transparent communication with patients and improving the uptake of clinical recommendations.

4.3 Limitations

Despite these strengths, the study has several limitations. The models were developed under a set of assumptions that may not fully generalize to complex clinical settings. For instance, comorbidities such as diabetes, hypertension, or placental dysfunction were not explicitly included, though these factors could affect fetal fraction dynamics. Similarly, the abnormality detection framework focused on trisomies 13, 18, 21, and the X chromosome, while rare aneuploidies (e.g., chromosomes 16 or 22) were not considered. Extreme technical errors, such as sequencing platform failures or contamination, were also outside the model scope.

Moreover, the relatively low sensitivity of the random forest classifier in female-fetus detection suggests that further refinement is necessary, particularly for balancing specificity with recall. Additionally, the dataset was drawn primarily from high-BMI populations, which may limit generalizability to broader maternal demographics.

4.4 Future Directions

Future research should expand the scope of maternal covariates by incorporating clinical comorbidities, lifestyle factors, and genetic history into predictive models. Multi-center validation across diverse populations will be essential to ensure robustness and external applicability. On the methodological side, hybrid machine learning approaches—such as ensemble stacking or deep learning models—may improve female abnormality detection without sacrificing interpretability. Finally, integrating cost-effectiveness analysis into model design could support clinical guideline development, ensuring both scientific rigor and healthcare efficiency.

5 CONCLUSION

This study proposed a quality-corrected modeling framework to optimize the timing of non-invasive prenatal testing (NIPT) for male fetuses and to improve abnormality detection strategies for female fetuses. By integrating nonlinear regression, ordered clustering, and risk-based optimization, we demonstrated that Y-chromosome fraction is strongly influenced by both gestational weeks and maternal BMI, and that higher BMI systematically delays the optimal detection window. The derived BMI-specific testing schedules, ranging from 16.5 to 23.5 weeks, provide actionable guidance for clinicians to improve reliability and reduce unnecessary re-testing.

Robustness analyses confirmed that sequencing quality is the dominant error source, especially in high-BMI groups, highlighting the importance of maintaining sufficient read depth in clinical practice. For female fetuses, a dual-model diagnostic approach combining logistic regression and random forest achieved reliable performance when integrated with quality control and BMI-specific correction. The structured workflow supports clinical decision-making by balancing accuracy, interpretability, and practicality.

Overall, the proposed framework enhances the scientific basis of NIPT, offering interpretable and clinically implementable solutions that can improve prenatal screening outcomes, reduce maternal-fetal health risks, and inform the development of personalized testing guidelines. Future extensions incorporating comorbidities, larger datasets, and advanced learning methods will further strengthen the generalizability and impact of this work.

COMPETING INTERESTS

The authors have no relevant financial or non-financial interests to disclose.

REFERENCES

- [1] Zhang R, Zhang H, Li Y, et al. External quality assessment for detection of fetal trisomy 21, 18, and 13 by massively parallel sequencing in clinical laboratories. Journal of Molecular Diagnostics, 2016, 18(2): 244-252.
- [2] Zhou Y, Zhu Z, Gao Y, et al. Effects of maternal and fetal characteristics on cell-free fetal DNA fraction in maternal plasma. Reproductive Sciences, 2015, 22(11): 1429-1435.
- [3] Yu D D, Li F J, Yao X Y, et al. Effectiveness of NIPT for detecting common fetal chromosomal aneuploidies in special-use populations. Chinese Journal of Family Planning & Gynecology, 2025, 17(3): 72-82.
- [4] Nan L L, Ma Y X, Zhang J, et al. Application analysis of 9,892 NIPT cases in prenatal screening in northern Linyi County. Chinese Journal of Prenatal Diagnosis (Electronic Edition), 2024, 16(3): 36-41.
- [5] Pan S Q, Pan X L, Ge L S, et al. Clinical value of non-invasive prenatal testing in prenatal screening. Zhejiang Medical Journal, 2024, 46(17): 1881-1884.
- [6] Lu Y F, Zhao J, Lei Y, et al. Clinical significance of non-invasive DNA testing for fetal chromosomal aneuploidy screening. Journal of Guizhou Medical University, 2022, 47(5): 598-603+620.
- [7] Zeng L, Deng Y, Wei P, et al. Analysis of 58,113 NIPT cases and pregnancy outcomes in Sichuan Province. Chinese Journal of Eugenics and Genetics, 2021, 29(5): 658-663.
- [8] Chen Y, Wu X, Li H, et al. Evaluation of the prenatal diagnostic value of non-invasive prenatal testing for the detection of rare fetal autosomal trisomies: a single center study of 83,842 cases. Scientific Reports, 2025, 15(1): 26254.
- [9] Bianchi B, Zaccaria G, Kang X, et al. Pregnancy outcomes in patients with increased nuchal translucency using non-invasive prenatal testing and first trimester ultrasound. European Journal of Obstetrics & Gynecology and Reproductive Biology, 2025, 313: 114-572.

58 ZhiJian Dai, et al.

[10] Yang M, Long D, Li Y, et al. An explainable machine learning model in predicting vaginal birth after cesarean section. The journal of maternal-fetal & neonatal medicine: the official journal of the European Association of Perinatal Medicine, the Federation of Asia and Oceania Perinatal Societies, the International Society of Perinatal Obstetricians, 2025, 38(1): 2546544.

- [11] Wang Y S, Qiao J, Wang R, et al. Development and external validation of an interpretable machine learning model for predicting perinatal depression in Chinese women during mid- and late pregnancy. International Journal of Medical Informatics, 2025, 203: 106000-106000.
- [12] Li J, Liu X, He S, et al. Interpretable Machine Learning for Predicting Adverse Pregnancy Outcomes in Gestational Diabetes: Retrospective Cohort Study. JMIR medical informatics, 2025, 13: e71539.
- [13] Hong S, Liu C, Kang X, et al. The development and validation of postpartum hemorrhage prediction models for pregnancies with placenta previa totalis based on coagulation function indexes: a retrospective cohort study. BMC Pregnancy and Childbirth, 2025, 25(1): 925-925.
- [14] Andonotopo W, Bachnas A M, Pribadi A, et al. Integrating NIPT and ultrasound for detecting fetal aneuploidies and abnormalities. Journal of Perinatal Medicine, 2025, 53(7): 789-802
- [15] Xu X, Wang L, Cheng X, et al. Machine learning-based evaluation of application value of the USM combined with NIPT in the diagnosis of fetal chromosomal abnormalities. Mathematical Biosciences and Engineering, 2022, 19(4): 4260-4276. DOI: 10.3934/mbe.2022197. PMID: 35341297.
- [16] Alberry MS, Aziz E, Ahmed SR, et al. Non invasive prenatal testing (NIPT) for common aneuploidies and beyond. European Journal of Obstetrics & Gynecology and Reproductive Biology, 2021, 258: 424-429.

Journal of Pharmaceutical and Medical Research

Print ISSN: 2663-1954 Online ISSN: 2663-1962

DOI: https://doi.org/10.61784/jpmr3047

RECENT ADVANCES IN THE NEUROPROTECTIVE EFFECTS OF TRADITIONAL CHINESE MEDICINE: FOCUS ON ACTIVE INGREDIENTS AND MECHANISMS OF ACTION IN ALZHEIMER'S DISEASE

YiWen Zhang

School of Pharmacy, Guangdong Pharmaceutical University, Guangzhou 510006, Guangdong, China.

Corresponding Email: 2200310458@stu.gdpu.edu.cn

Abstract: Alzheimer's disease (AD) is a senile brain disease characterized by insidious onset and neurodegenerative pathology. According to reports from the World Health Organization, the global population of individuals affected by AD exceeds 55 million, with a new case occurring approximately every three seconds. This number is projected to exceed 150 million by the year 2050. Given the unclear pathogenesis of AD, there are currently no available etiological treatments. Traditional Chinese Medicine (TCM) is known for its multi-target therapeutic approach, which provides several advantages, including a variety of treatment methods, minimal side effects, and the capacity to coordinate effects across multiple targets and pathways. This makes TCM particularly significant for research focused on the prevention and treatment of AD. This paper utilizes TCM as a foundation to review recent research findings regarding its treatment of AD, including ganolearins A–D, ulmoidol (30), Ganoderma lucidum polysaccharide, Ganoderma sinense crude polysaccharide and so on. It identifies newly discovered active ingredients and treatment methods, with the aim of providing a theoretical basis for TCM approaches to AD and serving as a reference for drug development.

Keywords: Alzheimer's disease; Traditional Chinese Medicine; Active ingredient; Mechanism of action; Neuroprotection

1 INTRODUCTION

Alzheimer's disease (AD), a degenerative brain disorder, is primarily characterized by the gradual onset of dementia symptoms, predominantly affecting the elderly population [1]. As the condition advances, patients typically experience a continuous decline in memory and cognitive abilities, including logical reasoning [2]. This process not only significantly diminishes the patient's quality of life but also places considerable strain on the daily lives of their families. Although the impact of AD is extensive, our current understanding is still relatively limited. Due to the incomplete elucidation of its exact etiology and pathological processes, achieving etiological treatment for AD remains challenging. Clinically, only symptomatic treatments are available to slow the progression of AD currently. The research has revealed a series of complex mechanisms underlying AD, including the toxicity of beta-amyloid protein (A β), excessive phosphorylation of tau protein, neuroinflammation, glucose metabolism disorders, and dysregulation of the gut microbiota [2]. Currently, the third core feature of the pathogenesis of AD is neuroinflammation, which has become an important research focus in this field, along with the deposition of β -amyloid protein and the formation of neurofibrillary tangles (NFTs) [3].

AD is divided into several categories by the theory of Traditional Chinese Medicine (TCM), such as "dementia," "psychosis," "forgetfulness," "consumptive disease," and "dullness disease." One important internal mechanism that is thought to be responsible for the development of these ailments is the lack of kidney essence, as well as the dual deficiency of Qi and blood [4]. TCM's multi-target characteristics allow it to offer benefits including a range of treatment options and low side effects, and it has demonstrated remarkable effectiveness in treating the neuroinflammation linked to AD [5]. The principles of holistic control, syndrome differentiation, and treatment are all upheld in TCM treatment. It has the ability to precisely target a number of AD pathogenesis pathways, including neuroinflammation, as well as related targets within the cascade reactions that these mechanisms initiate. Either individual herbs or intricate formulations are used to do this, allowing for a thorough regulatory impact on the body that affects numerous targets and pathways [6]. TCM has a great deal of promise as a therapeutic strategy for reducing the clinical symptoms of AD and slowing its progression because of this special therapeutic mechanism.

In contemporary clinical practice, the primary pharmacotherapeutic agents for the management of AD encompass central cholinesterase inhibitors, glutamate receptor antagonists, and anti-amyloid monoclonal antibodies [7]. Lecanemab, memantine, donepezil, and galantamine are examples of medicines having well-established clinical applications [8]. Unfortunately, there are presently no viable treatments for Alzheimer's disease. They can only slow the disease's progression. Therefore, prevention remains the most effective technique for addressing this illness. This study provides an in-depth analysis of recent breakthroughs in AD pathogenesis and research on active TCM constituents for therapy. This work systematically lists various TCM active ingredients, such as ginsenosides and quercetum, along with their mechanisms of action, in order to provide distinct TCM therapeutic strategies for the treatment of AD, as well as to further research and clinical applications of integrated Chinese and Western medicine for AD.

60 YiWen Zhang

2 ETIOLOGY OF AD

2.1 Aß Cascade Hypothesis

The aberrant accumulation of β -amyloid (A β) initiates AD, activating a cascade of pathogenic processes including tau protein hyperphosphorylation, neuroinflammation, and synaptic damage. That eventually leading to neuronal death and progressive cognitive impairment [9]. Aβ is a peptide that comes from the amyloid precursor protein (APP). APP is a transmembrane protein that is mainly expressed in neurons. Its physiological functions include synapse development, neural plasticity, cell adhesion, and signal transmission [10]. Under normal physiological circumstances, the α -secretase processing route cleaves APP, producing a membrane-anchored C83 fragment and soluble sAPPα, which has neuroprotective properties [11]. APP cleavage is changed in the clinical stage of AD, the first cleavage is carried out by β-secretase (BACE1) at the N-terminus of the Aβ domain inside APP, resulting in a membrane-bound C99 fragment [12]. The transmembrane region of the C99 fragment is next subjected to proteolytic cleavage by the γ-secretase complex, which releases A\$\beta\$ peptides of different lengths, primarily A\$\beta 40\$ and A\$\beta 42\$ [11]. A\$\beta 42\$ exhibits a significant tendency for aggregation and hydrophobicity [13]. Monomers aggregate into oligomers [14], which in turn aggregate into fibrous amyloid plaques, because to the hydrophobicity [15]. Inflammatory mediators released by excessive Aβ aggregation cause neuroinflammation, which in turn activates microglia and astrocytes. This activation creates a vicious cycle that worsens AD pathogenesis by encouraging more Aβ aggregation and generation [16]. There is clear pathological heterogeneity between the two types of AD, as tau can adopt distinct folds in the human brain in different diseases. [17].

2.2 Abnormal Modification of Microtubule-associated Protein Tau

Tau is a microtubule-associated protein that is essential to the physiological processes of neurons. Its primary role is to mediate microtubule-associated physiological functions and aid in intracellular microtubule assembly. It is also essential for controlling the intracellular transport of neurotransmitters and the development of neuronal axons [18]. Dysregulated tau protein function impairs neuronal development and repair and disrupts nerve impulse transmission across neurons [19]. Abnormal phosphorylation of tau protein is a mark pathogenic alteration in the brain neurons of AD patients [20]. Tau protein's innate disordered nature makes it susceptible to misfolding under pathological settings, exposing key motifs such as residues 275-280, which have been linked to vascular cognitive impairment. These misfolded motifs cause tau aggregation, which leads to the formation of neurofibrillary tangles (NFTs), a key clinical characteristic of AD [21]. Abnormal tau protein can spread trans-synaptically to undamaged brain areas, causing synaptic malfunction or loss, which leads to neuronal injury and progressive cognitive decline [21].

2.3 Oxidative Stress

Oxidative stress is a critical linked component in AD causation, which results from an imbalance between the organism's oxidative and antioxidant systems [22]. The primary oxidants in biological tissues are reactive oxygen species (ROS), whereas antioxidants consist mostly of enzymatic antioxidants such as superoxide dismutase (SOD) and non-enzymatic antioxidants such as vitamin C [23]. Given the brain's extraordinarily high oxygen consumption, a lack of antioxidant ability to combat the ensuing oxidants causes an accumulation of ROS. These excess ROS assault neuronal structures and biomolecules, disrupting cell membranes and eventually causing neuronal death [24]. Oxidative stress can trigger neuronal re-entry into the cell cycle, increase tau protein accumulation, and impede $A\beta$ breakdown, resulting in $A\beta$ buildup and neuroinflammation [24].

2.4 Cholinergic Receptor Deficiency

Short-term memory functions and synaptogenesis are supported by $\alpha 7$ nicotinic acetylcholine receptors ($\alpha 7$ nAChRs) in the healthy brain.Research employing $\alpha 7$ nAChR-deficient mice shows that receptor deficiency promote the generation of A β and abnormal aggregation of nAChRs. Additionally, it increases tau aggregation into NFTs and causes tau hyperphosphorylation by controlling glycogen synthase kinase-3 β [25]. According to this, cholinergic receptor insufficiency may serve as a precursor to aberrant tau phosphorylation and A β buildup, collaborating with other harmful elements to promote the pathophysiology of AD [25].

2.5 Genetic Factors

Certain differences between AD patients' and unaffected people's DNA have been found using molecular probe techniques. The condition may become more likely to develop if genes like *ZDHHC21* and *CHCHD2* are mutated [26]. According to research, family early-onset AD can result from mutations in genes such the amyloid precursor protein gene, *presenilin 1 (PSEN1)*, and *presenilin 2 (PSEN2)* [27]. Genetic variations such alpha-2-macroglobulin (*A2M*) and *apolipoprotein E* &4 (*APOE* &4) greatly increase the risk of sporadic AD in the general population [28–30]. *CHCHD2* is a mitochondrial protein with many functions that regulate respiratory chain complex production as well as the mitochondrial apoptosis pathway. CHCHD2 and CHCHD10 proteins, which are homologous proteins with 54% identity in amino acid sequence, belong to the mitochondrial coiled-coil-helix-coiled-coil-helix (CHCH) domain protein family

and have been found to be linked to neurodegenerative diseases [31]. Furthermore, a recently discovered novel pathogenic pathway for AD is *ZDHHC21* mutation-induced aberrant protein palmitoylation, which causes familial AD in Chinese cohorts [26].

3 ACTIVE INGREDIENTS OF TCM FOR TREATING AD

3.1 Terpenoids

Several terpenoids and terpenoid derivatives have been shown to be effective against AD, including carvone, ginkgolide B, salidroside, astragaloside IV, ginsenoside, tenuifolin, Gynostemma pentaphyllum, and Ganoderma triterpenes [32]. Plant-derived triterpenoids have anti-inflammatory, antioxidant, and other therapeutic qualities, making them interesting candidates for treating AD (Table 1). Triterpenoids, such as Ganoderma triterpenes and ginsenosides, can help AD patients by altering critical pathways such as neuroinflammation, oxidative stress, autophagy, mitochondrial dysfunction, and endoplasmic reticulum stress. Ganoderma lucidum contains significant amounts of triterpenoids, which could act as natural anti-inflammatory agents or functional meals to help prevent, delay, and treat AD [33]. Pathological tau protein is eliminated as a result of the efficient autophagy activation provided by the ganoderma triterpenes ganoapplin A and ganoapplin B [34]. To encourage the removal of Tau proteins, ganolearins A-D, which are produced from Ganoderma triterpenes, trigger the AMPK-ULK1 autophagy pathway [35]. By regulating key signaling pathways related to inflammation, triterpenoids extracted from Poria can reduce the incidence of Alzheimer 's disease. Additionally, it improves memory function by reducing oxidative stress, preventing tau hyperphosphorylation and neuronal death, and controlling the cholinergic system [36-37]. Gypenoside XLVI, a dammarane-type triterpenoid saponin found in Gynostemma pentaphyllum, has been shown to have therapeutic potential for AD by considerably improving learning and memory deficits in the 3×Tg-AD mouse model of the disease [38]. From the Eucommia ulmoides leaf extract's ethyl acetate fraction, thirty-eight chemicals were separated and identified. The nortriterpenoid ulmoidol showed the most anti-neuroinflammatory effect among them [39-41].

3.2 Flavonoids

Quercetin, genkwanin, dihydromyricetin, myricetin, myricitrin, puerarin, and the total flavonoids from *Drynaria* fortunei are examples of active flavonoids that are used to treat AD. By regulating the apoptosis-related proteins Bcl-2 and Bax and altering the PI3K/Akt signaling pathway, quercetin has neuroprotective effects [42]. By lowering intracellular ROS, improving mitochondrial dysfunction, and lowering tau hyperphosphorylation, genkwanin has neuroprotective benefits [43]. *Ampelopsis grossedentata's* dihydromyricetin exhibits strong research promise because to its biological activities, which include antioxidant, anti-inflammatory, and neuroprotective properties [44].

Extracted from *Pueraria lobata*, puerarin has neuroprotective, antioxidant, and anti-inflammatory properties [45]. Research shows that puerarin works better than β -sitosterol to improve cellular AD models. Puerarin dramatically increases NOS3 protein expression in AD cells at 100 μ M, indicating that NOS3 might be a possible target for puerarin's advantageous effects in AD [45]. In hydrocortisone-induced model mice, osteopractic total flavone may have neuroprotective properties against AD. The ER pathway mediates this possible therapeutic effect, which reduces brain tissue damage by upregulating the expression of the proteins NMDAR1 and GluR2 and downregulating that of CaMKII [46].

The plant *Scutellaria barbata* has antibacterial, antioxidant, and anticancer properties. Its active ingredients are flavonoids, which show promise in the treatment of ovarian and lung adenocarcinomas. According to recent research, *Scutellaria barbata* suppresses microglial (MG) proliferation and modifies the expression of pro-inflammatory factors and nitric oxide synthase activity to prevent A β complex-induced neuroinflammation. Its flavonoid concentration is responsible for its anti-AD therapeutic and preventative activities [47-48]. One of the most researched phytochemicals, luteolin, has neuroprotective properties. By blocking acetylcholinesterase activity, controlling the production and aggregation of A β , altering Tau protein phosphorylation and brain glucose metabolism, and exhibiting anti-inflammatory, antioxidant, and anti-apoptotic properties, it produces these effects in the context of AD [49].

3.3 Polysaccharides

Physalis alkekengi fruit, deproteinized Vitis vinifera, Ganoderma lucidum, and Schisandra chinensis are a few examples of medicinally active polysaccharides used to treat AD.Ganoderma lucidum reduces oxidative stress damage, improves immunological function loss, and lessens AD symptoms. In AlCl₃/D-gal-induced AD animal models, studies on Ganoderma lucidum polysaccharide (GLP) and Ganoderma sinense crude polysaccharide (GSP) showed that GSP was noticeably more effective than GLP in reducing cognitive impairments and dementia-related behaviors. This improvement included less memory loss, more time spent investigating new things, and improved spatial exploration [50]. Two fractions, GSP1 and GSP2, were produced by the separation and purification of GSP. GSP1 reversed AD-induced gut microbiota dysbiosis, increased the abundance of potentially beneficial bacteria (including taxa that produce short-chain fatty acids), significantly improved dementia-associated behavioral and pathological symptoms, and effectively attenuated cerebral Aβ deposition in AlCl₃/D-gal-induced AD model mice [50]. Furthermore, GSP1 may also influence AD progression through the gut-brain axis. Furthermore, by modifying the expression levels of antioxidant enzymes, polysaccharides obtained from deproteinized Vitis vinifera 'Thompson Seedless' reduce oxidative

62 YiWen Zhang

damage caused by $A\beta_{1-42}$, showing promise as a therapy for AD [51]. By reducing tau protein phosphorylation in the brain, *Lycium chinense* polysaccharides improved learning and memory impairments in AD combined with type 2 diabetes mellitus (AD+T2DM) model mice [52].

Four separate fractions were obtained from the fractionation of *Schisandra chinensis* polysaccharides (SCP). In AD rats, all pure polysaccharide fractions dramatically restored intestinal barrier integrity, reduced neuroinflammation, and enhanced learning and memory in a dose-dependent manner. However, the SCP2 group showed the most notable efficacy [53]. By blocking the TLR4/NF- κ B/NLRP3 pathway, SCP2 reduces neuroinflammation and has neuroprotective effects [53]. Fucoidan has the potential to be used in the development of natural product-based AD therapies, as evidenced by animal trials showing that it dramatically reduced scopolamine-induced cognitive impairment, decreased A β deposition, and activated the Nrf2/TLR4/NF- κ B neuroprotective pathway [54].

Table 1 The Main Active Components of TCM in the Treatment of AD and its Mechanism of Action

Traditional Chinese medicine	Active ingredient	Category	Specific mechanism	Literature
Ganoderma lucidum	Ganoderma triterpenes		the AMPK-ULK1 autophagy pathway	[34, 35]
Panax ginseng	ginsenosides		Activation of NLRP3 \downarrow \rightarrow cleaved caspase-1 \downarrow \rightarrow TNF- α \downarrow	[33]
Poria	Poria cocos triterpenes	Terpene	BACE1 $\downarrow \rightarrow$ APP $\downarrow \rightarrow$ A $\beta \downarrow$; GSK-3 $\beta \downarrow$;NF- κB pat hway $\downarrow \rightarrow$ TNF- $\alpha \downarrow$ IL-1 $\beta \downarrow$ IL- $6 \downarrow$; ROS \downarrow	[38]
Gynostemma pentaphyllum	Gypenoside XLVI		NLRP3↓→NLRP3↓→speck-like pro↓;PPM1A /NLRP3/tau axis↓ & PPM1A /nuclear factor -κB/CX3CR1 pathway	
Eucommia ulmoides	nortriterpenoid Ulmoidol (30)		$A\beta\downarrow;NF$ -κ B pathway $\downarrow\rightarrow TNF$ -α \downarrow IL-1 $\beta\downarrow$ IL-6 \downarrow	[40, 41]
Rutin	Quercetin		PI3K/AKT pathway change Bcl-2/Bax \rightarrow casp ase-3 \downarrow \rightarrow A β \downarrow ;GSK-3 β \downarrow CDK5 \downarrow MAPKs \downarrow \rightarrow Tu a pro	
Genkwa Flos	Genkwanin		NF-κB pathway $\downarrow \rightarrow$ TNF-α \downarrow IL-6 \downarrow ; ROS \downarrow RNS \downarrow	[43]
Ampelopsis grossedentata	Dihydromyricetin		$\begin{array}{c} BACE1{\downarrow} \to \!\! A\beta{\downarrow} \ ; NF\text{-}\kappa B \ pathway} \to \!\! TNF\text{-}\alpha{\downarrow} \\ IL\text{-}6{\downarrow}; AChE{\downarrow}; ROS{\downarrow} \ RNS{\downarrow} \end{array}$	[44]
Pueraria lobata	Puerarin	Flavonoid	NOS3↑	[45, 46]
Davallia mariesii	Osteopractic total flavone		$NMDAR1 \uparrow GluR2 \uparrow CAMKII \downarrow \rightarrow Prot\text{-ecting } th \\ e \ nerves$	[47]
Scutellariae Barbatae Herba	Scutellaria barbata flavonoids		$A\beta\downarrow;MG\downarrow;NOS\downarrow TNF-\alpha\downarrow IL-6\downarrow$	[48, 49]
Reseda odorata L.	Luteolin		AChE↓;Aβ↓;Tua pro	[50]
Ganoderma lucidum	GSP1		Aβ↓;Intestinal flora↑;the gut-brain axis way	[51]
Schisandra chinensis	SCP2		TLR4/NF- κ B/NLRP3 pathway $\downarrow \rightarrow$ TNF- $\alpha \downarrow$ I L-1 $\beta \downarrow$ IL-6 \downarrow ;A $\beta \downarrow$; MG \downarrow	[54]
Sargassum pallidum	Fucoidan	Polysaccharides	A $\beta\downarrow;$ NRf-2/TLR4/NF-kB pathway $\uparrow \rightarrow$ prote cting the nerves	[55]
Lycium chinense	Polysaccharides of <i>Lycium</i> chinense		ROS↓RNS↓ ;GSK-3↓	[53]

4 COMPARISON BETWEEN TCM AND CONVENTIONAL THERAPEUTIC DRUGS

4.1 Mechanism of Action

TCM's mode of action has advantages over Western medicine in the treatment of AD. Through mechanisms like heat shock protein activation, oxidative stress and inflammation modulation, and gut-brain axis regulation, TCM's distinctive multi-target strategy allows for synergistic benefits [55]. On the other hand, traditional pharmaceutical treatments for AD usually focus on a single pathway: memantine serves as an NMDA receptor antagonist, whereas donepezil just inhibits acetylcholinesterase. Neither directly addresses the control of tau phosphorylation or A β production [56]. Aducanumab and other monoclonal antibodies that target A β clearance are controversial in clinical settings and ineffective in repairing synaptic damage [57].

4.2 Efficacy and Safety

Since AD is a neurological condition, it requires ongoing medical care. TCM offers substantial benefits for such long-term treatment plans because of its natural multi-target effects and good safety record. Additionally, research suggests that integrating TCM with Western therapy could lessen the negative effects of traditional medications. When used with chemical medications like donepezil, for instance, TCM may be more successful than chemical medications alone at improving patients' cognitive impairment and lowering the risk of side effects like urticaria and sleeplessness [58].

4.3 Treatment Philosophy

The treatment philosophy of TCM integrates a systemic perspective, holism, and pattern differentiation-based treatment. The primary goals of current therapy approaches, which emphasize preventive measures, are to reduce symptoms and halt the progression of AD because the pathophysiology of the illness is yet unknown. With its ability to delay the beginning of disease and support health maintenance and recovery, TCM has intrinsic advantages in preventive medicine. This offers substantial research opportunities for AD therapy and prevention [59]. A foundation for dietary intervention is also provided by the TCM idea of the homology of medicine and food, which is extremely pertinent to the prevention and treatment of AD [60].

5 CONCLUSION AND OUTLOOK

In conclusion, the pathophysiology of AD, a neurodegenerative disease that poses a serious risk to the health of the aged, is still poorly understood, and the available clinical treatments for it have serious drawbacks. TCM's theoretical underpinnings provide special benefits for the treatment of AD. Through multi-component, multi-target herbal formulae, its therapeutic strategies—which emphasize "holistic regulation" and "syndrome differentiation and treatment (bian zheng lun zhi)"—execute synergistic effects. The clinical efficacy of traditional Chinese medicine in treating AD is currently not fully supported by evidence-based medicine. Nonetheless, further research is necessary to fully understand the complex mechanisms of action and the pharmacological underpinnings of important bioactive components.

Clarifying the targets and signaling pathways of TCM's mechanisms of action, examining how it integrates with other therapeutic modalities, and examining the processes underlying TCM's holistic regulatory effects within the intricate pathophysiology of AD should be the top priorities of future study. In order to clarify the mechanisms of TCM in the treatment of AD from a variety of viewpoints and biological levels, future research should use biomedical methodologies such as pharmacology, network pharmacology, immunology, bioinformatics, and data analytics. Research on the scientific analysis and processing methods of TCM formulations, as well as on combination treatment approaches that combine TCM and Western medicine, should be stepped up at the same time. This seeks to lessen harmful side effects while increasing therapeutic efficacy.

COMPETING INTERESTS

The authors have no relevant financial or non-financial interests to disclose.

REFERENCES

- [1] Cummings J. The National Institute on Aging—Alzheimer's Association Framework on Alzheimer's disease: Application to clinical trials. Alzheimer's & Dementia: The Journal of the Alzheimer's Association, 2019, 15(1): 172–178.
- [2] Wu C, Ma D, Chen Y. Association of pulse pressure difference and diabetes mellitus in Chinese people: A cohort study.International Journal of General Medicine, 2021, 14: 6601-6608.
- [3] Kamila P, Kar K, Chowdhury S, et al. Effect of neuroinflammation on the progression of Alzheimer's disease and its significant ramifications for novel anti-inflammatory treatments. IBRO Neuroscience Reports, 2025, 18: 771-82.
- [4] Miao Qi, Zhu Renyan, Li Niannian, et al. Progress in traditional Chinese medicine treatment of Alzheimer's Disease. Journal of Shaanxi University of Chinese Medicine, 2024, 47(1): 139-42.
- [5] Zhang Tao, Zhao Lei, Zhan Rui, et al. Novel mechanisms of some traditional chinese medicine for the therapy of neurocognitive disorders. Progress In Biochemistry and Biophysics, 2020, 47(8): 729-742.
- [6] Erli Fei, Yun Gu. Progress in the prevention and treatment of Alzheimer's disease with traditional Chinese medicine. Chinese Journal of Alzheimer's Disease and Related Disorders, 2025, 8(1): 67-72.
- [7] Yuan Fang, Wang Gang. Progress in pharmacotherapy for Alzheimer's disease. Acta Academiae Medicinae Sinicae, 2024, 41(5): 702-708.
- [8] Rafii M S, Aisen P S. Amyloid-lowering immunotherapies for Alzheimer disease: current status and future directions. Nature Reviews Neurology, 2025.
- [9] Zhang He, Zheng Yan. β Amyloid Hypothesis in Alzheimer's Disease: Pathogenesis, Prevention, and Management. Acta Academiae Medicinae Sinicae, 2019, 41(5): 702-708.
- [10] Wang Guoqing. Advances in the study of Aβoligomers and Alzheimer's disease. Journal of Apoplexy and Nervous Diseases, 2023, 40(7): 579-83.

64 YiWen Zhang

[11] Guo X, Li H, Yan C, et al. Molecular mechanism of substrate recognition and cleavage by human γ-secretase. Science, 2024, 384(6700): 1091-1095.

- [12] Zheng Y F, Song Z Y, Lyu W C, et al. A review of research on A β 1-42 oligomers and Alzheimer's disease. Journal of Regional Anatomy and Operative Surgery, 2016(2): 142-144.
- [13] Niu Z, Gui X, Feng S, et al. Aggregation mechanisms and molecular structures of Amyloid-β in Alzheimer's Disease. Chemistry, 2024: 1521-3765.
- [14] Zhang P, Song C, Shi J, et al. Endothelium-specific endoglin triggers astrocyte reactivity via extracellular vesicles in a mouse model of Alzheimer's disease. Mol Neurodegener, 2025: 1750-1326.
- [15] Azargoonjahromi A. The duality of amyloid-β: its role in normal and Alzheimer's disease states. Molecular Brain, 2024, 17(1).
- [16] Zhang X, Hu J, Zhong L, et al. Quercetin stabilizes apolipoprotein E and reduces brain Aβ levels in amyloid model mice. Neuropharmacology, 2016, 108: 179-92.
- [17] Benjamin Falcon, Wenjuan Zhang, Alexey G Murzin, et al. Structures of filaments from Pick's disease reveal a novel tau protein fold. Nature, 2018: 137–140.
- [18] Zhang Xin, Zhu Tiantian, Wei Yuting, et al. Research progress on the mechanism of acupuncture intervention in Alzheimer's Disease via regulation of tau protein. Western Journal of Traditional Chinese Medicine, 2025, 38(3): 98-102
- [19] Gaikwad S, Senapati S, Haque M A, et al. Senescence, brain inflammation, and oligomeric tau drive cognitive decline in Alzheimer's disease: Evidence from clinical and preclinical studies. Alzheimers Dement, 2024: 1552-5279.
- [20] Arakhamia T, Lee CE, Carlomagno Y, et al. Posttranslational modifications mediate the structural diversity of tauopathy strains. Cell, 2021: 1097-4172.
- [21] Wan H L, Hong X Y, Zhao Z H, et al. STAT3 ameliorates cognitive deficits by positively regulating the expression of NMDARs in a mouse model of FTDP-17. Signal Transduction and Targeted Therapy, Cell, 2020, 5(1): 295.
- [22] Zeng F X, Zhao R Q, Wang B. Neuroprotective mechanism of exercise on Alzheimer's Disease: Role of oxidative stress. Chinese Journal of Biochemistry and Molecular Biology, 2025, 41(5): 687-695.
- [23] Wen L, Bi D, Shen Y. Complement-mediated synapse loss in Alzheimer's disease: mechanisms and involvement of risk factors. Trends in Neurosciences, 2024: 1878-108X.
- [24] Puranik N, Song M. Oxidative stress and the role of immune cells in Alzheimer's Disease: therapeutic implications and future perspectives. CNS neurol disord drug targets, 2025: 1996-3181.
- [25] Bodur O C, Hasanoğlu Özkan E, Çolak Ö, et al. Preparation of acetylcholine biosensor for the diagnosis of Alzheimer's disease. Journal of Molecular Structure, 2021, 1223: 129168.
- [26] Li W, Pang Y, Wang Y, et al. Aberrant palmitoylation caused by a ZDHHC21 mutation contributes to pathophysiology of Alzheimer's disease. BMC Med, 2023, 21(1): 223.
- [27] Jiang Q W, Tang H D. Case report of a sporadic alzheimer's disease caused by psen2 gene mutation and literature review. Chinese Journal of Alzheimer's Disease and Related Disorders, 2021, 4(4): 302-305.
- [28] Bilousova T, Melnik M, Miyoshi E, et al. Apolipoprotein E/Amyloid-β Complex Accumulates in Alzheimer Disease Cortical Synapses via Apolipoprotein E Receptors and Is Enhanced by APOE4. The American Journal of Pathology, 2019, 189(8): 1621-1636.
- [29] Millet A, Ledo J H, Tavazoie S F. An exhausted-like microglial population accumulates in aged and APOE4 genotype Alzheimer's brains. Immunity, 2024, 57(1): 153-170.
- [30] Zhou X, Fu A K, Ip N Y. APOE signaling in neurodegenerative diseases: an integrative approach targeting APOE coding and noncoding variants for disease intervention. Current Opinion in Neurobiology, 2021, 69: 58-67.
- [31] Imai Y, Meng H, Shiba-Fukushima K, et al. Twin CHCH proteins, CHCHD2, and CHCHD10: Key molecules of Parkinson's Disease, Amyotrophic Lateral Sclerosis, and Frontotemporal Dementia. International Journal of Molecular Sciences, 2019, 20(4): 908.
- [32] Tao L Q, Zhang H. Research progress of triterpenoids in the prevention and treatment of Alzheimer's disease. Chinese Bulletin of Life Science, 2024, 36(4): 487-498.
- [33] Qi Z, Deng S, Wu Y, et al. The effects of Ganoderma leucocontextum triterpenoids treatment on the D-galactose and aluminum chloride-induced Alzheimer-like pathology in mouse brain. Journal of Ethnopharmacology, 2024: 1872-7573.
- [34] Peng X, Luo R, Ran X, et al. Ganoapplins A and B with an unprecedented 6/6/6/5/6-fused pentacyclic skeleton from Ganoderma inhibit Tau pathology through activating autophagy. Bioorganic Chemistry, 2023, 132: 106375.
- [35] Peng X R, Luo R C, Qiu, M H, et al. A-ring opening triterpenoid compounds and their pharmaceutical compositions and applications in Ganoderma lucidum, 2024, 01.
- [36] Shan X X, Zhou L L, Li D W, et al. Research progress on mechanism of classic famous prescription Kaixin Powder in treatment of Alzheimer's disease. Chinese Traditional and Herbal Drugs, 2023, 54(11): 3685-3695.
- [37] Wu Tong. Study on anti-Alzheimer's disease effect and active ingredient screening of triterpene extract of Poria cocos. Changchun University of Chinese Medicine, 2023, 12: R749.16 R285.5.
- [38] Lv J L, Shen X Y, Shen X Y, et al. NPLC0393 from Gynostemma pentaphyllum ameliorates Alzheimer's disease-like pathology in mice by targeting protein phosphatase magnesium-dependent 1A phosphatase. Phytotherapy Research, 2023, 37(10): 4771-4790.

- [39] Xiang Z, Li H J, Shen X Y, et al. Chemical Constituents, Pharmacological Effect, and Product Development of Eucommia ulmoides with Both Medicinal and Edible Values: A Review. Chinese Journal of Experimental Traditional Medical Formulae, 2024, 30(2): 190-202.
- [40] Han R, Yuan T, Yang Z, et al. Ulmoidol, an unusual nortriterpenoid from Eucommia ulmoides Oliv. Leaves prevents neuroinflammation by targeting the PU.1 transcriptional signaling pathway. Bioorganic Chemistry, 2021, 116: 105345.
- [41] Hu F, Lei Y, Han R, et al. The efficacy and pharmacological mechanism of Guilingji to prevent Alzheimer's disease. Alzheimer's Research & Therapy, 2025, 17(1): 157.
- [42] Wang H L, Fu Y Y, Tie F F. Protective Effects of Genkwanin and Other Flavonoids on Alzheimer's Disease and Its Mechanism. Qinghai Science and Technology, 2023, 30(4): 46-55.
- [43] Yan X N, Wang Z, Li R F. Research Progress on the Mechanism of Flavonoids from Ampelopsis grossedentata on Alzheimer's Disease. Modern Food Science and Technology, 2023, 39(8): 343-51.
- [44] Ma X N, Gao P, Wu Y, et al. The ameliorative effects of Vitis vinifera L. Suosuo polysaccharides on Aβ1-42-induced oxidative damage in HT22 cells. Journal of Hainan Medical University, 2024, 30(17): 1304-1312.
- [45] Fang D Y, Zhang L, Wu P, et al. Exploring the mechanism of pueraria lobata improving AD based on network pharmacology and experimental validation. Journal of Shenyang Pharmaceutical University, 2025, 42(2): 131-41.
- [46] Wang Y T, Xu Y M, Zhang Z B, et al. Effect of Drynaria total flavonoids on the expression of NMDAR1, GluR2 and CaMK II in the brain of hydrocortisone model mice. Journal of Hainan Medical University, 2022, 28(24): 1860-1866.
- [47] Liu X Y, Shang Y Z. Pharmacological research progress on extracting flavonoids from Scutellaria barbata. Journal of Chengde Medical University, 2021, 38(5): 421-426.
- [48] Liu X Y, LI H, Shang Y Z. Effects and regulatory mechanism of Scutellaria barbata flavonoids in inhibiting the neuroinflammation of AD rats induced by composited Aβ. Chinese Journal of Hospital Pharmacy, 2022, 42(12): 1197-203.
- [49] Sun H Y, Zhou L Y, Ren L X, et al. Recent progress of neuroprotective mechanisms of luteolin in Alzheimer's disease. Chinese Pharmacological Bulletin, 2022, 38(12): 1781-1785.
- [50] Liu X, Li Y, Wang J, et al. Polysaccharides from Ganoderma lucidum attenuate cognitive impairment in 5xFAD mice by inhibiting oxidative stress and modulating mitochondrial dynamics via the Nrf2/antioxidative axis activation. Metabolic Brain Disease, 2025: 1573-7365.
- [51] Wang L, Lu Y, Liu J, et al. Gegen Qinlian tablets delay Alzheimer's disease progression via inhibiting glial neuroinflammation and remodeling gut microbiota homeostasis. Phytomedicine, 2024, 128: 155394.
- [52] Ye H X, He Yingxi, Qi Y Q, et al. Effect of Lycium barbarum polysaccharides on learning and memory ability and Tau protein phosphorylation level in brain withAlzheimer's disease and type 2 diabetes mellitus mice. Journal of Shihezi University (Natural Science), 2023, 41(3): 360-366.
- [53] Fu J. Study on structural characterization, in vitro digestion and fermentation characteristics of Schisandrae Chinensis Fructus polysaccharides and its mechanism of improving Alzheimer's disease. Jilin University, 2023.
- [54] Shah Z, Iqbal A, Badshah SL, et al. Macroalgae polysaccharides enhance brain health by mitigating scopolamine-induced oxidative stress and inflammation via Nrf-2/TLR4/NF-kB Pathways. Journal of Neuroimmune Pharmacology, 2025: 1557-1904.
- [55] Campanella C, Pace A A-O, Caruso Bavisotto C A-O, et al. Heat shock proteins in Alzheimer's Disease: Role and targeting. Journal of Neuroimmune Pharmacology, 2025: 1422-0067.
- [56] Hajihosseini S, Zakavi SA, Farrokhi Z, et al. A meta-analysis update evaluating the treatment effects of donepezil alone versus donepezil combined with memantine for Alzheimer's disease. IBRO Neuroscience Reports, 2025, 19: 72-82.
- [57] Salloway S, Chalkias S, Barkhof F, et al. Amyloid-related imaging abnormalities in 2 Phase 3 studies evaluating aducanumab in patients with early Alzheimer Disease. JAMA Neurology, 2022: 2168-6157.
- [58] Xu L, Chen W J, Tian C J, et al. Efficacy and safety of chinese herbal medicines combined with chemical drugs for alzheimer's disease: A systematic review and meta-analysis. World Journal of Traditional Chinese Medicine, 2024, 10(1).
- [59] Wang J W, Wei B J. Prevention and treatment of Alzheimer's disease by traditional chinese medicine via regulating ROS: A review. Chinese Journal of Experimental Traditional Medical Formulae, 2024, 30(12): 281-8.
- [60] Aktary N, Jeong Y, Oh S, et al. Unveiling the therapeutic potential of natural products in Alzheimer's disease: insights from in vitro, in vivo, and clinical studies. Frontiers in Pharmacology, 2025: 1663-9812.

